Simulation of Gas Injection Processes

Jákupsstovu, Sigurd I.

Publication date:
2002

Document Version
Publisher's PDF, also known as Version of record

SIMULATION OF GAS INJECTION PROCESSES

By

Sigurð í Jákupsstovu

2002

IVC-SEP, Department of Chemical Engineering
Technical University of Denmark
Building 229
DK-2800 Lyngby
Denmark

Printed by Book Partner, Nørhaven Digital, Copenhagen, Denmark

ISBN 87-90142-89-6

Preface

This thesis is submitted as a partial fulfilment of the requirement for obtaining the Ph.D degree at the Technical University of Denmark (Danmarks Tekniske Universitet, DTU). The work has been carried out at the Department of Chemical Engineering (Institut for Kemiteknik), at Chevron Petroleum Technology Company in San Ramon and at the University of the Faroe Islands (Fróðskaparsetur Føroya). The project has been supervised by Professor Erling H. Stenby.

I will take this opportunity to thank my friend Dengen Zhou for inviting me to work with him at the Chevron offices in San Ramon, California.

I thank the The Faroese Research Council and the Nordic Energy Research Council for supporting the project financially.

Finally I thank my beloved wife Gunvør for her support and endless patience.

Tórshavn, August 2002

Sigurð í Jákupsstovu

Summary

Upscaling of Miscible Displacement.

Accurate predictions of reservoir flow and recovery is important for planning a development of an oil and gas field. To accomplish this task we require, as a starting point, detailed information about the reservoir geology as well as accurate information of the fluid types present in the reservoir. In order to make any predictions on reservoir flow and recovery we also need accurate and robust models for fluid-fluid and fluid-rock interactions.

Reservoir simulation is a numerical tool which is used to dynamically model fluid flow through porous underground reservoirs. The structural and geological features of the reservoir are described by a 3 dimensional mesh of grid blocks. The reservoir rock properties, fluid properties and fluid saturations are assigned to each of the grid blocks ensuring hydrodynamic and capillary equilibrium. After defining boundary conditions and the location of the production and injection wells within the grid block system, dynamic simulations of an oil field development can be carried out.

Modern geo-statistical methods are capable of providing highly detailed, statistically realistic representations of permeability and porosity structures of petroleum reservoirs and these frequently consist of more than 10^7 grid blocks. The Finite Difference reservoir simulators commonly used, such as ECLIPSE, can not be used for routine simulations on grids of this size, as a single simulation run may last for weeks depending on the complexity of the model. To overcome this problem, the geological description is upscaled for use on the coarser simulation scale. Upscaling can be regarded as an attempt to conserve the effective properties of the fine scale system and the transfer of these onto the coarse scale, to ensure that the coarse scale flow is representative of the actual system. More or less advanced upscaling methods have been developed over the last decades to account for the loss of detail between the geological model scale and the flow simulation scale.

The motivation for using an upscaling methodology is thus to reduce the simulation run times. When planning a field development it is necessary to carry out a large number of sensitivity simulation runs in order to evaluate well spacing and production - injection strategies. By employing a suitable upscaling methodology it is possible to obtain a reduction in the computing time for a single simulation run by 2 - 3 orders of magnitude, from days to minutes.

Gas injection has become very important as a means to increase oil recovery as well as for environmental considerations in oil field development. As a

means to increase oil recovery, gas injection processes are most effective when the injected gas is nearly or completely miscible with the oil in the reservoir. In theory it is possible to recover all the oil by a miscible displacement.

In order to understand the effects of the resulting flow behavior it is important to use modelling tools that allow us to account for effects resulting from fluid mixing, sub grid heterogeneity, viscous forces, capillary forces and from gravity.

In this work we present a methodology for upscaling miscible displacement processes, which may result when gas is injected into an oil zone. The method combines the Todd Langstaff formulation for miscible displacement with the use of pseudo relative permeability curves. For each grid block a pseudo relative permeability curve and a mixing parameter, ω, are specified.

The results from the coarse grid simulations have been compared to fine grid reference results and to coarse grid simulations using straight line relative permeability functions, i.e. with no upscaling of relative permeability functions, and a constant global mixing parameter, ω. Simulations have been carried out on systems of different heterogeneity correlation lengths.

The results show that in most cases the Standard Boundary Conditions (STBC) with Volume Averaged concentrations provide the best results. The volume averaging controls numerical dispersion and the pseudo relative permeability functions are able to transfer the flow behavior of the fine grid heterogeneity on to the coarse grid. For highly heterogeneous systems with long correlation lengths this becomes particularly true.

When using the Effective Flux Boundary Conditions (EFBC) in combination with Outlet Averaging, the displacement front is seen to be more dispersed. Breakthrough generally occurs early due to the dispersive effects of the outlet averaging while for systems of long heterogeneity correlation lengths the breakthrough may be delayed due to the attenuation, imposed by the EFBC conditions, of flow through high permeability channels.

For some systems of short correlation lengths it may not be necessary to use pseudo relative permeability functions as the systems exhibit a rather homogeneous behavior which can be transferred to the simulation scale by means of permeability averaging. For these systems it may be sufficient to use straight line permeability functions with a global viscosity mixing parameter, ω, to control the physical solvent dispersion and a critical solvent concentration to control numerical dispersion.

Viscosity

The Friction theory method for calculating viscosity has been implemented into the Chears reservoir simulator in order to compare the performance of the Friction Theory (FT) method to the normally used Lohrenz Bray Clark (LBC) correlation. The Lohrenz Bray Clark method uses a 4^{th} order polynomium in the reduced density to calculate the viscosity and therefore the accuracy of the LBC method is dependent on the accuracy of the fluid density calculations. In compositional reservoir simulation the density is calculated using cubic equations of state such as the Soave Redlich Kwong (SRK) or the Peng Robinson (PR) equations of state. It is well known that the density calculations from these equations of state are not very accurate and consequently the accuracy of the viscosity calculation will suffer from this also. By applying the Peneloux volume shift for the molar volume calculations, the Lohrenz Bray Clark viscosity predictions can in many cases be improved.

The Friction Theory model takes advantage of the accurate pressure predictions that can be obtained from the PR and SRK equations, when correlating the attractive and repulsive pressure terms of the equation of state to model the viscosity. The models have been derived by correlating 12 parameters to a viscosity database for methane to n-octadecane.

The two viscosity calculation methods have been compared for 12 reservoir oils before and after tuning of the models. The results show that the Friction Theory method is superior to the Lohrenz Bray Clark method, in particular for the heavier oils. The FT method does not increase computing time compared to the LBC method. The method is presently being improved further for a wider range of oils.

Resumé

Nøjagtige beregninger af reservoirstrømninger og indvinding er vigtigt for at kunne planlægge en udbygning af et gas-olie felt. For at kunne udføre disse beregninger er det nødvendigt at indsamle detaljeret information om reservoirets geologi og de væsker som er indeholdt i reservoiret. Endvidere er det nødvendigt at have nøjagtige og robuste metoder til beregning af vekselvirkning mellem gas, olie og vand samt reservoir-bjergartens indflydelse på fasestrømninger.

Hvis man kan beskrive reservoiret tilstrækkeligt fint er det muligt at beregne reservoirstrømninger med god nøjagtighed. For at kunne udføre disse beregninger indenfor en rimelig tidshorisont, kræves meget stor regnekraft som ikke er tilgængelig i de fleste tilfælde. I praksis udføres derfor, reservoirsimulering på et numerisk grid der er væsentligt grovere end den tilsvarende geologiske beskrivelse. Hvis ikke der kompenseres for den manglende detaljeringsgrad i det grovere grid er der risiko for at beregningerne i mange tilfælde vil blive fejlagtige.

Ved opskalering overføres det fine grids egenskaber til det grovere grid ved hjælp af såkaldte pseudo relativ permeabilitets funktioner. I dette arbejde præsenterer vi en metode for dynamisk opskalering af den blandbare fortrængningsproces, som kan opnås når gas injiceres i en oliezone. Metoden er baseret på Todd Langstaff teorien for blandbar fortrængning i kombination med pseudo-funktioner og blandingsparametre beregnet for hver enkelt grid blok i den grove model.

Ved generering af pseudo-funktionerne, til brug for simuleringer på det grove reservoirgrid, har vi sammenlignet 2 forskellige kombinationer af grænsebetingelser og midlingsmetoder, Standard grænsebetingelser og Effective Flux grænsebetingelser. Resultater fra de grove simuleringer er blevet sammenlignet med de fine reference simuleringer samt med grove simuleringer hvor der ikke er foretaget nogen opskalering af den relative permeabilitet. For de systemer vi har arbejdet med viser det sig at Standard grænsebetingelserne giver de bedste resultater, både med hensyn til skarphed af fortrængnings front og gennembrudstidspunkt. Ved brug af Effective Flux grænsebetingelser ses at fortrængningsfronten er mere udvisket i forhold til simuleringsresultaterne fra den fine model og at gennembrud som regel forekommer for tidligt.

Viskositet

Friction Theory metoden til beregning af viskositet er blevet inkluderet i Chears reservoir simulerings programmet, således at det er muligt at sammenligne metoden med den normalt anvendte Lohrenz Bray Clark metode (LBC). Lohrenz Bray Clark metoden benytter sig af en 4 ordens korrelation af reduceret massefylde (densitet) til beregning af viskositet. I kompositionel reservoirsimulering beregnes densitet ved hjælp af kubiske tilstandsligninger, som f.eks. Peng Robinson (PR) eller Soave Redlich Kwong (SRK). Det er et velkendt problem med disse ligninger at beregning af det molære volumen og dermed densiteten er behæftet med en unøjaktighed, der i mange tilfælde påvirker den beregnede viskositet i en uacceptabel grad. Ved at benytte sig af den såkaldte Peneloux volumen korrektion, kan dette problem afhjælpes i nogen grad, specielt for de lettere olier.

Friktion Theory metoden korrelerer viskositeten med det attraktive og det repulsive bidrag af trykket fra de ovennævnte kubiske tilstands ligninger, som netop er velegnede til nøjagtige trykberegninger. Friktions parametrene er baseret på eksperimentelle viskositets data af rene alkaner fra metan til n-octadecane.

Metoderne er blevet afprøvet på 12 reservoir olier, fra lette olier med en viskositet omkring 0.15 cP til tungere olier med en viskositet på 12-15 cP. Resultaterne viser at Friction Theory metoden er LBC metoden overlegen. For de 12 olier er det muligt efter tuning at reproducere de eksperimentelle data indenfor 3 % nøjagtighed ved brug af Friction Theory metoden og indenfor 16% ved brug af LBC metoden.

Contents

Nomenclature

k	Permeability [mD]
k_e	Effective permeability [mD]
k_r	Relative Permeability
h	reservoir thickness [m]
s	Saturation
c	Concentration
p, P	Pressure [Psia, Bara]
α	Alfa, miscibility parameter
ω	Omega, mixing parameter
f_s	Fractional Flow (solvent)
μ	Viscosity [cP]
q	Darcy velocity [ft/day, m/sec]
λ	Mobility
ρ	Density [kg/m^3]
v	Molar volume [m^3/mole]
η	Viscosity [cP]
κ_a	Attractive term for Friction Theory
κ_r	Repulsive term for Friction Theory
κ_{rr}	Quadratic repulsive term for Friction Theory
ε	Mixing exponent for Friction Theory
Q	Darcy flow rate
q	Darcy flow velocity
L	Length
τ_{xy}	Shear force
R	Universal gas constant
T	Temperature
a	Factor for intermolecular attractive forces
b	Factor for intermolecular repulsive forces
c	Peneloux volume correction term
σ	Interfacial tension
φ	Porosity
A_T	Adhesion tension
I_H	Heterogeneity Index
ϕ	Pressure potential
θ	Dip angle
API	American Petroleum Institute
SG	Specific Gravity
d	Dimension number (Effective Flux Boundary Conditions)

χ	Constant for use in the dimensionless volume shift
Ψ	Constant for use in the dimensionless volume shift

Subscripts

m	Mixture (used for the 1/4 power mixing rule)
s	Solvent
w	Water
o	Oil
t	Total property
he	Effective hydrocarbon property
se	Effective solvent property
oe	Effective oil property
c	Critical Property, concentration
k	Permeability
H	Heterogeneity

Superscripts

^{o}	Reference state
cor	Corrected

1 Exploration and Production

Exploration for oil takes place all over the world in order to meet the ever increasing demand for energy sources. The exploration takes place both onshore and offshore in remote areas and at increasing water depths.

The oil reserves are not evenly distributed around the world. From the following graph it is seen that some 67% of the reserves are located in the Middle East while only 2 and 5 % are found in Western Europe and North America respectively. For energy-political reasons it is probably important to locate additional hydrocarbon reserves outside the Middle East.

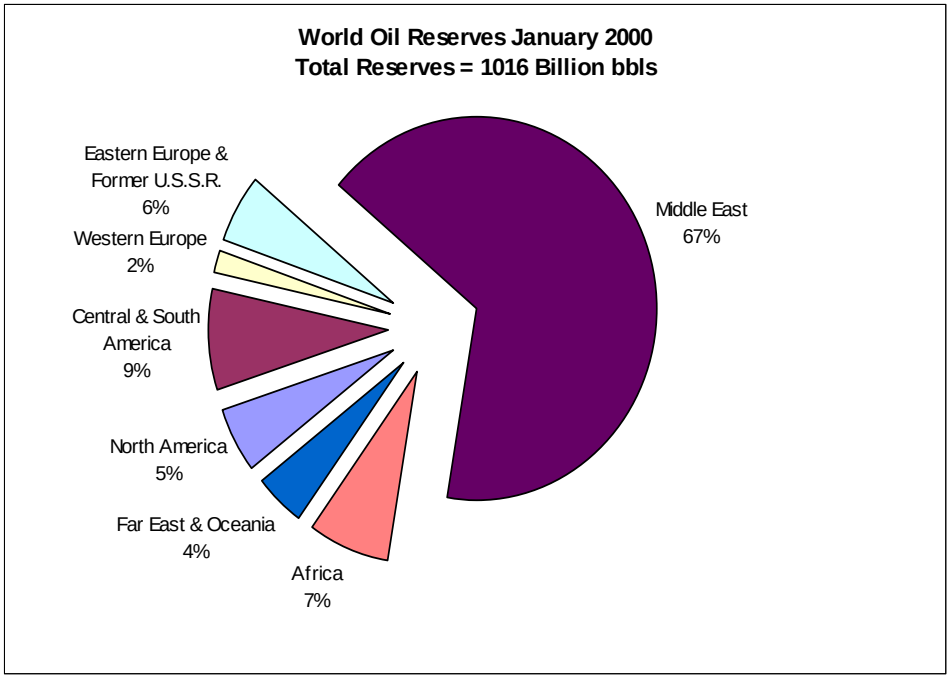

Figure 1.1: The world oil reserves estimate at 1 January 2000. (*Ref.: Energy Information Administration EIA*)

When exploration is carried out, it is attempted to locate underground accumulations of hydrocarbons by means of geophysical surveying methods, including seismic surveys as well as magnetic and gravimetric surveys.

For an underground accumulation of hydrocarbons to exist several conditions must be fulfilled, among these, the most important are:

- A source rock must be present in the area from which the hydrocarbons are generated
- A porous reservoir rock must exist in which the hydrocarbons can be contained
- A migration path must be available for the hydrocarbons to migrate from the source rock to the reservoir rock
- The reservoir rock must be capped upwards in order to trap the hydrocarbons

The geophysical surveys are therefore directed towards areas where sedimentary basins are believed to exist.

Where and when did it begin.

The first attempt to drill for oil was carried out by Edwin L. Drake who drilled for oil in Pennsylvania and found oil on 27 august 1859 [62]. Up to this point oil had only been collected from surface seepages. The main use of oil had been for illumination and lubricating purposes.

After Drake had demonstrated that it was possible to drill for oil and to pump it out of the subsoil in large quantities, a new industry was established. The initial wells were produced by pumping, but in 1861 the first flowing well was found which flowed at a rate of three thousand barrels pr. day. When the oil shot in the air the escaping gases were ignited which caused a huge explosion and fire, killing 19 men.

The production in west Pennsylvania rose from 450,000 bbls/day in 1860 to more than 3 million bbls/day in 1862. The oil price in January 1861 was 10$/bbl, in June 1861 the price was 50 cents/bbl and by the end of 1861 the price was down to 10 cents/bbl. At these prices all competition was reduced quickly and soon demand caught up with supply and by the end of 1863 the prices were up to more than 7 $/bbls.

The years after the first discoveries were made were truly like a gold rush. Fortunes were made and lost in days. The initial pioneering days ended when the oil corporations were founded and the ultimate concentration was found in Standard Oil which was founded by John D. Rockefeller. The company's monopoly was later divided by a court ruling via the anti thrust act into 7 companies, termed the 7 sisters.

Ref.: The Price

Chapter Outline

A brief introduction on the generation and accumulation of hydrocarbons will be given here together with an overview over the processes from exploration through to development and production.

1.1 Generation of Hydrocarbons

The hydrocarbons found in nature were formed by the action of heat and pressure on the remains of ancient plant and microscopic animal life. The organic matter that constitutes the main source for oil and gas generation is regarded to be algae, plankton and bacteria. The organic matter is deposited on the sea bed together with shale sediments. If the resulting shale has a high enough content of organic matter it is classified as an oil shale. When the source rock (oil shale) undergoes burial by being covered by younger sediments, the process of petroleum generation is initiated. At an early stage the organic matter is anaerobically decomposed by bacteria into a substance called Kerogen, which is the raw material of petroleum. After further burial the bacterial life is destroyed and at a temperature of about 339 K (150° F), oil starts to be formed from the Kerogen. At higher temperatures progressively lighter oils are formed. At temperatures above 450 K (350° F) only dry gas is produced. At even higher temperatures all hydrocarbons are destroyed.

1.2 Petroleum Migration

After the hydrocarbons have been generated within the source rock they are expelled and travel towards the surface along available migration paths. The migration can be divided into a primary and a secondary migration process. The primary migration being the transport of generated oil and gas through and out of the source rock. As we normally think of the oil shale or source rock as being completely impermeable it has not been explained how the oil migrates through the source rock. The Secondary migration takes place outside the source rock and is explained as a buoyancy driven transport through a porous media and/or along fracture planes. The secondary migration will continue until the oil reaches the surface or until it is trapped by an impermeable structure.

1.3 Formation of Reservoirs

There are in general two types of oil reservoirs, being sandstone reservoirs and carbonate reservoirs. The sandstone reservoirs are deposited from eroded

material which is transported by rivers to the sea shore (Deltas). In some instances when large amounts of deposits build up at the shelf, sudden slides occur resulting in large fans of sand bodies being deposited on the deeper seabed, as illustrated by figure 1.2 and 1.3. These slides are commonly termed turbidites. As the reservoir sands are buried by finer sediments through geologic time, the sand is compacted and altered into sandstone through diagenetic processes.

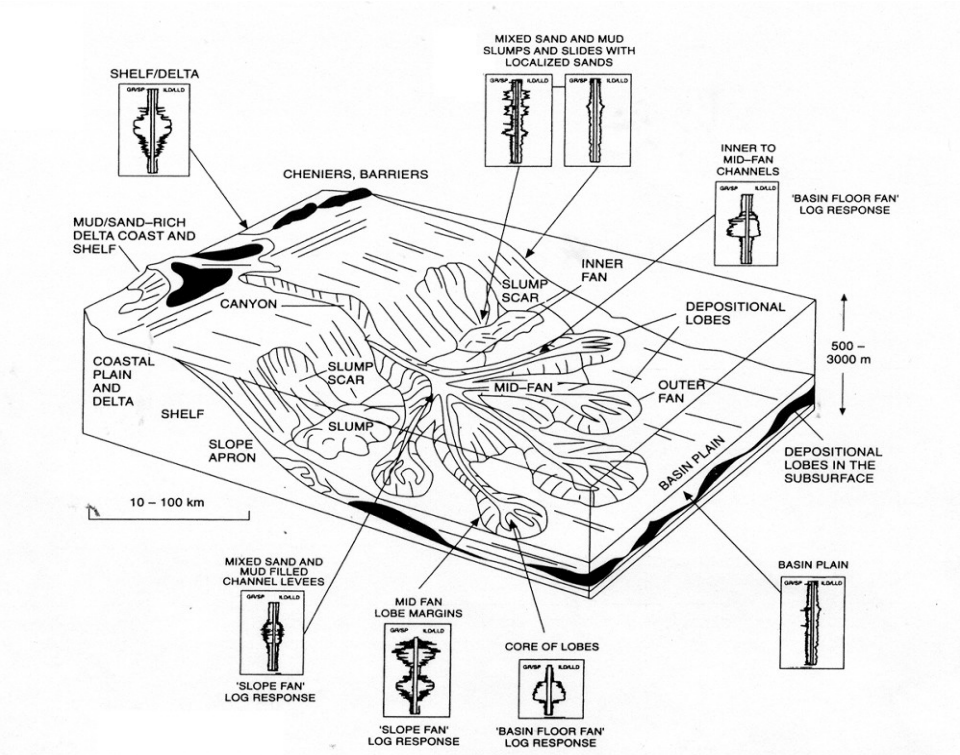

Log signatures from selected depositional lobe and channel–levee elements of a single point-source, mixed sand–mud fan system. Note variation in log character with respect to the position within the fan (after Richards and Bowman, in press)

Figure 1.2: Sand is deposited on the deeper seafloor forming potential hydrocarbon reservoirs.

Figure 1.3: Deepwater turbidite sandstone fan (Karoo Basin 2002)

Carbonate reservoirs consist mainly of remains from socalled lime secreting organisms, algae, shellbearing animals and corals. These remains may be crushed into smaller parts by wave action reworked and transported until deposited much in the same way as silici-clastic deposits. When the carbonate sediments are subjected to burial and cementation the result is a hard rock consisting mainly of calcium carbonate ($CaCO_3$). The carbonate reservoir consisting of Calcite, unlike the sandstone reservoir consisting of Silica, is very prone to dissolution and reprecipitation by formation waters percolating through the reservoir.

1.4 Traps

In order to facilitate an accumulation of hydrocarbons, a trapping mechanism is needed which prevents further migration of the hydrocarbons. The types of traps normally encountered are structural traps or stratigraphic traps or a combination of these.

A structural trap is formed by deformation of the formation beds after these have been deposited. A typical example of a structural trap is the anticline, or 4-way dip closure.

Figure 1.4: The anticline is an example of a strucural trap.

A stratigraphic trap is formed by changes in the beddings themselves, for example the reservoir rock pinching out, preventing further migration.

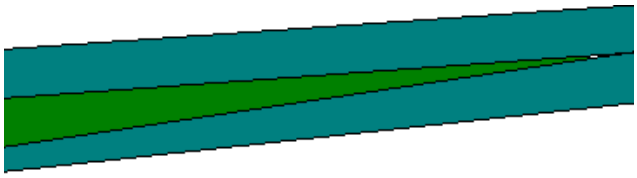

Figure 1.5: The reservoir rock (porous layer) is pinching out forming a statigraphical trap.

1.5 Reservoir Properties

The reservoir properties of the most significance with respect to hydrocarbon recovery, apart from overall reservoir dimensions, are permeability and porosity.

Porosity

Porosity is defined as the proportion of pore space to the total bulk volume of the sample. The porosity of a sandstone reservoir depends on the shape and

size distribution of the sand grains constituting the rock. Other factors that affect the porosity are the depth of burial and degree of cementation. The porosity as a general rule decreases with depth due to compaction. After deposition and burial the sandstone porosity may be altered by formation waters that percolate through the rock and precipitate salts.

Figure 1.6: The porosity of sandstone reservoirs normally range between 10 and 30 %

The building blocks of carbonate reservoirs are much more irregularly shaped than sand grains and therefore the porosity function for carbonates is more complex. The carbonates are also very sensitive to dissolution and re-precipitation due to formation waters flowing through the reservoir. The porosity for carbonate reservoirs may be as high as 45 %.

Permeability

The absolute permeability, *k*, can be regarded as the hydraulic conductivity of the porous media, i.e. the ability of the rock to allow fluid flow through its interior. The concept of permeability and its important role in hydrocarbon recovery will be introduced in chapter 2.

1.6 Diagenesis

Diagenesis can be defined as the physical, chemical or biological processes that turn sediments into sedimentary rock by modifying the mineralogy and/or texture. Diagenesis occurs where the mineralogy of the rock becomes unstable as a result of changes in the conditions or chemistry. Instability usually occurs at grain contacts and in pore space between the grains. Changes in pressure and temperature cause new minerals to form or pre-existing minerals to become modified as the sediment (or rock) adjusts to new equilibrium conditions. Compaction and precipitation of salts are examples of diagenetic processes.

1.7 Fluid Distributions

Before the porous space of the reservoir rock is being charged with hydrocarbons migrating upwards from below, the reservoir rock was filled with water. Due to density differences the water is being displaced by the hydrocarbons. Not all the water, however, is being displaced, as a proportion is left within the pore space as "residual water". This residual water is trapped by capillary forces and is regarded as immobile. The Free Water Level (FWL) is defined as the point where the capillary pressure is zero. Above the free water level a transition zone exists where the water saturation gradually decreases upwards from 100 % water at the FWL to residual water saturation S_{wc} above the transition zone. The height and shape of the transition zone saturations are a function of capillary forces and of pore size distributions.

In the transition zones both the oil and the water phases are mobile.

1.8 Prospectivity

From already published information, it is possible, combined with remote sensing methodologies such as satellite imaging, to locate areas where sediments have been accumulated in large quantities forming socalled sedimentary basins. These areas will then be the subject for further geophysical prospecting. The methods for identifying prospects are e.g. geological mapping where the shape of the subsurface layers is interpreted from the surface mapping. Screening of the surface for oil seepages may also give confidence in that a hydrocarbon system exists. More advanced prospecting methods are in use today where it is attempted to indirectly sense the geological aspects of the subsurface. Among these methods are the gravitational and magnetic surveying methods where local variations in the earths gravitational and magnetic fields are used to interpret the subsurface. By far the most important method is the seismic reflection survey where a sound wave is propagated downwards through the formation layers in the subsurface. At formation boundaries, where rock properties change, a portion of the transmitted energy is reflected back towards the surface. By recording and analysing two way travel times for the sound waves, an image of the subsurface can be generated.

Based on these subsurface images and other available information, possible prospects are identified. In order to decide if a prospect is significant enough to warrant an exploration well it is necessary the determine likely hydrocarbon volumes that the prospect can hold.

1.9 Exploration Drilling

After a prospect has been identified from geophysical surveys, the prospect has to be tested. This is done by drilling a well. The main objective of an exploration well is therefore to prove a prospect. In a success case where a hydrocarbon column of sufficient height is found, the objectives are to gather the necessary information in order to base a decision for the next phase of operations.

In a failure case, where the prospect for some reason or other does not work, the objective of the well becomes to gather information that can assist in explaining the reason for failure as well as further exploration decisions.

The success/failure mechanisms are the ones that are listed in the beginning of this chapter.

- Source rock
- Migration Path
- Reservoir
- Trap
- Seal

A probability is assigned to each of the 5 criteria and the combined likelihood of success is found by multiplying the likelihood associated with each criteria.

1.10 Wire Line Logging

When the well is drilled, each hole section is logged prior to being cased of. The logs are carried out by lowering different instruments down into the borehole measuring the formation response to the signals sent out by the logging tools. The purpose of logging is to obtain information on reservoir characteristics such as:

- Lithology
- Porosity
- Reservoir Pressure
- Fluid types
- Fluid saturations

- Fluid contacts
- Flow potential
- Geophysical properties for calibrating seismic data
- Coring
- Formation bedding and natural fractures
- …

1.11 Well Testing

If a hydrocarbon column is found, it is important to evaluate the production potential of the reservoir. The wire line logging methods only provide indirect measurements of the bulk productivity. In order to obtain productivity information it is normally decided to carry out a well test. In order to conduct a well test, temporary production equipment is installed in the well and on the drilling rig. The fluids that are being produced during the well test is disposed of by flaring.

Main purposes for the well test is to obtain information on:

- Productivity of the reservoir zone
- Reservoir fluid type and properties
- Reservoir characteristics in terms of size, boundaries, drive mechanisms etc.

1.12 Appraisal Well Drilling

If an exploration well and the subsequent evaluation has proven successful, the next step is usually to drill one or more appraisal wells in order to delineate the reservoir and to gather additional information on reservoir and fluid properties.

From the information gathered from the exploration and appraisal activities the decision is taken whether or not to develop the field. If it is decided to develop the field it is necessary to generate a development plan which outlines how the field should be developed and produced in the most efficient way. Reservoir simulation plays an important role in generating the development plan and to test the optimum recovery strategy.

1.13 Hydrocarbon Recovery

Primary recovery is related to the recovery which can be obtained from depletion alone and is dependent on the system properties such as reservoir pressure, permeability, solution gas, system compressibility, the presence of a gas cap or a water aquifer etc.

In order to increase the recovery beyond what can be obtained from depletion, it is necessary to use secondary recovery methods where water and/or gas is injected into the reservoir. The injection serves 2 purposes, 1) the reservoir pressure and production is not declining at the same rate as under pure depletion and 2) the injected fluid displaces the reservoir oil towards the production wells. The efficiency of the displacement is dependent on the reservoir heterogeneity and the mobility ratio between the injected fluid and the in-situ oil. For adverse mobility ratios where the injection fluid is more mobile than the reservoir fluid the recovery factor may be reduced due to oil being bypassed by the injection fluid. For high viscosity oils, steam injection is sometimes used to heat up the oil in order to reduce the viscosity.

During secondary recovery where injection is used to maintain pressure and to displace the oil towards the production wells, it becomes very important to understand the effects of the reservoir heterogeneity and the interactions between the injected fluid and the reservoir oil in order to determine a realistic recovery factor for any given secondary recovery scheme.

In this project we are concerned with the modelling of miscible displacement of oil by gas in highly heterogeneous reservoirs.

2 Simulation of Miscible Gas Injection.

2.1 Introduction

Gas injection has become very important as a means to increase oil recovery as well as for environmental considerations in oil field development. As a means to increase oil recovery, gas injection processes are most effective when the injected gas is nearly or completely miscible with the oil in the reservoir. When injecting gas into the oil zone of a reservoir, under the right conditions, miscibility may be obtained between the injected gas and the in-situ oil. In theory it is possible to recover all the oil by a miscible displacement.

When producing from an oil reservoir, associated gas will also be produced. The gas is not easily stored and transported as is the case for oil and therefore, in remote areas where it is not economically feasible to recover the produced gas, re-injection of the gas provides the only viable and environmentally friendly alternative for disposal of produced gas. The re-injection of produced gas may also provide an economic benefit in terms of added oil production.

To evaluate the effect of gas injection on a reservoir scale it is necessary to carry out reservoir simulation studies.

Oil and gas reservoirs are complex sedimentary structures, within which fluid flow is controlled by the interaction between driving forces, such as pressure gradients between wells and gravity and the properties of the reservoir rock and the reservoir fluids. When gas is injected and comes in contact with the in-situ oil the properties of the fluid phases may undergo dramatic changes. In order to understand the effects of the resulting flow behavior it is important to use modelling tools that allow us to account for effects resulting from fluid mixing, sub grid heterogeneity, viscous forces, capillary forces and from gravity.

In this project we are focusing on reservoir simulation of gas injection into oil reservoirs. We are mainly concerned with miscible displacement processes as these processes have a significant potential with respect to enhanced oil recovery. The governing transport properties in a miscible displacement process are viscosity and density of the fluids interacting with the permeability heterogeneity of the system. Capillary effects are negligible in a miscible displacement.

It is possible to simulate a miscible displacement through a heterogeneous system with good accuracy if the grids are sufficiently fine. For field-scale simulations, however, the required number of grid blocks can be orders of

magnitude larger than what is effectively handled with the available computation power. To bridge this gap of detail it is necessary to conserve the effective properties of the fine scale model to ensure that the coarse scale flow is representative of the actual system. The methodology for transferring the properties from a fine scale to a coarser scale is referred to as upscaling.

2.2 Objective of the Project

The aim of this project is to improve the description of selected physical processes in miscible reservoir flow simulation which potentially have a large influence on the oil recovery during gas injection, including:

- Relative permeability curves and how these are affected by sub-grid heterogeneity, scale and fluid property changes. We have applied a dynamic up-scaling method to processes where oil is miscibly displaced by gas in heterogeneous systems in order to investigate the interaction of miscibility and adverse viscosity ratios to the degree of system heterogeneity and the development of resultant effective system properties suitable for the simulation scale.
- The use of improved methods for calculating fluid viscosity. We have implemented a new method, the Friction Theory Method, for calculating viscosity into the CHEARS reservoir simulator and subsequently tested and compared the new method to the widely used Lohrenz-Bray-Clark method.

Chapter Outline

In this chapter an introduction will be given to some of the basic concepts and definitions within oil recovery and gas injection, the processes involved and to the modelling of these processes.

2.3 Reservoir Simulation / Modelling of Recovery Processes

Reservoir simulation plays a central role when planning the development and production of an oil and/or gas field. Reservoir simulation is a numerical tool which is used to dynamically model fluid flow through porous media. The structural and geological features of the reservoir are described by a 3 dimensional mesh of grid blocks. The reservoir rock properties, fluid properties and fluid saturations are assigned to each of the grid blocks ensuring hydrodynamic and capillary equilibrium. After defining boundary

conditions and the location of the production and injection wells within the grid block system, dynamic simulations of an oil field development can be carried out. The properties that are assigned to each grid block, e.g. porosity and permeability, are usually based on average values calculated from well logs and core measurements. Between wells the properties are generated by means of geo-statistical tools or by more or less advanced inter- and extrapolation methods.

When production data become available from a reservoir these can be used to adjust reservoir parameters in the model. The process of adjusting reservoir parameters in order to calibrate the model against real production data is termed history matching.

When oil, gas and water are flowing simultaneously through a porous medium the effective flow of each phase is affected by the affinity of the porous media towards the phase and by the presence of other phases. These interactions are accounted for by relative permeability functions. In the 2 phase case of oil being immiscibly displaced by water, the relative permeability functions describe the flow of oil and water as a function of water saturation relative to the single phase flow of the same fluid. Adding phases and miscibility effects will increase the complexity of the system. Reservoir simulation programs are generally grouped by how they handle the phase behavior. In Black Oil simulation the oil phase properties are functions of pressure and solution gas content while gas and water properties may be functions of pressure only. In miscible simulation the phase properties are controlled by mixing rules, combining the component properties into resultant phase properties. In compositional simulation the phase properties are based on equation of state and flash calculations.

The following figure illustrates the central role of reservoir simulation.

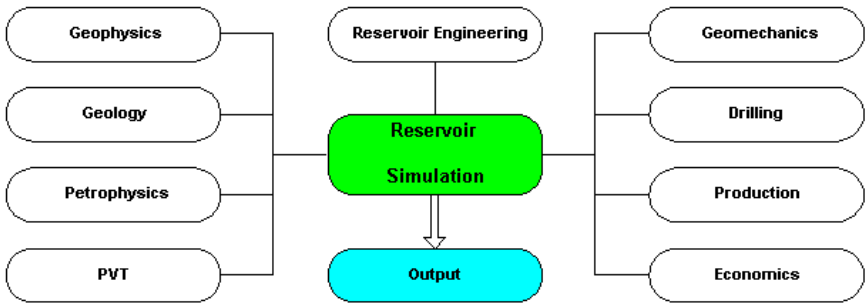

Figure 2.1: Reservoir Simulation combines the outcome of different disciplines into a powerful decision making tool.

2.4 Darcy's Law and Conservation of Mass

Darcy's law and the law of mass conservation are the fundamental laws that reservoir flow modelling is built upon. The concepts of these laws will be introduced here.

2.4.1 Conservation of Mass

The isothermal mass balance for flow through a control volume is illustrated in figure 1.2 and can be expressed by equation 2.1

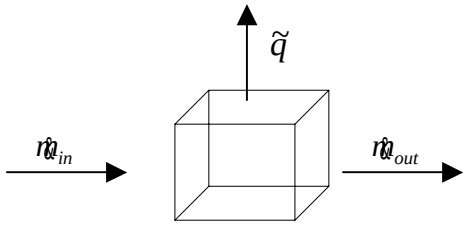

Figure 2.2: The mass balance through a control volume

2.1 $$\hat{m}_{in} A\Delta t - \hat{m}_{out} A\Delta t = \frac{\partial(\rho\phi\Delta V)}{\partial t}\Delta t - \tilde{q}\Delta V\Delta t$$

where $\hat{m}$ = flux (mass flow per area per time), A is the face flow area, ρ is the fluid density, ϕ is the porosity, V the control volume, t the time and $\tilde{q}$ = source – sink strength, (mass per volume per time). Dividing by volume and time results in the following equation (2.2), where the different component have the units of (mass unit per volume unit per unit time).

2.2 $$\frac{\hat{m}_{in} - \hat{m}_{out}}{\Delta x} = \frac{\partial(\rho\phi)}{\partial t} + \tilde{q}$$

The mass flux m_l can also be expressed as $m_l = \rho \cdot q$, where ρ is the density and q is the Darcy velocity which can be obtained from the Darcy equation (2.3) for phase flow.

2.4.2 Darcy's Law

Darcy´s law was extended to multiphase flow by Muskat and Meres (1936). The equation is given here to illustrate which fluid and rock properties are of importance for calculations of flow in porous media.

2.3 $$q_l = -\frac{kk_{rl}}{\mu_l}\left(\frac{dp_l}{dx} + \rho_l g \sin\varphi\right) \qquad l = o,w,g$$

Where q_l is the bulk velocity of the fluid phase , dp_l/dx is the phase pressure gradient, k is the absolute permeability, k_{rl} is the phase relative permeability, μ_l is the fluid phase viscosity, ρ_l is the fluid phase density, g is the acceleration of gravity and φ is the dip angle relative to the horizontal plane, as seen in the following figure.

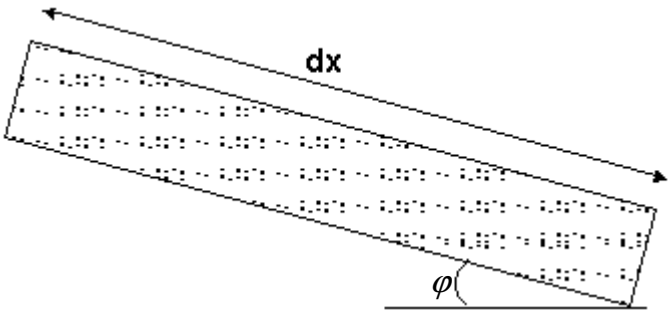

Figure 2.3: Darcy's law gives the flow velocity through porous media as a function of permeability, viscosity, external pressure gradient and dip angle.

2.4.3 Absolute Permeability

The absolute permeability, *k*, can be regarded as the hydraulic conductivity of the porous media, i.e. the ability of the rock to allow fluid flow through its interior. The permeability was defined by Henri Darcy from the following relation for single phase flow.

2.4 $$k = \frac{Q\mu L}{A\Delta P}$$

where Q is the total flow rate (volume/time) passing through the media, L is the distance between inlet and outlet, A is the cross sectional area through which the fluid flow takes place and ΔP is the pressure difference between inlet and outlet. Eq. 2.4 is a simplification of eq. 2.3 assuming single phase flow in the horizontal plane.

2.4.4 Relative Permeability

The relative permeability k_r, is used to calculate the effective permeability of the actual phase and is measured in laboratories under immiscible conditions.

If two fluids flow simultaneously through a porous medium each fluid has its own effective permeability within the same pore network. The effective permeability for the particular fluid phase is dependent on the saturation of each fluid and by the surface properties of porous rock. The relative permeability, k_r, is defined as the effective permeability, k_e ,normalised by the absolute permeability, *k*.

2.5 $$kr = ke/k$$

The relative permeability functions are measured on small samples (core-plugs) of reservoir rock in the laboratory. Due to the size of the sample and the process of bringing the sample from the reservoir to the laboratory, the relative permeability measurements are subject to large uncertainties when used in reservoir flow simulation.

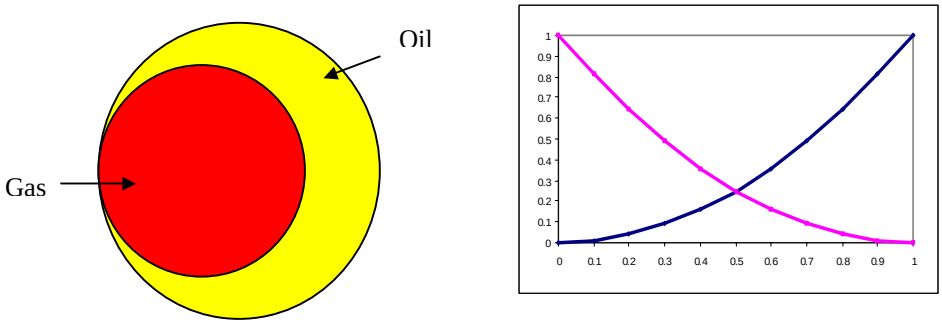

Figure 2.4: The effective permeability of the fluid is dependent on the saturation of each fluid and by the surface properties of the porous rock.

2.4.5 Viscosity

From the Darcy equation it is seen that the flow velocity is inversely proportional to the viscosity of the fluid phase. When carrying out reservoir simulation studies it is necessary to accurately represent the viscosity of the reservoir fluids and how the viscosity of the fluids change when the in-situ fluids interact with the injected fluids.

The viscosity is defined by the following relationship:

2.6 $$\mu = -\frac{\tau_{xy}}{du_x / dy}$$

where τ_{xy} is the shear force and du_x/dy is the fluid velocity gradient in the direction orthogonal to the flow direction. This is illustrated by the following figure where the fluid is contained between an outer wall moving at constant velocity and an inner static wall.

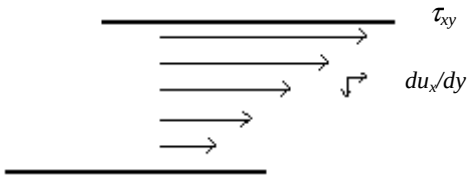

Figure 2.5: The viscosity is defined as the ratio of shear force, $\tau_{xy,}$ over velocity gradient, du_x/dy, orthogonal to the flow direction.

If the injected and in-situ fluids are considered to be immiscible, the viscosity is a function of pressure and temperature only and therefore the viscosity behavior can be included in reservoir models using look up tables.

If the fluids are miscible, the viscosity picture becomes more complicated and therefore not easily handled by look up tables. In compositional reservoir simulation the *Lohrenz-Bray-Clark* [36] correlation has been widely used. In this correlation a reduced viscosity is correlated to a 4th order polynomium of the reduced fluid density of the mixture. The fluid density may be calculated by an equation of state.

A new method for calculating hydrocarbon mixture viscosities has been developed at the IVC-SEP, Technical University of Denmark. The theory is termed the *Friction Theory* [35]. As part of this project the *Friction Theory* methodology has been implemented in the Chears reservoir simulator in order to compare its performance to the standard *Lohrenz-Bray-Clark* correlation.

2.4.6 Density

The density of the fluid is also an important parameter in multiphase flow. If there is a large density difference between the injected fluid and the in situ fluid, this may result in either gravity segregation or gravity override. In such cases breakthrough may occur early resulting in a poor recovery.

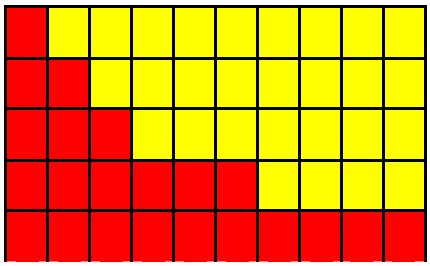

Figure 2.6: If the density of the injected fluid is higher than the in-situ fluid, this may result in gravity segregation and consequently in a poor sweep efficiency.

Density is defined as the mass of the fluid per unit volume. The density is dependent on pressure and temperature. The specific gravity SG is defined as the ratio of the density of the liquid to the density of water at standard conditions. In the oil industry the specific gravity is frequently measured in degrees API which can be calculated by the following relation:

2.7 $$^{0}API = \frac{141.5}{SG} - 131.5$$

If the specific gravity is equal to 1 this corresponds to an API gravity of 10.

In black oil reservoir simulation the density is calculated from surface densities and tabulated values of the formation volume factor and solution gas. In miscible reservoir simulation the density is calculated by mixing rules combining the tabulated component densities into a resultant phase density. In compositional reservoir simulation the density is calculated by means of a cubic equation of state. The most common equations of state used in reservoir simulation are the Peng Robinson (PR) [42] and the Soave Redlich Kwong (SRK) [41] cubic equations of state.

The 2 parameter Peng Robinson equation of state is given by the following equation

2.8 $$P = \frac{RT}{v-b} - \frac{a}{v^2 + 2bv - b^2}$$

where P is the pressure, R is the universal gas constant, v is the molar volume and the 2 parameters a and b represent intermolecular attractive and repulsive forces respectively.

The 2 parameter cubic equations of state, however, are not very well suited for accurate liquid density calculations due to the inaccuracy of the molar volume calculations. Peneloux [43] introduced a method for including a volume correction term in the equations of state in order to improve the molar volume calculation. The volume shift takes the following form:

$$v^{cor} = v - c \tag{2.9}$$

In reservoir simulation, where the density dependent Lohrenz Bray Clark correlation is used to calculate viscosity, the concept of volume shift may improve the viscosity predictions. Correlations are available for calculating the volume shift for both the SRK and the PR equation and by use of these it is possible to obtain improved values for the molar volume and the density.

If very accurate density calculations are needed, a specific density correlation can be used.

2.4.7 Contact Angle, Wettability and Capillary Forces

When a liquid is placed on a solid surface it is seen that the liquid either spreads out like a film on the surface or it forms small well defined drops on the surface. If the fluid spreads out, the fluid is said to be wetting the surface. When the fluid forms small confined droplets which roll of the surface when tilted, this is a non-wetting fluid to the surface.

The wettability describes the affinity of the rock for a specific fluid. The wettability is controlled by interfacial forces between the solid surface and the fluid phases, as illustrated from the following figure.

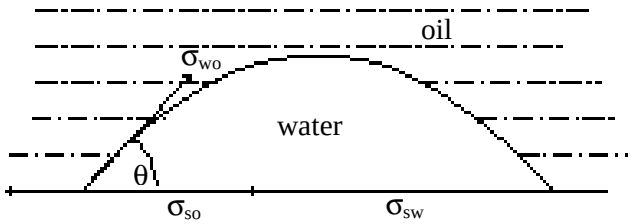

Figure 2.7: The contact angle is controlled by the interfacial tensions between the solid surface and fluid phases.

The contact angle θ is defined by the following relation between the interfacial tensions

2.10 $$\cos\theta = \frac{\sigma_{so} - \sigma_{sw}}{\sigma_{wo}}$$

where σ_{so} is the interfacial tension between the surface and the oil phase, σ_{sw} is the interfacial tension between the surface and the water phase and σ_{wo} is the interfacial tension between the oil and water phases.

If the contact angle is less than 90 degrees when measuring through the water phase the water is *wetting* the surface.

The *Adhesion Tension* is a function that determines, which fluid will preferently wet the solid. In the case of a water-oil-solid system, the adhesion tension is defined as

2.11 $$A_T = \sigma_{so} - \sigma_{sw} = \sigma_{wo}\cos\phi$$

2.4.8 Interfacial Tension

When two fluids are immiscible, a clearly defined interface exists between the fluids. Under conditions where miscibility is approached, this interface breaks down and the fluids begin to mix. The reduction of the interfacial tension (IFT) affects the relative permeability; as the fluids become more and more

equal the surface effects are eliminated and the relative permeability functions becomes a linear function of the phase component concentration. The interfacial tension is normally predicted by means of so-called Parachor methods [47]. The following correlation between the vapor-liquid interfacial tension and the density difference.

$$\sigma^{1/4} = P_\sigma\left(\rho^L - \rho^V\right) \tag{2.12}$$

where ρ^L and ρ^V are the molar density of the liquid and vapor phase respectively, σ is the interfacial tension and P_σ is a proportionality constant known as the Parachor. When modelling the transition from immiscible fluid flow to miscible flow this is usually carried out by linear interpolation between the two endpoints using the IFT as the interpolation parameter as illustrated below.

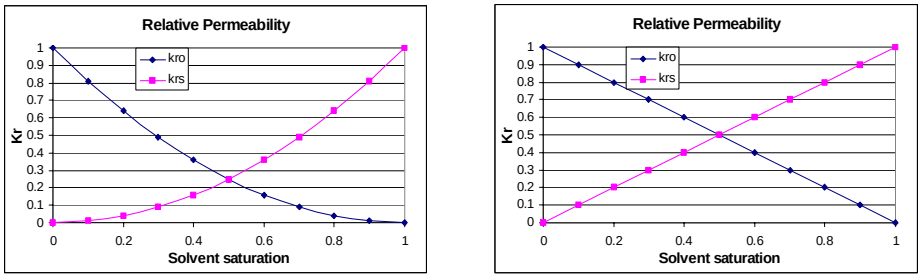

Figure 2.8: The relative permeability is modelled as a function of the Interfacial tension. If the fluid phases are fully miscible, the IFT is equal to zero and in effect only one phase exists. In this case the component fractional flow is proportional to the component concentration and can be modelled using straight line relative permeability functions and appropriate viscosity mixing rules.

2.5 Heterogeneity

In this context we consider heterogeneity as a measure for how the absolute permeability is changing within the simulation domain. It is well known that the absolute permeability may change orders of magnitude on a scale that is significantly less than the simulation scale used. It is inherently difficult to quantify the nature and importance of the system heterogeneity.

A definition for a Heterogeneity Index, I_H, can be defined [16] as follows

2.13 $$I_H = \sigma^2_{\ln k} \lambda_c$$

where $\sigma^2_{\ln k}$ is the square of the variance of ln k, and λ_c is the dimensionless correlation length in the flow direction. The index combines information on the variability of the permeability with information on the structure of the heterogeneity through the correlation length. As the correlation length is evaluated for a specific flow direction, the index may not be representative for flow in a different direction, e.g. the system may behave heterogeneous in one direction and homogeneous in another direction. The higher the heterogeneity index, the more heterogeneous the system is considered to be.

The following pictures illustrate qualitatively the nature of some deepwater sandstone deposits (Turbidites). It is seen that the sequences are in general laminated with varying layer thickness and properties.

Figure 2.9: An example of heterogeneity in a sandstone formation, it is seen that the relative massive homogeneous sandstone sequence at the base of the picture is overlain by thinner laminated layers with more shaly inter-bedded layers. (Karoo Basin 2002)

Figure 2.10: A sequence of massive homogeneous sandstone layers where the bed-thickness is thinning downwards. (Karoo Basin 2002)

Figure 2.11: Thin interbedded sandstone / shale intervals overlain by a thicker more homogeneous sandstone sequence. (Geologists at work, Karoo Basin 2002)

2.6 Upscaling

For heterogeneous systems the rock properties may vary orders of magnitude on a scale much smaller than the simulation scale. To bridge this gap of detail it is necessary to conserve the effective properties of the fine scale model to ensure that the coarse scale flow is representative of the actual system. The methodology for transferring the properties from a fine scale to a coarser scale is referred to as up-scaling.

To run full field simulation on a very fine scale may be impractical due to time constraints, and therefore a certain degree of up-scaling is usually applied. The methodology for upscaling may be system dependent and therefore it is necessary to verify the methodology by comparing upscaled simulation results to fine grid reference results. Once this has been accomplished the pseudo functions can be used to generate fast results on a number of model sensitivities.

In some cases it is sufficient to only upscale static parameters such as permeability and porosity. In other cases the heterogeneity is such that it is necessary to upscale the relative permeability functions also. In a case where the simulation scale contains sub-grid heterogeneity, direct use of laboratory measured relative permeability curves may result in misleading results. It is necessary to evaluate the effect of the heterogeneity and include this in the effective relative permeability functions. The resulting curves are called pseudo relative permeability functions.

In the following figure, an example of an heterogeneous block is illustrated. Assume that the simulation scale is illustrated by the block to the right and the sub-grid heterogeneity by the block on the left and the permeability of the blocks to be illustrated by the colours. If we assume that the orange streak has a permeability 10 times higher than the area in grey it is easy to see that it is difficult to transfer the flow characteristics of the block to the left to the simulation block to the right only by means of permeability up-scaling.

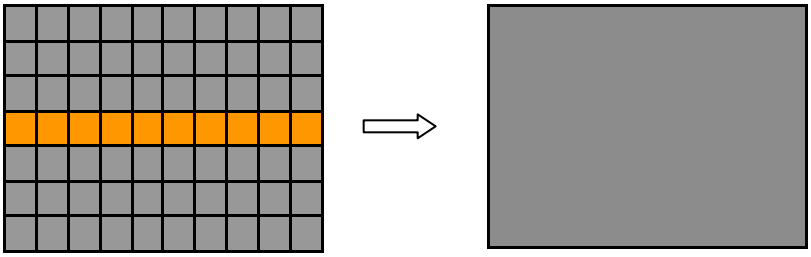

Figure 2.12: The fine grid block contains a high permeability streak which must be incorporated on the simulation scale.

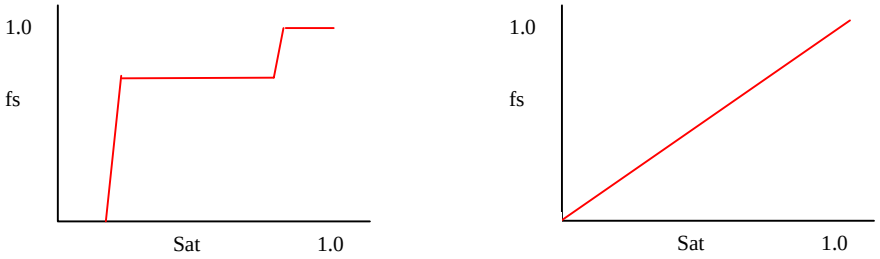

Figure 2.13: Qualitative flow behavior of the fine grid and of a corresponding coarse grid without use of pseudo relative permeability curves.

The fractional flow figures above illustrate schematically how fluid injected uniformly at the right block face would exit at the left block face as a function of the block concentration of the injected fluid, using straight line relative permeability functions for both the fine grid and the corresponding coarse block. It is seen that the effect of the high permeability layer is not accounted for in the fractional flow curve on the coarse scale. The effects of reducing the number of grid blocks in the flow direction is also seen to promote flow at the outlet face too early. If the up-scaling shall succeed it is necessary to recreate the correct fractional flow on the coarser scale. By introducing a pseudo relative permeability function it is possible to maintain the qualitative behavior of the sub grid. The procedure for doing this is called dynamic up-scaling. This is treated further in chapter 3.

As part of this thesis we have extended the *Renorm*[10] methodology for use with fully miscible flow. The methodology is based on a combined use of an extension of the Todd Langstaff miscible formulation proposed by Zhou et.al [8] and the dynamic *Renorm* up-scaling code for WAG processes developed by Mike Christie and Los Alamos National Laboratories. [10, 16].

3 Upscaling of a Heterogeneous Medium

Upscaling is the transfer of fine grid flow behavior onto a coarser scale by means of effective flow properties and flow functions ……

3.1 Introduction

Gas injection becomes increasingly important for oil recovery and environmental considerations in oil field development. Gas injection processes are most effective when the injected gas is nearly or completely miscible with the oil in the reservoir, however, as a result of strong interaction between reservoir heterogeneity and gas-oil properties, continuous miscible gas injection is commonly found to be unstable. In theory one can simulate such processes with great accuracy if the grids are sufficiently fine.

Modern geo-statistical methods are capable of providing highly detailed, statistically realistic representations of permeability and porosity structures of petroleum reservoirs and these frequently consist of more than 10^7 grid blocks. The Finite Difference reservoir simulators commonly used, such as ECLIPSE, can not be used for routine simulations on grids of this size, as a single simulation run may last for weeks depending on the complexity of the model.

The problem of incorporating available geological information into the reservoir simulator is not a new problem. The continuously increasing computing power available enables us to build more and more complex models, however, the gap between the amount of data and the degree of complexity that we would like to incorporate into our simulators and what the simulator can practically handle, is continuing to be present, and it is therefore necessary to use alternative methods to help us run our simulations.

By increasing computing power and by running parallel computing, the problem can be reduced, but the amount of resources required are high and not always justified. A new simulation method, the Streamline Simulator, provides very fast simulation results on large grids[24, 37, 38]. The saving in computing time compared to the conventional Finite Difference simulator can be orders of magnitude depending on the nature of the problem. The Streamline simulator, however, is best suited for special cases, such as voidage replacement, and does not, at present, provide the versatility of the Finite Difference simulator.

More or less advanced upscaling methods have been developed over the last decades to account for the loss in detail between the geological model scale and the flow simulation scale. Upscaling can be regarded as an attempt to conserve the effective properties of the fine scale system and the transfer of

these onto the coarse scale, to ensure that the coarse scale flow is representative of the actual system.

In some cases it may be sufficient to upscale static parameters such as the absolute permeability and porosity distributions. In other cases however, where the heterogeneity is significant and the mobility ratio between the in-situ fluid and the injected fluid is large, it may be necessary to use a dynamic upscaling technique to reproduce the fine scale behavior. Heterogeneity can be described through equation 2.13 by the variance and the correlation length of the permeability distribution. In a system with long correlation lengths in the direction of flow, channelling may take place and the use of pseudo relative permeability functions are required in order to capture this effect on a coarser grid.

Taken to the limit pseudo functions should be generated for each flow direction for every grid block on the coarse scale resulting in a total of 6 pseudo relative permeability curves for each grid block. In practice, however, by considering only the major flow directions and by lumping similar curves into classes, the number of curves can be reduced. The high number of relative permeability curves, results in an extensive input deck but does not increase the computing time.

In this project we are focusing on upscaling a continuous miscible gas injection process in which water is immobile. The motivation for using an upscaling methodology is to reduce the simulation run times. When planning a field development it is necessary to carry out a large number of sensitivity simulation runs in order to evaluate well spacing and production - injection strategies. By employing a suitable upscaling methodology it is possible to obtain a reduction in the computing time for a single simulation run by 2 - 3 orders of magnitude, from days to minutes.

3.2 Miscible Flow

When the injected gas or solvent is fully miscible with the reservoir oil, only one phase exists. A black oil simulation program can not distinguish between components or fractions within a single phase. Therefore, in simulating such processes, it is necessary to use either a miscible or a compositional formulation for reservoir flow. In this work we focus on the miscible simulation approach. If the injected solvent is completely miscible, i.e. only a single phase is formed over the range of pressures and temperatures present in the reservoir, then the displacement is said to be First Contact Miscible (FCM) and the residual oil saturation in a swept zone can theoretically be reduced to zero. In many cases, however, miscibility is achieved in-situ after the solvent

has contacted the oil repeatedly leading to mass transfer between the injected solvent and the oil in place. These cases are referred to as Multi Contact Miscible (MCM). The multiple contact steps between the solvent and the oil, results in a gradual transfer of components between the phases leading to full miscibility and only one phase. The transfer between the separate phases may occur by means of condensation or vaporisation or a combination of the processes. As the miscibility is obtained immediately in a first contact miscible system this requires higher pressure than for a multi contact miscibility process to develop.

An important concept related to miscible displacement is the Minimum Miscibility Pressure (MMP). At this pressure the injected gas and initial oil become Multi Contact Miscible leading to a more efficient displacement process. The determination of MMP is important when designing a gas injection project. If the injection pressure is too low, full miscibility is not achieved leading to a less satisfactory recovery. If the injection pressure is too high the cost of compressing the gas is higher than necessary.

In miscible simulation, the miscibility is controlled explicitly by one parameter from the input deck. In compositional simulation, the development of miscibility is controlled by the algorithms used for calculating phase equilibrium in a multi component system.

3.3 Numerical Dispersion

A numerical finite difference simulator such as Eclipse and Chears consider each grid block as an element in which all properties are averaged. When the injected fluid enters one side of a grid block it is immediately dispersed throughout the grid block due to the averaging of properties. Consequently the saturation of the injected fluid will be the same at the outlet as at the inlet instantaneously. This means that the injected fluid can travel through a coarsely gridded model more quickly than through a fine gridded model, resulting in front smearing and a premature breakthrough of the injected fluid. This effect is called numerical dispersion. The effect of numerical dispersion is therefore related to the ratio of gridblocks between the fine and the coarse gridded model.

In compositional simulation the effects of numerical dispersion are more severe due to the strong nonlinearities introduced from thermodynamic equilibrium calculations. The impact of numerical dispersion in compositional simulation is to mitigate the mobility and density contrasts of the fluids through mixing and thereby underestimate channeling and gravity override, and by this predict an overly optimistic recovery.

Another difficulty with compositional simulation is the computational expense of handling many hydrocarbon components and the use of flash calculations to represent the phase behavior of the fluid. Attempts to use fine grids with more geological detail combined with a detailed compositional description of the reservoir fluid may quickly lead to computational costs, too high for practical reasons. This is particularly true for full field development studies. Upscaling of compositional processes has received significant attention as it has been recognized that compositional simulation is extremely sensitive to numerical dispersion and may give very misleading results using a coarse grid.

Miscible simulation provides an attractive alternative to compositional simulation, as it is possible to account for effects of miscibility on properties such as viscosity and density through the miscibility factor, α, and the mixing factor, ω. The calculations are fast as we are only handling 3 components (4 if a free gas phase is present) and do not require flash and equilibrium calculations as is the case for compositional simulation. In the cases treated here we are considering the water to be immobile.

3.4 Historical Overview

In the following section an overview is given on the development of some of the upscaling methods that have been used in reservoir simulation.

3.4.1 Coats

One of the earlier methods for upscaling includes the Vertical Equilibrium Method by Coats et.al. [40]. In this approach it is assumed that the thickness of the reservoir is insignificant compared to the lateral extent and further that the vertical fluid distribution is dominated by gravitational and capillary forces and therefore that the fluids redistribute immediately in the vertical direction. A 3 dimensional model can then be reduced to a 2 dimensional (one layer) areal model. This method can not be used for cases where viscous forces are dominant.

3.4.2 Hearn

Hearn[19] developed a method for upscaling water flooding of layered reservoirs. The method calculates pseudo relative permeability functions from the total outlet face water saturation as each layer floods out. The method assumes constant properties of each layer and does not account for numerical dispersion.

3.4.3 Jacks

In the method proposed by Jacks et al. [39] dynamic pseudo functions were derived for x-z cross sections of the reservoir and used in a 2-dimensional areal model. In this approach, the vertical saturation distribution is developed through simulation of the fluid displacement in a vertical cross-section (x-z) model of the reservoir. Results of the cross-section simulations are subsequently processed to give depth-averaged fluid saturations and dynamic pseudo-relative permeability values for each column of blocks in the cross-section model at each output time.

3.4.4 Kyte and Berry

Kyte and Berry [6] proposed a method, similar to the method proposed by Jacks et. al, for dynamic upscaling. The pseudo curves are calculated from vertical cross section and transfers the vertical flow behavior onto the areal model. Also the model can account for differences in computing block lengths between the cross sectional and the areal model. This is done by using pore volume weighted average saturation from all the cross sectional blocks represented by the areal block.

The pseudo relative permeability functions are calculated, by Kyte and Berry, by using Darcy's law where the total phase flow rate was calculated by a summation over the fine grid blocks multiplied by an oil flow weighted average of the viscosities dividing with averaged fine grid pressures and transmissibilities.

3.1
$$\bar{k}_{ro} = -\frac{\bar{\mu}_o \sum_j q_{oj}}{\bar{T}_x \Delta\bar{\Phi}_o}$$

where $\bar{\mu}$ is an effective viscosity, $\bar{T}_x$ the average transmissibility in the x direction and $\Delta\bar{\Phi}_o$ the average pressure potential difference. The use of pressure potential difference can cause problems as it is possible for the average net flow of a phase to be in the opposite direction of the average pressure direction[22].

3.4.5 Stone

Stone [1] proposed a method where the total mobility and phase fractional flow is calculated. The pseudo relative permeability can be calculated directly from the fractional flow curve if the gravity and capillary forces are neglected. This method avoids the problems that can arise from using the average pressure in the Kyte and Berry method [7].

3.4.6 Darman

Darman et. al.[3] proposed a method for gravity dominated immiscible gas displacement. The method is based on the Kyte and Berry method and using pore volume weighted saturations. The method is found to give better results than the conventional Kyte and Berry method for high gravity cases. This is explained by using a different weighting method to calculate the average pressure potential differences.

3.4.7 Renormalization

The concept of renormalization is to replace the single upscaling step from the fine grid to the coarse grid by a series of steps which pass from the fine grid to the final coarse grid through increasingly coarser intermediate grids. This method is less time consuming than going through the upscaling in one step. Christie et. al. [10] have used the renormalization method to upscale first contact miscible WAG floods.

The work carried out in this project is based in part on the work by Christie et. al. as we have used a code which originates from their work and was further developed by a group from Los Alamos National Laboratories[10, 16] to upscale immiscible displacements.

3.4.8 Effective Flux Boundary Conditions

Wallstrom, Durlofsky et. al. proposed to use the concept of Effective Flux Boundary Conditions[16, 17, 18] for dynamic upscaling of immiscible displacements. The EFBC method takes into account the global background permeability in the upscaling simulations. This method is termed by the authors as a "quasi-global" method. First the global permeability is calculated from single phase simulations and then the "global" information is subsequently used in the upscaling of the local flow

3.4.9 Non Uniform Upscaling

Durlofsky[46] proposed a method for non-uniform upscaling where the coarse grid block sizes are dependent on the permeability of the field, i.e. highly communicating layers are discretized more finely than low permebility layers. This method upscales the absolute permeabilities only and has been reported to work very well for intermediate levels of upscaling.

3.4.10 Zhang, Sorbie

Zhang and Sorbie[2] have developed a general 2 phase simulator that can be used for simulation of both immiscible and miscible simulations. The simulator can handle non-monotonic directional relative permeability curves. While the fine grid simulations are carried out, effective properties for a coarsened grid can be calculated. The upscaling part of the code uses the method proposed by Stone to calculate relative permeability functions, based on the concept of fractional flow and the effective mobility.

3.4.11 Fayers

Fayers[7] uses a 4-component Todd Langstaff method to upscale near miscible WAG projects. In this method an omega factor for viscosity (ω_μ) and for density (ω_ρ) are found using a matching technique against the fine grid reference results. Phase behavior is included in the model by calculating equilibrium constants and compressibility factors from differential liberation data and single stage compositional flashes. One of the conclusions in this work is that for grid sizes much larger than the reference compositional model, it becomes necessary to use $\omega_\rho = 0$ and variable values for ω_μ. For smaller grid sizes a $\omega_\mu = 1$ and values of ω_ρ which decrease with the degree of gravity segregation should be used.

3.4.12 Compositional Upscaling

Upscaling of compositional processes has received significant attention as it has been recognized that compositional simulation is extremely sensitive to numerical dispersion and may give very misleading results, when carried out on a coarse grid.

α-factor approach

Barker and Fayers[20] proposed a method where the fine grid simulation results are processed to generate a set of compositional correction factors (α-

factors) for use in the coarse grid simulation model. Christie and Clifford [13] have combined the alfa factor method with a streamline simulation technique giving good results in much less time than using a conventional compositional simulator.

3.5 Our approach

The work carried out in this project is, as mentioned, based in part on the work by Christie et. al. as we have used a code which originates from their work where they used the renormalization method to upscale first contact miscible WAG floods. The code was, at a later stage, further developed by a group from Los Alamos National Laboratories[10, 16] to upscale immiscible displacements. In the work carried out by the Los Alamos group they used the Effective Flux Boundary conditions to upscale water - oil displacements with good results.

The upscaling code was received from Los-Alamos National Laboratories. As Los Alamos had used the code for upscaling immiscible displacements, the miscible part from the original WAG code had not been used and was effectively deactivated. The code was very extensive as it was integrated with the Mistress reservoir simulator in order to allow fine grid simulation, upscaling and coarse grid simulation through one workflow.

In our case we used the Chears simulator for the fine and coarse grid simulations and Renorm for the upscaling. In order to facilitate the input for Chears we separated the upscaling part from the code and modified the post processing and the output file formats to be compatible with Chears. Extensive debugging was carried out to separate the code and to activate the miscible option.

We present a systematic approach where the Todd-Langstaff formulation is used with grid specific pseudo relative permeability functions and mixing parameters, ω, which have been calculated from fractional flow curves and effective viscosity functions generated for each upscaled sub-grid using our adapted version of the Renorm upscaling software. The method is similar to the Stone method as the pseudo relative permeability curve is generated from the total mobility and fractional flow functions, calculated from the fine scale sub grid simulations. Further more we propose a concept for estimating the Todd -Langstaff mixing parameter,ω, for each coarse grid block.

In the following chapter we will give an introduction to the Todd-Langstaff miscible formulation as well as to the application that we have used the method for.

4 Upscaling of Miscible Flow

4.1 Introduction

The method used for upscaling miscible simulation is outlined here. We are concerned with the upscaling of continuous miscible gas injection process in which water is immobile and capillary forces are absent. The upscaling is carried out for 2 dimensional systems in the x-z plane. Fine grid and coarse grid simulations are carried out under influence of gravity. The upscaling simulations, however, are carried out without the effects of gravity.

For fine and coarse grid field simulation we use the Chevron in house simulator Chears. The Chears simulator has been modified to include the T-L model with pseudo relative permeability curves and a local grid-specific mixing factor, ω.

First an introduction is given to the miscible flow formulation of Todd and Langstaff [21] and subsequently it is explained how we use the method for upscaling miscible flow through a highly heterogeneous medium.

4.2 Todd Langstaff Miscible Flow Formulation

The miscible formulation can be regarded as an extension of the Black-Oil formulation, using mixing rules to determine effective fluid properties and effective relative permeability curves. The miscible formulation was first proposed by Todd and Langstaff in 1972. They defined effective properties as functions of the empirical parameter omega, ω. The ω parameter takes a value between 0 and 1 and is used to controll physical dispersion by e.g. accounting for the effects of the heterogeneity of the porous media on the mixing of the injected fluid with the reservoir fluids. If for example a high permeability zone between injector and producer exists, this zone would favour channelling of the injected fluid and therefore result in poor mixing of the fluids. In a system which is more homogeneous the injected fluid would disperse leading to a more effective mixing than in the channel case. By setting omega equal to 1 we are assuming a fully homogeneous system where the fluids are fully mixed. If omega is set to 0 the heterogeneity is considered to promote channeling to such a degree that virtually no mixing of the in situ and injected fluids takes place.

The Todd Langstaff model was later extended to include the miscibility dependent parameter, α. The α parameter also takes a value between 0 and 1 and is used to represent the ability of the injection fluid to mix with the

reservoir oil when contacted. If α is set to 0 the fluids are treated as immiscible and the system would behave like the corresponding black oil system. Conversely if α is set to 1, the fluids are treated as first contact miscible with effective oil and solvent properties calculated according to the mixing rules specified.

If we consider a coarse grid block with sub grid heterogeneity wherein flow of solvent and oil is taking place it is necessary to describe this flow via average or effective properties. The properties that we need to define are permeability, k, relative permeability, kr, and viscosity.

The effective viscosity and relative permeability are used to account for the flow behavior of the phase-components within the coarse grid.

4.2.1 Relative Permeability

The effective relative permeability, k_{re}, in the Todd-Langstaff formulation is given by the following equation

4.1 $$k_{re} = (1-\alpha)k_{rim} + \alpha k_{rm}$$

where k_{rim} is the relative permeability function used for immiscible conditions and k_{rm} the relative permeability function used for miscible conditions. For α=1.0, the system is considered to be fully miscible and the component (oil or solvent) flow is consequently governed by straight line relative permeability functions, k_{rm}, i.e. proportional to the component concentration.

4.2.2 Viscosity

The effective viscosity is calculated by equation 4.2. The effective viscosity depends on α as well as on ω, and therefore the effective fluid properties and the effective relative permeability are coupled through α.

4.2 $$\mu_{le} = \mu_l^{(1-\alpha\omega)} \mu_m^{\alpha\omega}, \quad l = o,s$$

where the mixture viscosity, μ_m, is calculated from the quarter power law given in Eq. 4.3.

4.3 $$\frac{1}{\mu_m^{1/4}} = \frac{c}{\mu_s^{1/4}} + \frac{1-c}{\mu_o^{1/4}}$$

where c is the solvent concentration.

4.2.3 Density

The effective fluid density is calculated as follows

4.4 $$\rho_{le} = (1-\alpha\omega)\rho_l + \alpha\omega\rho_m, \quad l = o,s$$

and the mixture density from

4.5 $$\rho_m = \rho_o(1-c) + \rho_s c$$

It is seen that the mixing parameter, ω, is also used in the calculation of the effective density. One could argue that a separate mixing factor should be used for density calculations in order to account separately for gravity effects. Fayers[7] is using separate factors for density and viscosity and concludes that for grid cells much larger than the reference grids a density mixing factor of 0 should be used in connection with a non zero viscosity mixing factor.

We use the same ω-factor for both viscosity and density calculations.

4.3 Upscaling Methodology

When modelling fully miscible processes, the omega factor, ω, is the only up-scalable parameter in the original T-L formulation, as the relative permeability curves are retained as straight lines. This means that the only method available to us to incorporate sub grid heterogeneity is by adjusting the ω-factor in the interval from 1 to 0. The effect of changing the ω-factor changes the mobility of the phase via the phase component viscosity. In a highly heterogeneous system it is suggested that the fine grid flow behavior can not be adequately captured only by manipulation of the ω-factor when upscaling to a significantly coarser grid.

To capture the channelling effects that results from adverse viscosity ratios and heterogeneity we propose to use pseudo relative permeability curves specified for each grid block in addition to the ω-factor. This is done by effectively eliminating equation 4.1 and instead use a pseudo relative permeability curve for each grid block. The pseudo relative permeability functions are generated from sequential fine grid simulations as illustrated in figure 4.1. The upscaling is carried out not taking gravity into account, i.e. the upscaled functions are results of heterogeneity and of mobility contrasts only. The fine and coarse grid simulations, however, are carried out with gravity.

Figure 4.1 illustrates the upscaling procedure. Sequential fine grid simulations are carried out for sub domains of the fine grid permeability field. Based on these simulations the calculation of effective properties and flow functions are carried out.

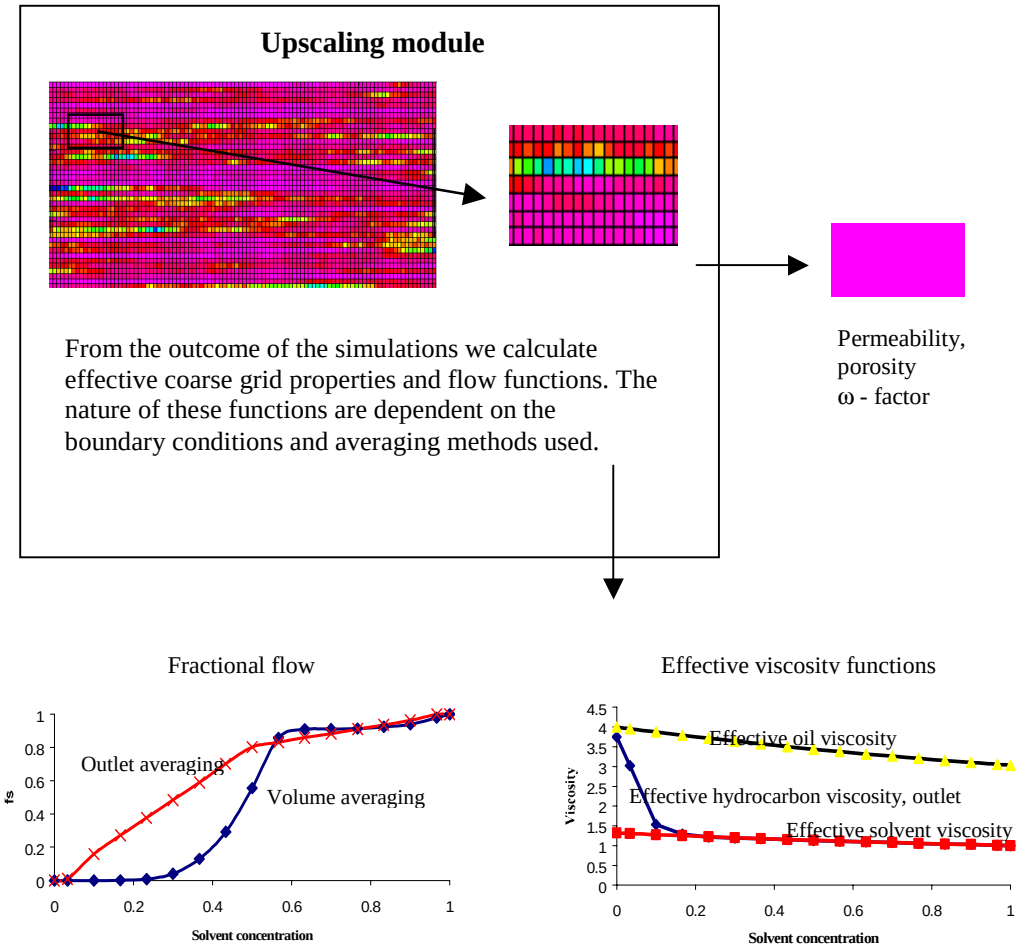

Figure 4.1: The upscaling is carried out by running successive fine grid simulations on sub domains of the fine grid permeability distribution. The outcome from these simulations are coarse grid rock properties and flow functions. The rock properties are permeability and porosity. The flow functions generated are fractional flow and effective hydrocarbon viscosity (eq. 4.11). The flow functions are dependent upon the boundary conditions and the averaging schemes used to associate the solvent concentration with the flow functions. The concentration averaging schemes can be either volume averaging or outlet averaging. If the ω-factor = 1.0 then the effective oil viscosity and the effective solvent viscosities become the same and equal to the 1/4 power law mixture viscosity (eq. 4.3).

As seen from the flow chart in figure 4.1, the dynamic upscaling gives, for each coarse grid block, a fractional flow curve, an effective hydrocarbon viscosity curve and a mixing parameter, ω as functions of chosen boundary conditions and concentration averaging method. Based on this we can calculate coarse grid pseudo relative permeability functions as input for the reservoir simulation, as outlined in the following sections.

Calculations of fluid properties are carried out in the same manner as in the original T-L formulation. In simulating fully miscible processes, one can use straight-line relative permeability in fine grid simulations and use pseudo relative permeability curves for coarse grid simulations. Thus, we have two up-scalable parameters, ω and the pseudo relative permeability functions. We use ω to ensure the correct injectivity and pressure drop across the grid block and the pseudo relative permeability to obtain correct fractional flow.

4.4 Boundary Conditions and Concentration Averaging

When carrying out dynamic upscaling the effective properties and flow functions are generated from sequential fine grid simulations on the sub domains corresponding to a coarse grid block. The outcome of the simulations are dependent on the boundary conditions applied for the simulations and on the method used to average the concentrations that the effective properties are dependent on.

4.4.1 Introduction

The boundary conditions most frequently used, have been a constant pressure or a constant pressure gradient at the grid inlet and a constant pressure at the grid outlet while the boundaries parallel to the flow direction are assigned to be no-flow boundaries. One potential drawback with this type of boundary conditions is that these do not include any effects that the surrounding flow field may have on the resultant flow through this particular block, i.e. we are trying to estimate a local flux without knowing the global solution. This is sometimes termed a "local" upscaling technique. Different upscaling methods can be grouped by to what extent they include global information. Using a "global" method, the local flow functions and parameters are estimated from the fine grid solution. This in itself does not lead to a reduction in computational expense for a single run but can be very useful in cases where the pseudo functions can be used to carry out sensitivity studies without re-calculating the pseudos**.** Between the "local" and "global" methods a number of "quasi-global" and "quasi-local" methods exist where more or less advanced methods are used to incorporate information from the surroundings.

The Effective Flux Boundary Conditions (EFBC) [16, 17, 18] proposed by Wallstrom et. al., have been used to upscale immiscible displacement processes with good results. The EFBC method takes into account the global background permeability in the upscaling simulations. This method is termed by the authors as a "quasi-global" method. First the global permeability is calculated from single phase simulations and the "global" information is subsequently used in the upscaling of the local flow.

The coarse grid effective flow functions, fractional flow and effective mobility, are calculated from the fine grid flow and total mobility at the outlet face. As the effective flow functions are functions of saturation it is important how we calculate the saturations that these functions are assigned to. Kyte and Berry [6] introduced a total pore volume weighted averaging scheme in which the saturations are averaged over all the fine grid blocks within the sub-grid. One of the benefits of the pore volume weighted averaging method is that it controls numerical dispersion, in that phase flow is not allowed through the block until a certain "critical" saturation has been reached.

It has been argued[10], that the total pore volume weighted method gives compounding errors when using the renormalization technique for upscaling and in fact overcompensates for numerical dispersion and therefore an outlet averaging method was used. In the paper, previously mentioned, by Wallstrom et. al., the saturations were also calculated using an outlet volume weighted method.

We compare results using pseudo functions calculated from the Effective Flux Boundary Conditions with outlet averaged concentrations to results from pseudo functions based on a constant pressure gradient at the inlet and a constant pressure at the outlet and volume weighted averaged concentrations. We term these conditions as Effective Flux Boundary Condition (EFBC) and Standard Boundary Conditions (STBC) respectively. The results obtained by using pseudo functions are also compared to a system where only the absolute permeability distribution have been upscaled and a global omega factor is used to account for sub grid heterogeneity.

4.4.2 Methods for Calculating Saturation / Concentration

The pore volume weighted method proposed by Kyte, averages over the entire sub-grid volume. As we compare this method to one where averaging is carried out over the outlet face it has been chosen here to term the methodologies as Volume Averaging and Outlet Averaging respectively.

The **Volume Averaging** method is given by the following equation.

4.6 $$\bar{S} = \frac{\sum_{i,j,k} S_{i,j,k} V_{i,j,k} \varphi_{i,j,k}}{\sum_{i,j,k} V_{i,j,k} \varphi_{i,j,k}}$$

where S is the saturation or concentration, V is the block volume and φ is the block porosity of grid block (i,j,k).

The **Outlet Averaging** method is given by:

4.7 $$\bar{S} = \frac{\sum_{j,k} S_{j,k} V_{j,k} \varphi_{j,k}}{\sum_{j,k} V_{j,k} \varphi_{j,k}}$$

It is seen that the only difference between the two methods is that for the Volume Averaging method, the saturation is averaged for all the grid blocks within the sub domain, while for the Outlet Averaging method the summation is only over the outlet face.

When using the Outlet Averaging method for saturations, this means that coarse grid phase flow is allowed to pass through immediately without numerical compensation for the grid block size. The impact of this is dependent on the number of coarse grid blocks in the flow direction. If the number is sufficiently large on the coarse scale, the numerical dispersion may not significantly change the simulation results. In cases where the upscaling is significant the outlet averaging may lead to breakthrough much too early.

The following figures illustrate qualitatively the difference of the two averaging methods.

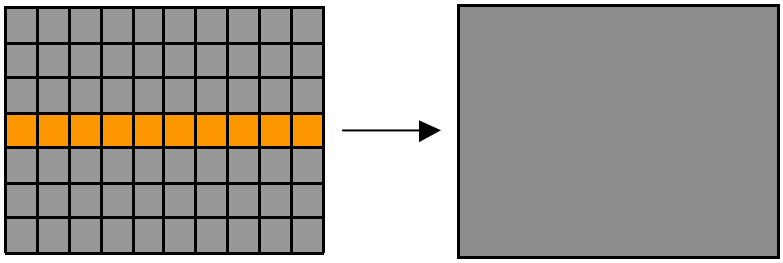

Figure 4.2: The fine grid block contains a high permeability streak which must be incorporated on the simulation scale.

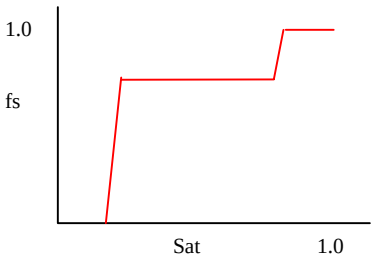

Figure 4.3.a

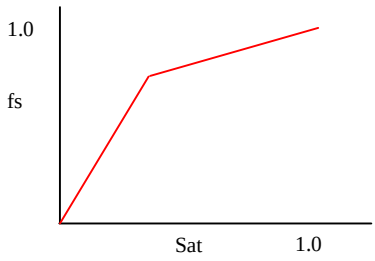

Figure 4.3.b

Figure 4.3: Qualitative flow behavior of an upscaled coarse grid using Volume Averaging 4.3.a and Outlet Averaging 4.3.b respectively. It is seen that the fractional flow function of figure 4.3.b allows flow of solvent to pass through the block immediately while the Volume averaged fractional flow curve 4.3.a requires a certain critical saturation before the phase becomes mobile.

4.4.3 Boundary Conditions

The boundary conditions that we will discuss here are for the boundaries orthogonal to the flow direction, i.e. the same boundaries at which flow enters and exits. All other boundaries are in this context parallel to the flow direction and are assigned no flow boundaries.

The boundary conditions that we have used are

1) **Standard Boundary Conditions,** which uses a constant pressure gradient at the inlet and constant pressure at the outlet. This method is a local upscaling technique which does not account for the effect of the surrounding flow field.

When using a constant pressure gradient at the inlet, the flux becomes proportional to the block permeability as follows:

4.8 $$q_{in} \approx k_x$$

2) **Effective Flux Boundary Conditions**, has been termed a quasi-global upscaling technique. The method scales the local flux by the background, global flux and permeability.

When using the Effective Flux Boundary Conditions, the flux of an inlet or outlet cell is scaled by the background permeability of an infinite medium in which the subgrid is imbedded. The permeability of the infinite medium is taken to be the effective permeability of a selected subdomain of the actual medium. In the cases considered here the effective background permeability is calculated from single phase simulations over the entire fine grid permeability domain.

The inlet flux q_{in} for a fine grid block using the effective flux boundary conditions is proportional to the following expression:

4.9 $$q_{in} \approx d \frac{k_x}{k_x + (d-1)k_0} q_0$$

where k_x is the block permeability in the x direction, k_0 is the background permeability of the medium and d is the number of dimensions. q_0 is The background flux calculated from single phase simulations on the fine grid.

It is seen that when k_0 is approaching infinity the flux through the local grid approaches zero and when the background permeability goes towards 0, the flux converges to $d*q_0$, i.e. for a two dimensional case the maximum inlet flux for any sub grid is 2 times the back ground flux.

4.5 Fractional Flow and Effective Properties

The solvent fractional flow curve and effective hydrocarbon viscosity are calculated by performing fine grid simulations on a sub-grid using appropriate boundary conditions. By setting the fine grid fractional flow equal to the coarse grid fractional flow, pseudo relative permeability curves can be found

for each coarse grid. The pseudo relative permeability curves can be used as region specific curves in Chears via the modified miscible formulation. The procedure for derivation of the resulting pseudo relative permeability curve and ω-factor is given below.

If we consider a miscible displacement where the fine grid is sufficiently fine to capture the heterogeneity, the solvent fractional flow can be calculated from the following expression, i.e. the solvent fractional flow is the ratio between solvent flow and the total flow at the grid block outlet.

4.10 $$f_s = \frac{q_s}{(q_o + q_s)} = \frac{q_s}{q_t}$$

The fractional flow function is calculated on the fine scale by summation over the sub-domain outlet.

The fractional flow function is related to the concentration by using a volume averaging or an outlet averaging scheme as outlined in section 4.4.1

4.5.1 Effective Viscosity

The effective viscosity is defined as the ratio between a summation of outlet permeabilities and the outlet mobilities. The mobility of a fine grid block is defined as $\lambda = k_{xi} / \mu_{mi}$, where k_{xi} is the permeability of the ith grid block on the outlet face of the sub-domain and μ_{mi} is the corresponding mixture viscosity calculated from the quadratic mixture rule, equation 4.3

The effective hydrocarbon viscosity is calculated as

4.11 $$\mu_{he} = \frac{k_{xi}}{k_{xi} / \mu_{mi}}$$

where summation is carried out over the outlet face of the simulation grid. If we consider a heterogeneous grid block where the solvent breaks through

early the pressure drop across this grid block is controlled by the solvent viscosity. In an up-scaled grid we could use an effective viscosity in order to obtain a correct pressure gradient across the cell. However the simulators that we use can not handle grid specific viscosity functions. Instead the Todd Langstaff mixing rules can be used with a grid block specific mixing parameter, ω.

The effective hydrocarbon viscosity function is related to the concentration in the same manner as the fractional flow functions, by using either a volume averaging or an outlet averaging scheme.

In the following sections the method for calculating the pseudo relative permeability function and evaluation of the ω-factor is outlined.

4.6 Calculation of Pseudo Relative Permeability Functions

On the coarse scale the solvent and oil flow can be expressed as follows

4.12 $$q_s = \frac{\bar{k}k_{rs}}{\mu_{se}}\nabla\bar{p} \qquad q_o = \frac{\bar{k}k_{ro}}{\mu_{oe}}\nabla\bar{p}$$

and the total flow by

4.13 $$q_t = \frac{\bar{k}}{\mu_{he}}\nabla\bar{p}$$

An alternative expression for the effective hydrocarbon viscosity is thus seen to be:

4.14 $$\frac{1}{\mu_{he}} = \frac{k_{rs}}{\mu_{se}} + \frac{k_{ro}}{\mu_{oe}}$$

The fractional flow for solvent and oil in the coarsened grid cell can be expressed by the following equations.

4.15 $$f_s = \frac{q_s}{q_s + q_o} = \frac{q_s}{q_t} = \frac{k_{rs}\mu_{he}}{\mu_{se}}$$

and

4.16 $$f_o = \frac{k_{ro}\mu_{he}}{\mu_{oe}} = 1 - f_s$$

where k_{rs} and k_{ro} , can be regarded as a solvent and oil pseudo relative permeability functions respectively. Rearranging equation 4.15 and 4.16 the following expressions for pseudo relative permeability is obtained.

4.17 $$k_{rs} = \frac{f_s\mu_{se}}{\mu_{he}} = \frac{f_s\mu_s^{(1-\omega)}\mu_m^{(\omega)}}{\mu_{he}}$$

and

4.18 $$k_{ro} = \frac{(1-f_s)\mu_{oe}}{\mu_{he}} = \frac{(1-f_s)\mu_o^{(1-\omega)}\mu_m^{(\omega)}}{\mu_{he}}$$

In the above equations it is seen that in order to calculate the correct relative permeability curves we need the fine grid fractional flow curve, the effective hydrocarbon viscosity curve and the mixing parameter, ω. The fractional flow and the effective viscosity curves are obtained from the fine grid simulation through equations 4.6 and 4.11. The ω-factor is evaluated from the effective hydrocarbon viscosity. It is seen from equations 4.17 and 4. 18 that when the mixing parameter $\omega = 1$, the block is homogeneous and consequently $\mu_{he} = \mu_m$ and the $k_{rs} = f_s$ and $k_{ro} = f_o$. When ω approaches 0, the block is heterogeneous to such a degree that virtually no mixing takes place and therefore the effective hydrocarbon viscosity, μ_{he}, rapidly approaches the effective solvent viscosity, μ_{se}, after the solvent breaks through. For a highly heterogeneous block the solvent will break through at a low block saturation (concentration) and it is seen from equation 4.17 that in the limit where $\mu_{he} = \mu_{se}$ the k_{rs}

function will be equal to the f_s function. When $\mu_{he} > \mu_{se}$ then the solvent relative permeability will always be lower than the solvent fractional flow ($k_{rs} < f_s$).

For the oil relative permeability, k_{ro}, it is seen that when the effective hydrocarbon viscosity approaches the effective solvent viscosity then the oil relative permeability, k_{ro}, may increase above unity, dependent on the viscosity ratio between oil and solvent, and the solvent fractional flow function (i.e. of heterogeneity).

In the following two sections, 4.6.1 and 4.6.2 examples are given of pseudo relative permeability functions calculated by equations 4.17 and 4.18 under the following conditions.

- Standard boundary conditions with volume averaged concentrations (bc0va)
- Effective Flux boundary conditions with outlet averaged concentrations (bc2oa)

4.6.1 Standard Boundary Conditions w. Volume Averaging

Fractional Flow

Figure 4.4 shows an example of the fractional flow for oil and solvent function using Standard Boundary conditions and Volume averaging (bc0va). It is seen how the volume averaging compensates for numerical dispersion by not allowing solvent flow until a critical concentration of 0.25 has been reached.

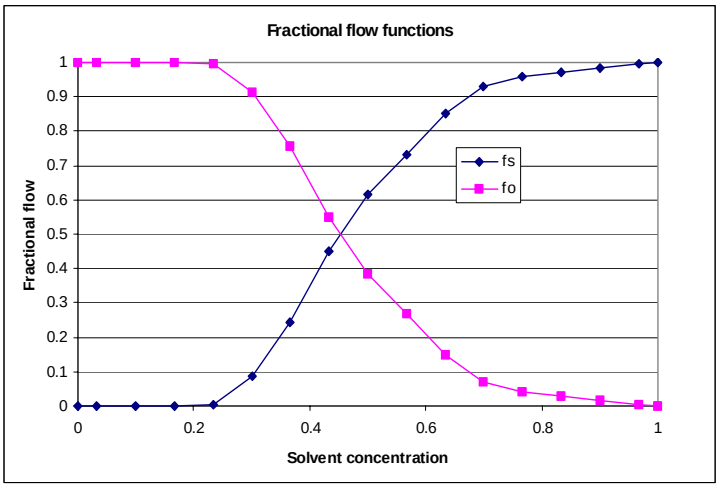

Figure 4.4: Fractional flow curves using Standard boundary conditions and volume averaging.

Effective Viscosity

Figure 4.5 shows the effective oil and solvent viscosities calculated from equation 4.2 with an ω-factor of 0.2 together with the effective hydrocarbon viscosity and the 1/4 power mixture viscosity functions calculated from equations 4.11 and 4.3 respectively.

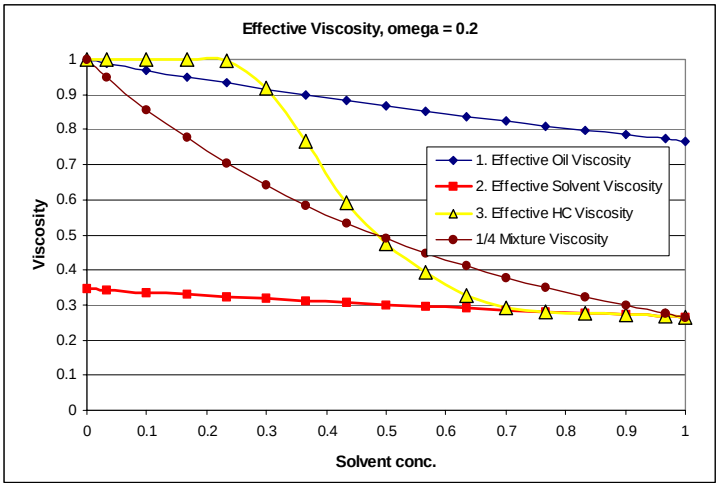

Figure 4.5: The figure shows the effective solvent, oil and hydrocarbon viscosities and the 1/4 mixture viscosity. The effective hydrocarbon viscosity is calculated for volume averaged concentrations.

Pseudo Relative Permeability

Figure 4.6 shows the resultant pseudo relative permeability functions calculated on basis of the above fractional flow curves and effective viscosity curves and an omega factor of .2 at a viscosity ratio of 3.75. It is seen that the oil relative permeability curve decreases monotonically due to the effective oil viscosity being lower than the effective hydrocarbon viscosity at concentrations up to 0.3.

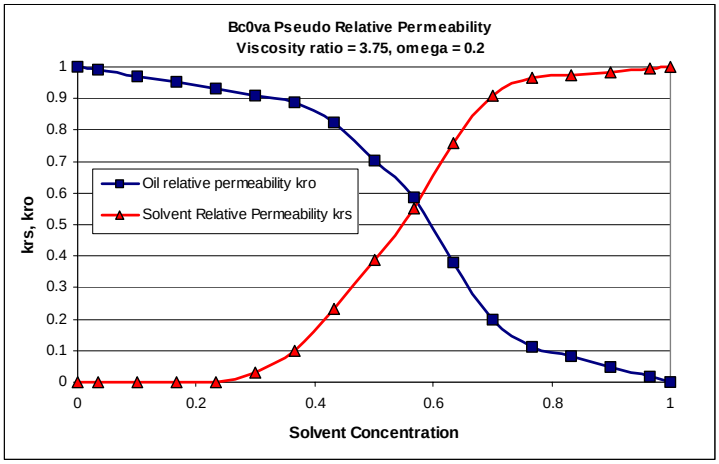

Figure 4.6: Pseudo relative permeability function for a specific grid block calculated from dynamic upscaling using the standard boundary conditions and volume averaging (bc0va) with a viscosity ratio of 3.75 and an ω-factor of 0.2.

4.6.2 Effective Flux Boundary Conditions w. Outlet Averaging

Fractional Flow

Figure 4.7 shows an example of the fractional flow for oil and solvent function using Effective Flux Boundary Conditions and Outlet averaging (bc2oa). It is seen that the Outlet averaging does not compensate for numerical dispersion and that solvent is allowed to flow out of the block at very low concentrations.

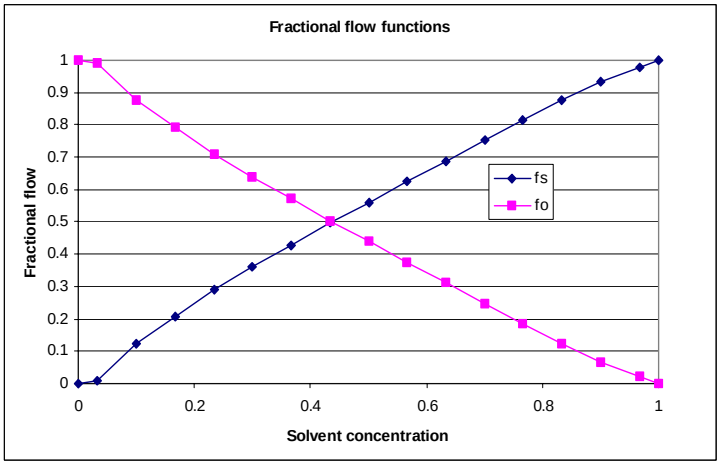

Figure 4.7: Fractional flow curves using Effective Flux boundary conditions and outlet averaging.

Effective Viscosity

Figure 4.8 shows the effective oil and solvent viscosities calculated from equation 4.2 with an ω-factor of 0.2 together with the effective hydrocarbon viscosity and the 1/4 power mixture viscosity functions calculated from equations 4.11 and 4.3 respectively.

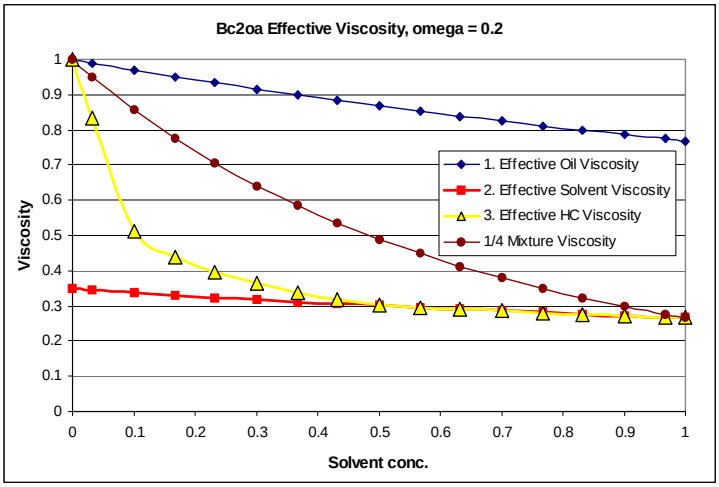

Figure 4.8: The figure shows the effective solvent, oil and hydrocarbon viscosities and the 1/4 mixture viscosity. The effective hydrocarbon viscosity is calculated for outlet averaged concentrations..

Pseudo Relative Permeability

Figure 4.9 shows the resultant pseudo relative permeability functions calculated on basis of the above fractional flow curves and effective viscosity curves and an omega factor of .2 at a viscosity ratio of 3.75. It is seen that the oil relative permeability curve exhibits a non-monotonic behavior increasing to 1.7 at a concentration of 0.17 before decreasing with increasing concentrations.

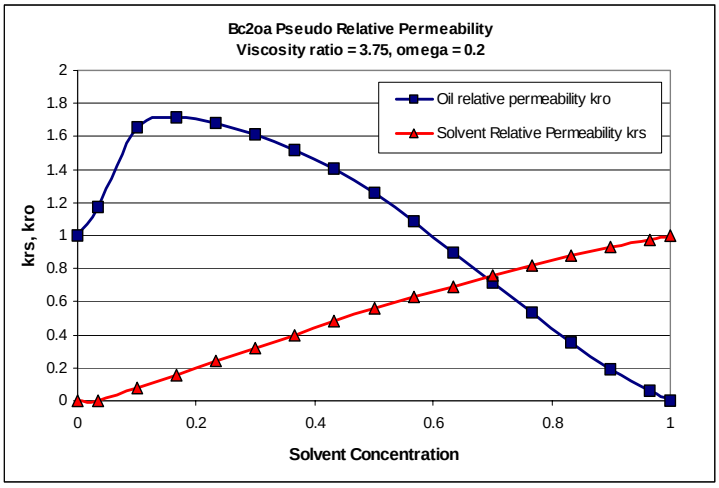

Figure 4.9: Pseudo relative permeability function for a specific gridblock calculated from dynamic upscaling using the Effective Flux boundary conditions and outlet averaging (bc2oa) with a viscosity ratio of 3.75 and an ω-factor of 0.2.

4.6.3 Non-Monotonic Relative Permeability Functions

From equations 4.17 and 4.18 it is seen that the pseudo solvent relative permeability function, k_{rs}, will be equal or less than the corresponding fractional flow curve f_s. If k_{rs} increases above f_s this will be caused by an incorrect ω-factor. The pseudo oil relative permeability function, k_{ro}, may increase above 1.0 depending on the ratio between μ_{he} and μ_{oe}. The Chears simulator is capable of handling non-monotonic relative permeability functions in the miscible option.

4.7 The ω-Factor

The effect of changing the ω-factor is illustrated in the following 2 figures. Curve 1 and 2 illustrates the effective oil and solvent viscosities as calculated by equation 4.2. Curve 3 is the effective hydrocarbon viscosity as calculated by equation 4.11 and curve 4 is the quarter power mixing rule viscosity from equation 4.3. It is seen that the effective hydrocarbon viscosity is very close to the effective solvent viscosity in the saturation range between 0.5 and 1.0. in figure 4.2 where ω is set to 0.2. In figure 4.3 where we have introduced a higher degree of mixing by increasing the ω-factor to 0.8 it can be seen that the effective solvent viscosity and the effective hydrocarbon viscosity do not match. It is proposed that the similarity of the effective solvent curve and the

effective hydrocarbon viscosity curve can be used to evaluate the omega factor. This can be carried out by adjusting the ω-factor until a satisfactory match is obtained between the effective solvent and hydrocarbon curve.

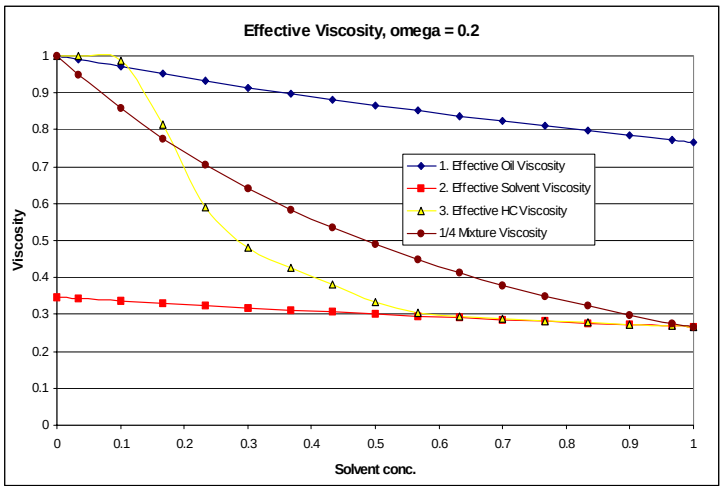

Figure 4.10: Effective viscosity with the ω-factor = 0.2

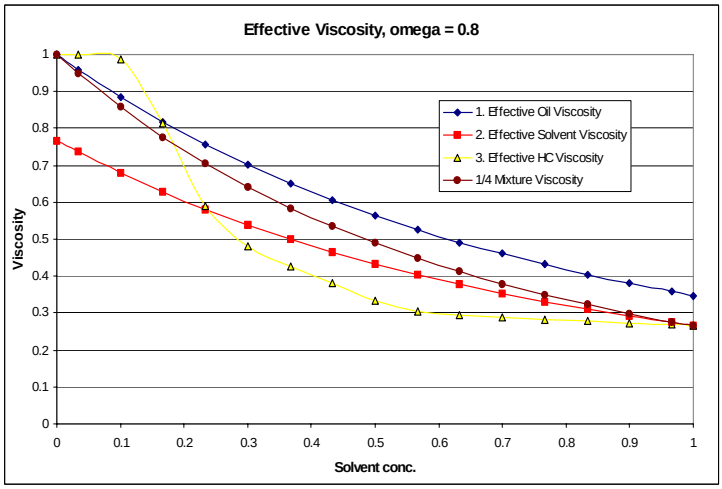

Figure 4.11: Effective viscosity with the ω-factor = 0.8

4.8 Evaluation of the ω Factor

As ω is a value representing the degree of heterogeneity it is suggested that this value may be derived implicitly from the sub-domain fine grid simulations resulting in one specific omega value for each coarse grid block of the system.

Assuming that the effective hydrocarbon viscosity rapidly becomes similar to the effective solvent viscosity, omega can be estimated from the following relation.

4.19 $$\mu_{he} = \mu_{se} = \mu_s^{(1-\omega)} \mu_m^{\omega}$$

we can use the above relation to estimate the ω-factor at a certain solvent concentration where the best match is obtained between the effective hydrocarbon viscosity curve and the effective solvent viscosity curve. As it can be a complex task in itself to match the effective solvent viscosity curve to the effective hydrocarbon viscosity curve in order to find the optimum omega factor for each coarse grid-block, we have chosen to use the following simple procedure.

At a solvent concentration of 0.57 the omega factor has been calculated by rewriting equation 4.19 as follows:

4.20 $$\omega = \frac{\log(\mu_{he} / \mu_s)}{\log(\mu_m / \mu_s)}$$

where μ_{he} and μ_m are calculated from equations 4.11 and 4.3 respectively. It is seen that when μ_{he} is equal to μ_s, ω is equal to 0.0 and when μ_{he} is equal to μ_m, ω is equal to 1. If the μ_{he} is found to be higher than μ_m , ω is set to 1.0.

By using this procedure we obtain grid specific ω-factors evaluated on the basis of sub-grid heterogeneity indirectly through the effective hydrocarbon viscosity calculation in equation 4.11.

The choice of using 0.57 is based on the observation that at this concentration the effective hydrocarbon viscosity and the effective solvent viscosity in most cases are very close. Using this method it is possible to capture the variation of sub grid heterogeneity between the coarse grid blocks through the ω-factor. However, using the same concentration to evaluate the ω-factor for every grid

block, is not quite correct and will for highly heterogeneous blocks yield a too high ω-factor, which will slow down the solvent.

4.9 Summary

In this section we have outlined the method for calculating pseudo relative permeability functions and a local ω-factor for each coarse grid block. The calculations are carried out using Standard Boundary Conditions with Volume averaged concentrations (bc0va) as well as Effective Flux Boundary Conditions with Outlet averaged concentrations (bc2oa). In the following chapter the methodology will be tested on several examples where we compare to fine grid results and to coarse grid results where we use straight line relative permeability functions and a global ω-factor, e.g. SL-0.3 or SL-1.0, where the number refers to the ω-value chosen.

5 Case Studies

5.1 Introduction

In this section the upscaling methodology is tested on several permeability realisations of different characteristics. The systems range from a layered system through synthetic systems of varying correlation lengths to examples of real data. The objective of the test is to compare the method using the Standard Boundary conditions and the Effective Flux Boundary conditions with local mixing parameter, ω, to cases where we use straight line permeability functions and a global mixing factor, ω.

When comparing the results we look at solvent break through times, solvent production profile, average reservoir pressure and the oil saturation distribution.

The following cases for upscaling will be studied. The heterogeneity index is calculated by equation 2.13.

Name	Description	Fine grid blocks	Coarse grid blocks	Het. Index / Corr length.
L1	Layered system, 1/10 mD	100x100	10x10	1.76 / 1.0
	Layered system, 1/100 mD	100x100	10x10	28.12 / 1.0
P4	Synthetic system, short correlation lengths	100x100	10x10	2.06 / 0.25
P5	Synthetic system, long correlation lengths	100x100	10x10	3.40 / 0.7
P5	Synthetic system, long correlation lengths	100x100	5x5	3.40 /0.7
S1	Obtained from the StreamSim homepage	100x100	10x10	1.30 / 0.3
T2D	Real permeability case, long correlation lengths	243x435	9x15	4810 / 0.7
SPE10-XZ	Top XY layer of the SPE10 comparative case, used as XZ	60x220	10x11	4.5 / 0.15

5.2 Fluid System

For all the cases we have used a fluid system, related to the Chevron oil example given as oil-2 in appendix A. The fluid properties used for simulation input is given in appendix D.

The viscosity and density ratio between solvent and oil are given below.

Reservoir temperature	383 K (231 F)
Reservoir pressure	586 Bar (8500 psia)
Oil/Solvent Viscosity Ratio	3.75
Oil/Solvent Density Ratio	1.6

5.3 Well Constraints:

for all the cases the simulation has been controlled by the following constraints.

Injection Pressure	827 Bara (12000 psia)
Min production BHP	255 Bara (3700 psia)
Maximum Oil production Rate	12.72 SM^3 (80 stb/day)

An oil production of 12.72 SM^3 (80 stb/day) is associated with some 5666 SM^3/day (200 Mscf/day) of gas.

5.4 A Layered System

A layered system is difficult to upscale when combining high permeability and low permeability layers. This case is well suited for checking the efficiency and validity of the two boundary conditions + averaging scheme combinations, the bc0va and the bc2oa respectively. A layered systems becomes a homogeneous system with constant permeability when upscaled.

2 different layered systems have been upscaled using a ratio between the high permeability and low permeability layers of 10 and 100 respectively. Using a horizontal correlation length, for a layered system, of 1.0, the heterogeneity index for the 2 distributions, 1/10 and 1/100, are calculated to be 1.76 and 28.12 respectively.

The 100x100 fine grid has the following dimensions:

Fine Grid dimensions:

Number of x-direction grid blocks	100
Number of z direction grid blocks	100
x-direction grid block size	3.048 m (10 ft)
y-direction grid block size	6.096 m (20 ft)
z-direction grid block size	1.524 m (5 ft)
kz-multiplier for fine grid simulations	0.1
Porosity	0.08

The grid is upscaled to 10x10 grid blocks.

Layered System 1/100 Fine grid permeability

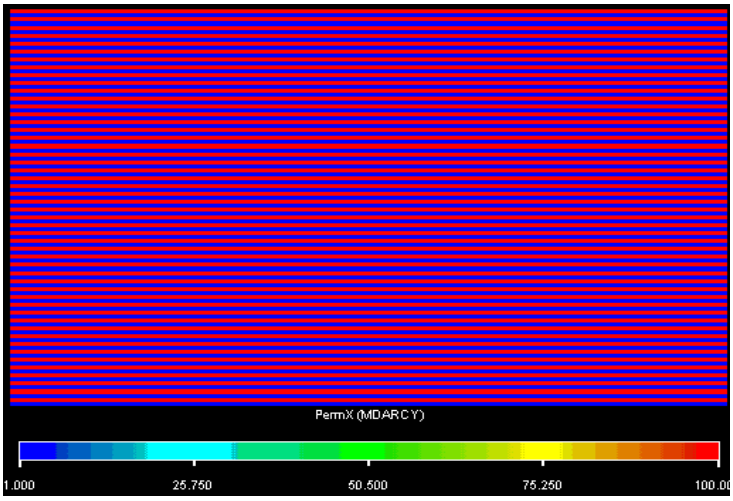

Figure 5.1: 100x100 permeability distribution for a layered systems where the layers are alternating between 1 and 100 mD. When upscaled the resultant permeability distribution becomes a 10x10 homogeneous grid with a permeability of 50.5 mD.

Layered System 1/100Fine grid oil saturation

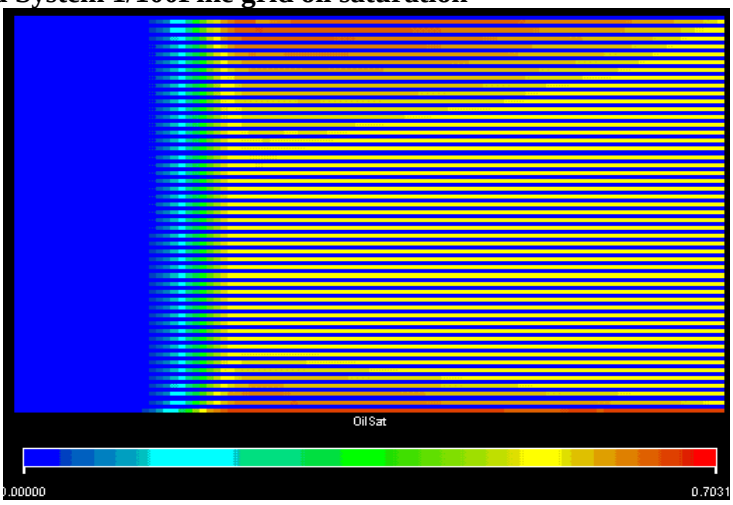

Figure 5.2: Layered system, 100x100 fine grid oil saturation after 3 months solvent injection. It is seen that the high permeability layers have been completely displaced while the low permeability layers still contain some 70 % solvent.

Coarse grid oil saturation, Standard boundary conditions w. outlet averaging (bc0va)

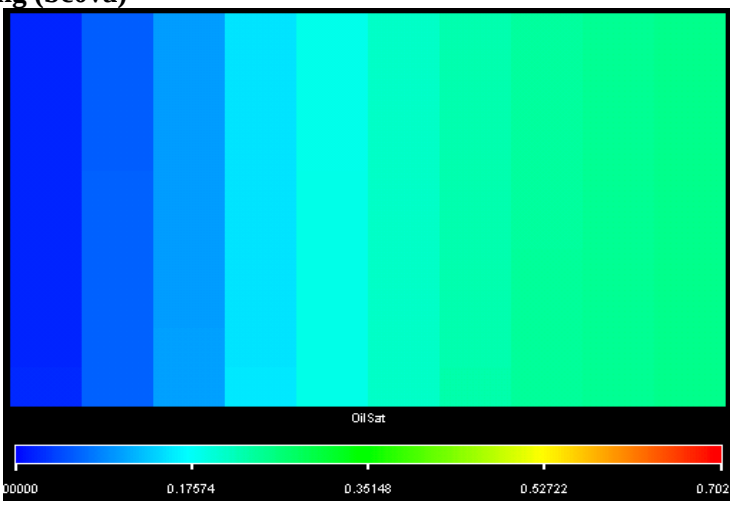

Figure 5.3: Layered system, bc0va-10x10 oil saturation after 3 months solvent injection. When comparing to the fine grid simulations it is seen that the saturation profile is quite well preserved.

Coarse grid oil saturation, Straight line functions and ω = 0.3. (SL-03)

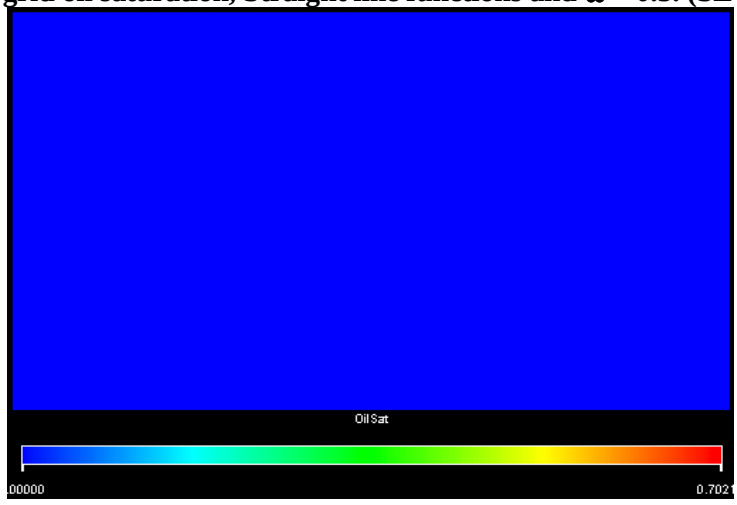

Figure 5.4: Layered system, SL0.3-10x10 oil saturation after 3 months solvent injection. It is seen that the oil has been displaced too early when using straight line relative permeability functions. This is also true if the mixing parameter is increased or if using the Effective Flux Boundary Conditions.

Layered system 1/100 oil production rate

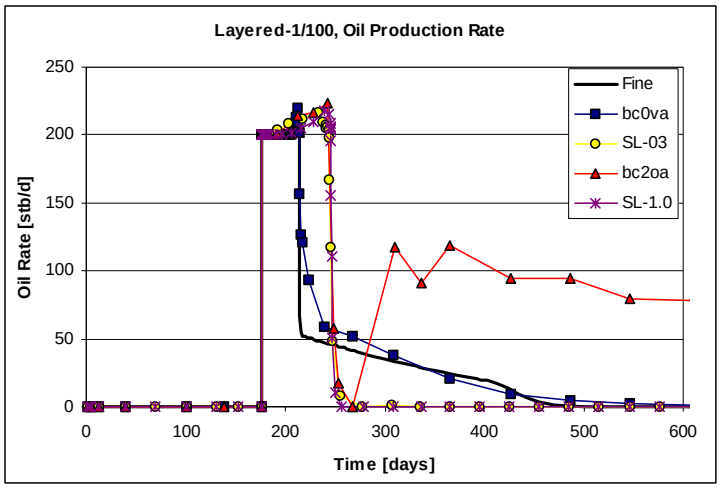

Figure 5.5: The figure compares the layered 1/100 fine grid oil production rate and the oil production rate from the upscaled model using standard boundary conditions, Effective flux boundary conditions and straight line relative permeability functions with a global mixing factor. It is seen that only the Standard boundary conditions captures the correct flow profile.

Layered system 1/100 cumulative oil production

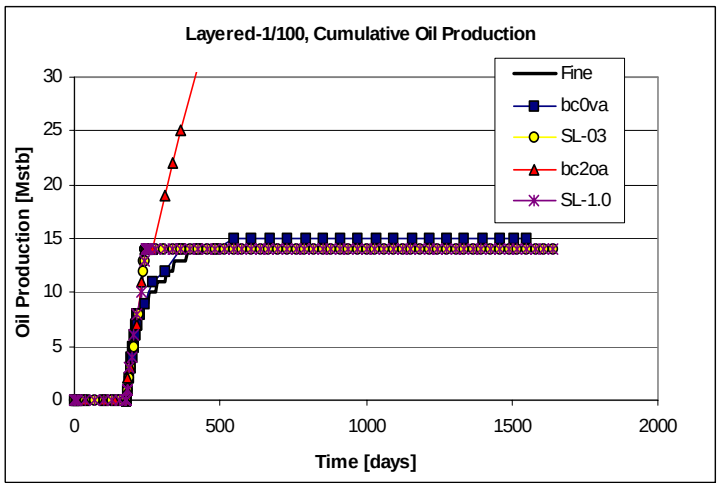

Figure 5.6: The figure compares cumulative oil production of the layered 1/100 fine and the upscaled 10x10 model using standard boundary conditions, Effective flux boundary conditions and straight line relative permeability functions with a global mixing factor. The bc2oa experiences numerical instabilities after solvent breakthrough.

Layered system 1/100 reservoir pressure

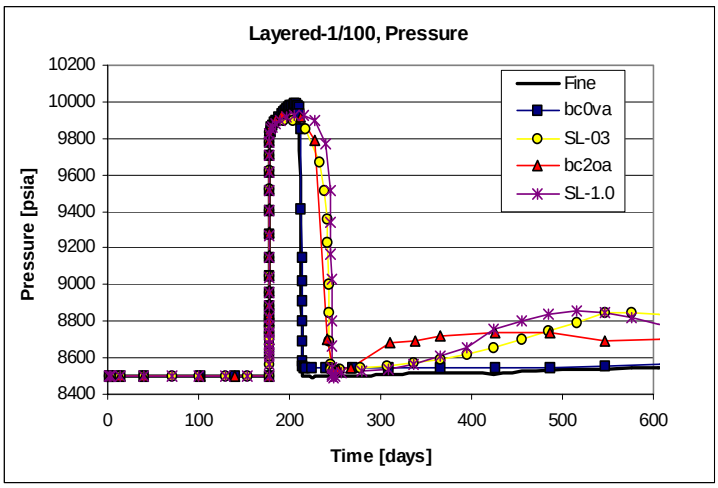

Figure 5.7. The figure compares the average pressure of the layered 1/100 fine and the upscaled 10x10 model using standard boundary conditions, Effective flux boundary conditions and straight line relative permeability functions with a global mixing factor.

Layered system 1/100 solvent production

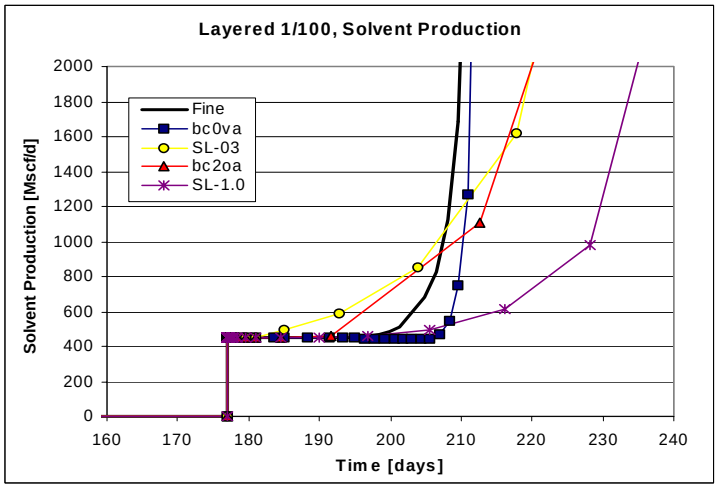

Figure 5.8. The figure compares the average pressure of the layered 1/100 fine and the upscaled 10x10 model using standard boundary conditions, Effective flux boundary conditions and straight line relative permeability functions with a global mixing factor. The bc0va captures the breakthrough and production profile quite well.

Layered system 1/10 solvent production

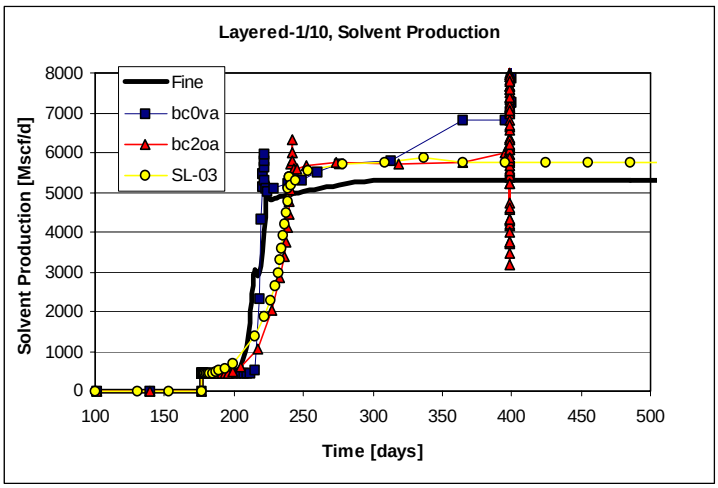

Figure 5.9. The figure compares the solvent production of the layered 1/10 fine and the upscaled 10x10 model using standard boundary conditions, Effective flux boundary conditions and straight line relative permeability functions with a global mixing factor. It is seen that the bc0va model correctly reproduces solvent production profile.

Layered system 1/10 reservoir pressure

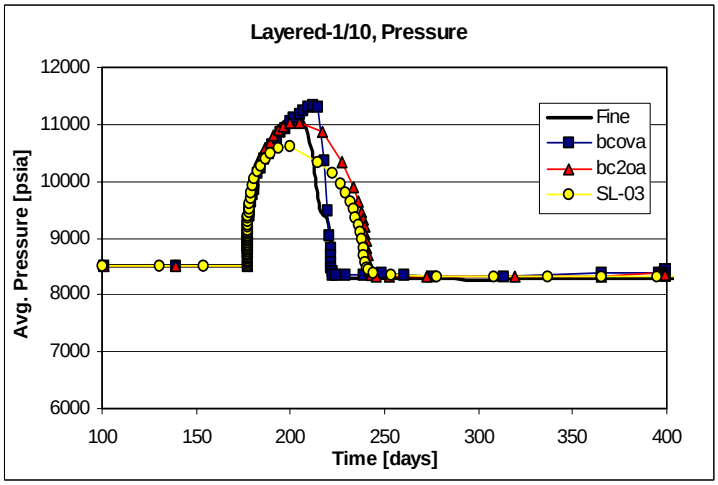

Figure 5.10. The figure compares the average pressure of the layered 1/10 fine and the upscaled 10x10 model using standard boundary conditions, Effective flux boundary conditions and straight line relative permeability functions with a global mixing factor. It is seen that the bc0va model is capable of capturing the correct pressure behavior.

5.5 2 Synthetic Cases with Varying Correlation Lengths

We have generated 2 different 2-dimensional synthetic permeability distributions, P4 and P5, for testing the sensitivity of the upscaling method and boundary conditions to the horizontal permeability correlation lengths. The fine grid permeability distributions are 100x100 grid blocks with the following dimensions and properties. The distributions have been obtained by using the SGSIM software from the Stanford GSLIB software package.

The P4 distribution has a correlation length of 0.25 and the heterogeneity index is calculated to 2.06.

The P5 distribution has a correlation length of 0.7 and a heterogeneity index of 3.40.

Fine Grid dimensions:

Number of x-direction grid blocks	100
Number of z direction grid blocks	100
x-direction grid block size	3.048 m (10 ft)
y-direction grid block size	6.096 m (20 ft)
z-direction grid block size	1.524 m (5 ft)
kz-multiplier for fine grid simulations	0.1
Porosity	0.2

The results of the simulations are shown in the following figures. It is seen that the results for the 2 distributions are quite similar. For both cases using straight lines with a global mixing parameter yields reasonable results. Matching the breakthrough time can be obtained by adjusting the mixing parameter, ω. When comparing the results for the bc0va and the bc2oa models it is seen that the bc2oa performs better for the P4 case with the shorter correlation lengths while bc0va better captures the flow behavior for the P5 distribution.

The P4 case has been upscaled to 10x10 grid blocks.

The P5 case has been upscaled to 10x10 grid blocks as well as to 5x5 grid blocks.

P4 fine grid permeability distribution

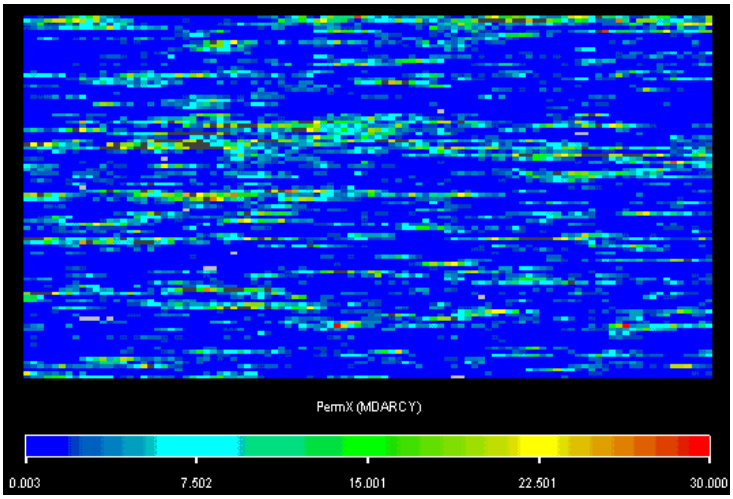

Figure 5.11. P4-Fine 100x100 permeability distribution. The horizontal correlation length is about .25 and the vertical correlation length is less than 0.1.

P4 coarse grid permeability distribution

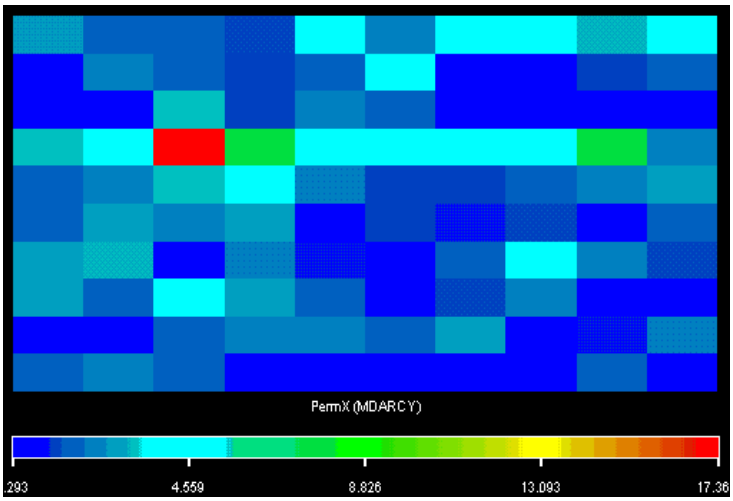

Figure 5.12. P4-Coarse 10x10 permeability distribution.

P4 fine grid oil saturation

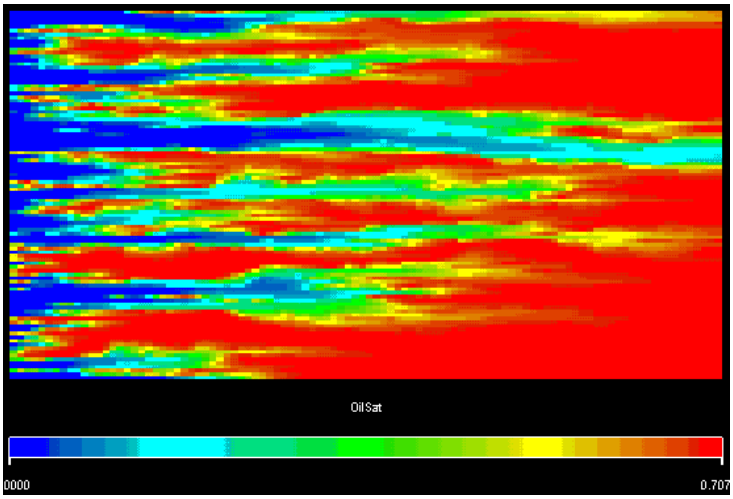

Figure 5.13. P4-Fine, Oil saturation after 1 year solvent injection.

P4 coarse grid oil saturation using standard boundary conditions and volume averaging (bc0va)

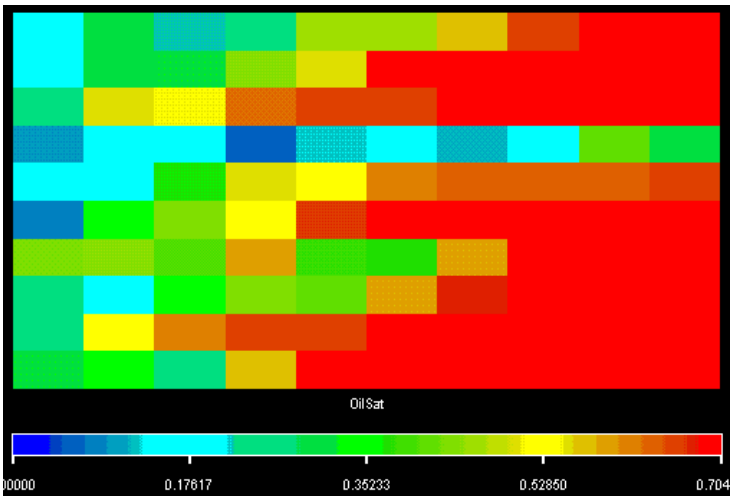

Figure 5.14. P4-bc0va, Oil saturation after 1 year solvent injection. It appears from the saturation plot that the solvent front is behind relative to the fine grid results.

P4 coarse grid oil saturation using effective flux boundary conditions and outlet averaging (bc2oa)

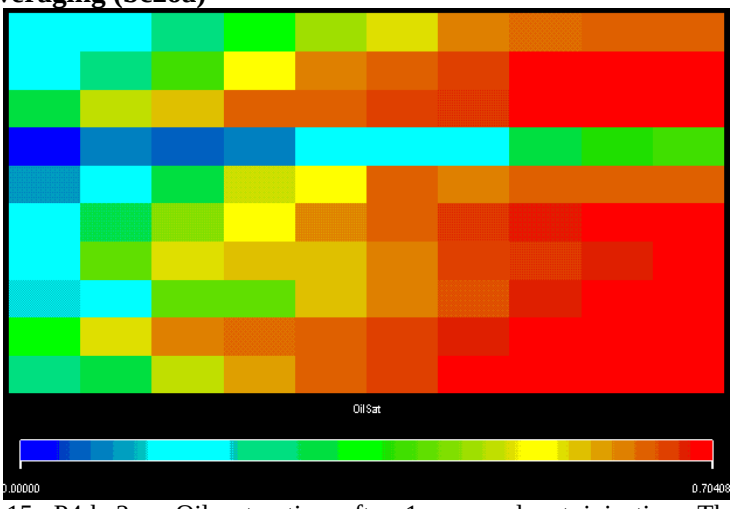

Figure 5.15. P4-bc2oa, Oil saturation after 1 year solvent injection. The solvent saturation front resembles the fine grid results quite well.

P4 coarse grid oil saturation using straight line functions and constant ω factor (SL-03)

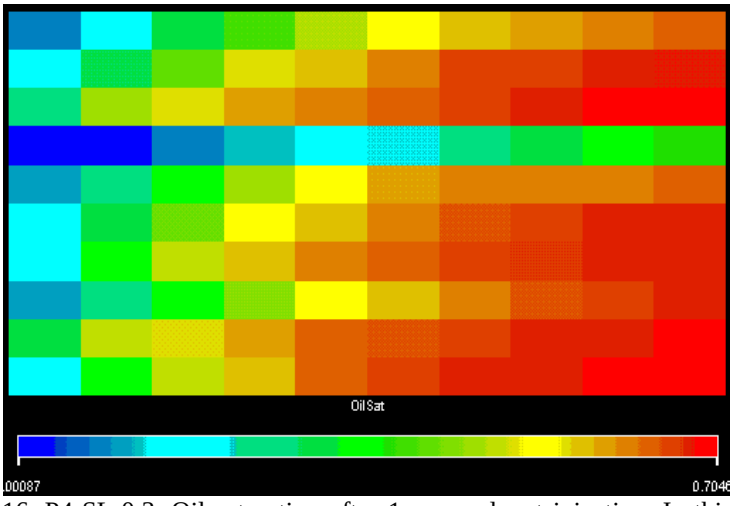

Figure 5.16. P4-SL-0.3, Oil saturation after 1 year solvent injection. In this case the solvent saturation front seems ahead of the fine grid results.

P4 reservoir pressure

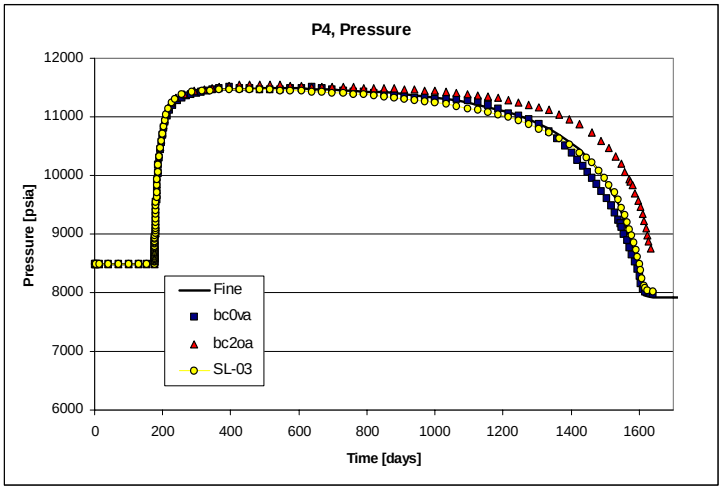

Figure 5.17. The figure compares the average pressure of the P4 fine and the upscaled 10x10 model using standard boundary conditions, Effective flux boundary conditions and straight line relative permeability functions with a global mixing factor. The pressure profile is captured very well by the bc0va and by the SL-03 conditions. For bc2oa conditions the pressure profile is slightly high at late time.

P4 solvent production

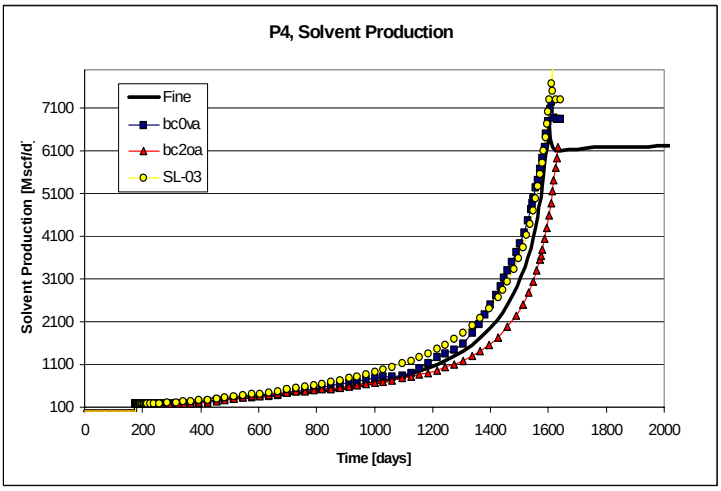

Figure 5.18-a. The figure compares the solvent production rate of the P4 fine and the upscaled 10x10 model using standard boundary conditions, Effective flux boundary conditions and straight line relative permeability functions with a global mixing factor. It is seen that bc0va and SL-03 predicts a too high solvent production at late time, while the bc2oa solvent production is too low consistent with the pressure plot above.

P4 solvent production

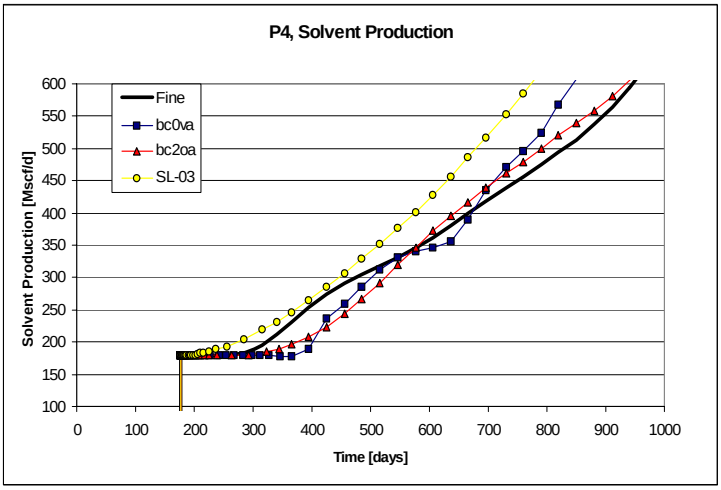

Figure 5.18-b. The figure compares the solvent production rate, at breakthrough time, of the p4 fine grid and the upscaled 10x10 model using standard boundary conditions, Effective flux boundary conditions and straight line relative permeability functions with a global mixing factor. It is seen that the bc2oa model reproduces breakthrough time very well while the bc0va predicts breakthrough about 80 days late. The SL-03 on the other hand predicts the breakthrough to occur about 100 days early.

P5 fine grid permeability distribution

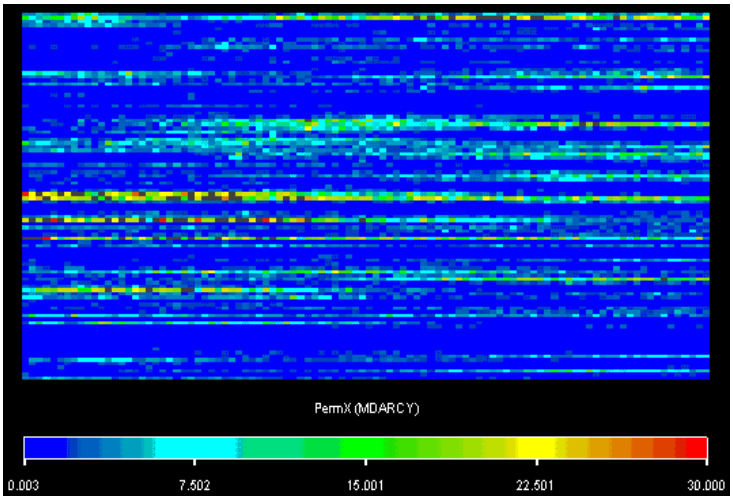

Figure 5.19. P5-Fine 100x100 permeability distribution. The horizontal correlation length is about .7 and the vertical correlation length is less than 0.1.

P5 coarse grid permeability distribution

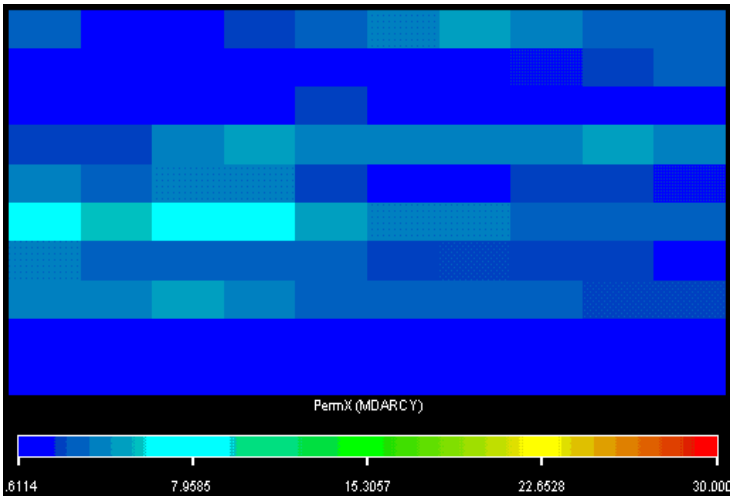

Figure 5.20. P5-Coarse 10x10 permeability distribution.

P5 fine grid oil saturation

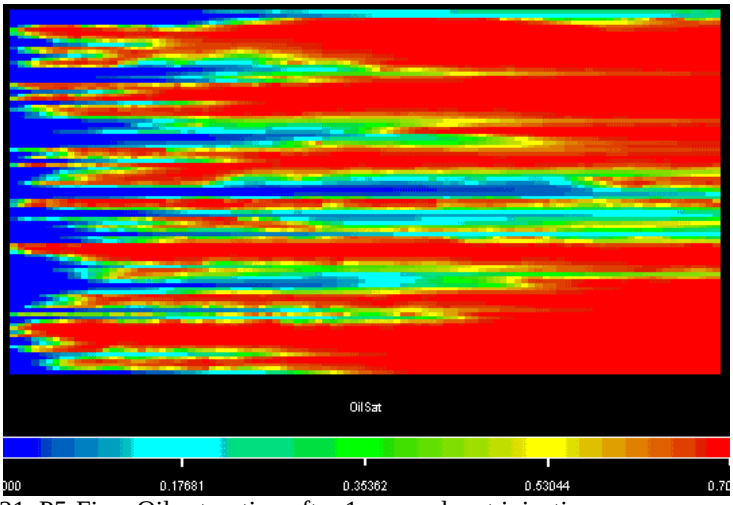

Figure 5.21. P5-Fine, Oil saturation after 1 year solvent injection.

P5 coarse grid oil saturation using standard boundary conditions and volume averaging (bc0va)

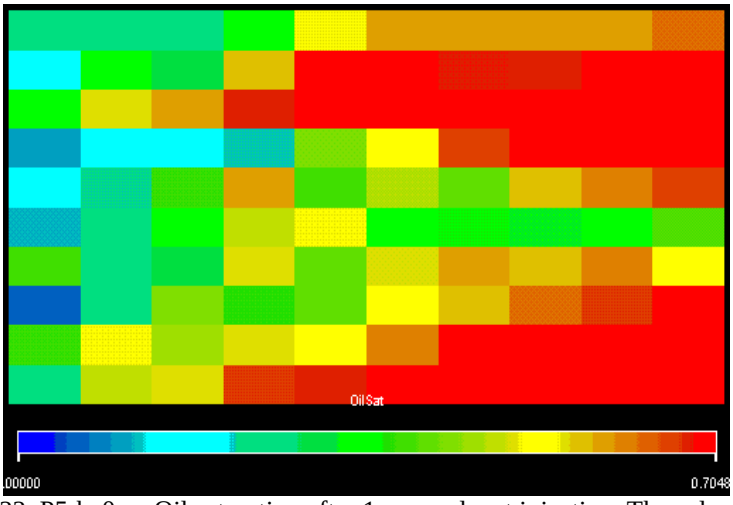

Figure 5.22. P5-bc0va, Oil saturation after 1 year solvent injection. The solvent profile matches the fine grid results very well.

P5 coarse grid oil saturation using effective flux boundary conditions and outlet averaging (bc2oa)

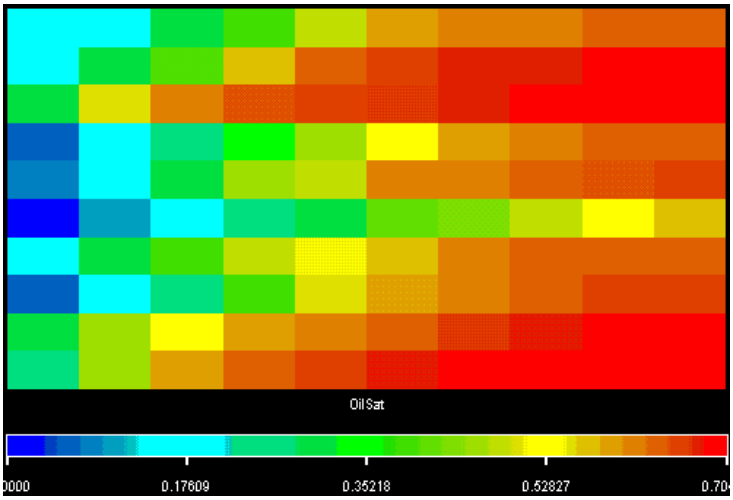

Figure 5.23. P5-bc2oa, Oil saturation after 1 year solvent injection. The solvent profile matches the fine grid results very well but appears to be more dispersed than the bc0va.

P5 coarse grid oil saturation using straight line functions and constant ω factor (SL-03)

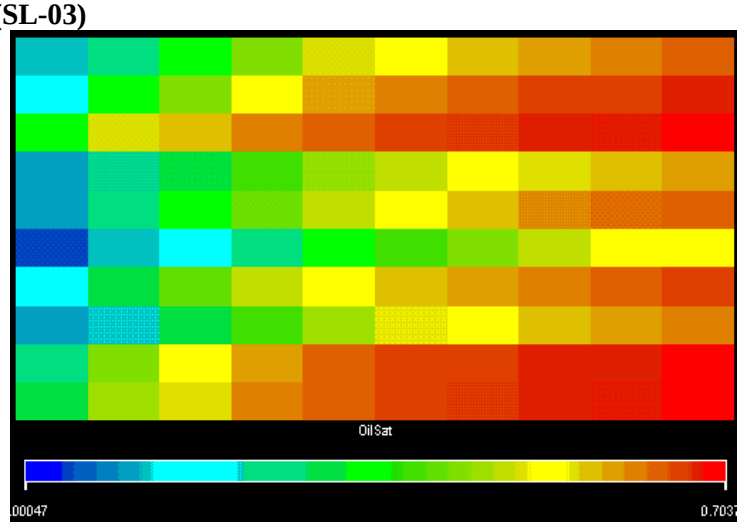

Figure 5.24. P5-SL-0.3, Oil saturation after 1 year solvent injection. The solvent front is seen to be much more dispersed compared to the fine grid results.

P5 reservoir pressure

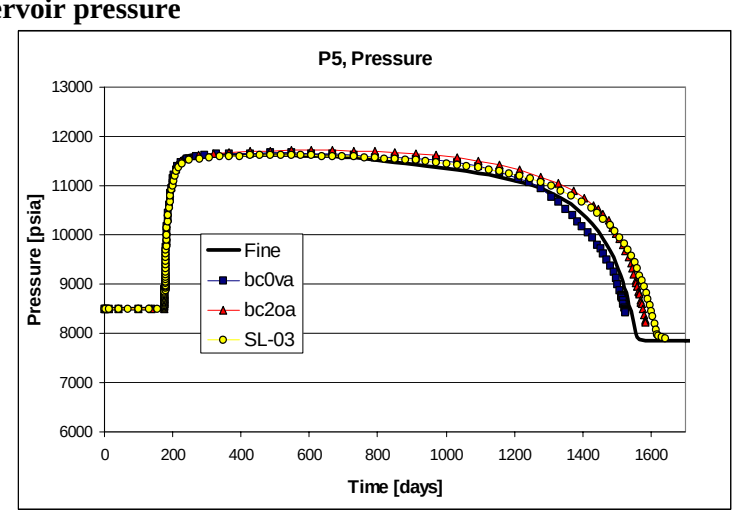

Figure 5.25. The figure compares the average pressure of the P5 fine grid and the upscaled P5-10x10 model using standard boundary conditions, Effective flux boundary conditions and straight line relative permeability functions with a global mixing factor. The bc0va conditions quite well follow the fine grid results, while the bc2oa and Sl-03 pressures are too high at late time.

P5 solvent production

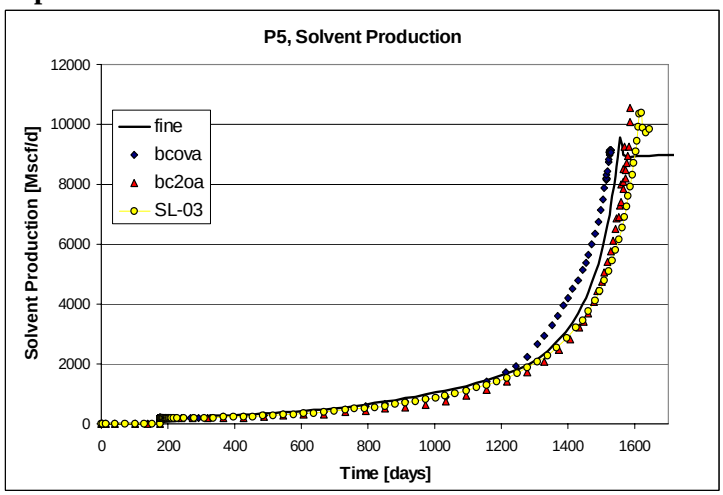

Figure 5.26-a. The figure compares the solvent production rate of the P5 fine grid and the upscaled P5-10x10 model using standard boundary conditions, Effective flux boundary conditions and straight line relative permeability functions with a global mixing factor.

P5 solvent production

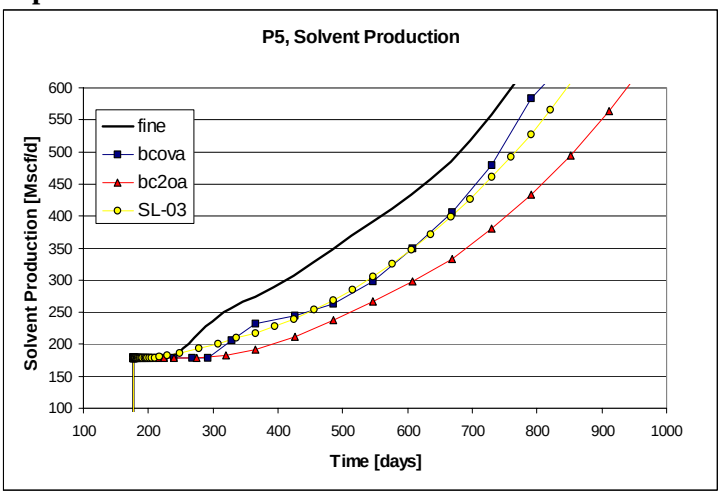

Figure 5.26-b. The figure compares the solvent production rate of the P5 fine grid and the upscaled P5-10x10 model using standard boundary conditions, Effective flux boundary conditions and straight line relative permeability functions with a global mixing factor. The bc0va and bc2oa predict a slightly late breakthrough. The bc0va profile matches the fine grid very well.

P5 5x5 reservoir pressure

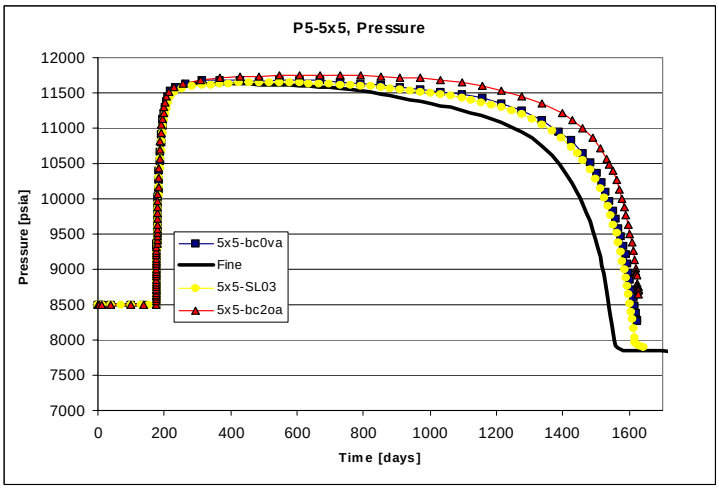

Figure 5.27. The figure compares the average pressure of the P5 fine grid and the upscaled P5-5x5 model using standard boundary conditions, Effective flux boundary conditions and straight line relative permeability functions with a global mixing factor. All 3 models predict too high pressure at late time compared to the fine grid model.

P5 5x5 solvent production

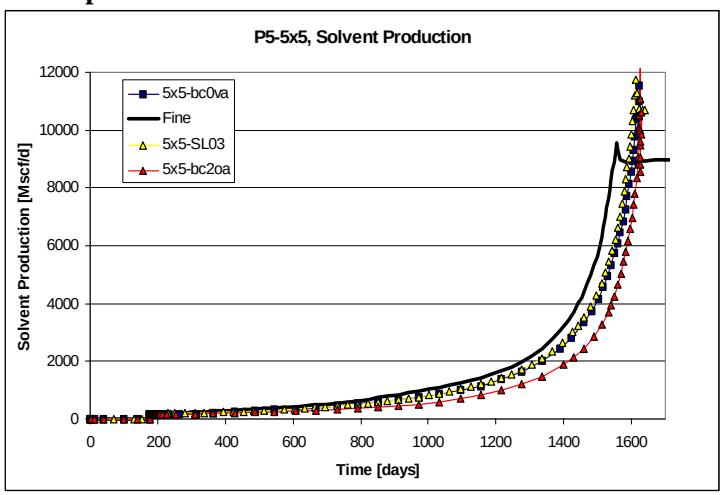

Figure 5.28. The figure compares the solvent production rate of the P5 fine grid and the upscaled P5-5x5 model using Standard boundary conditions, Effective flux boundary conditions and straight line relative permeability functions with a global mixing factor.

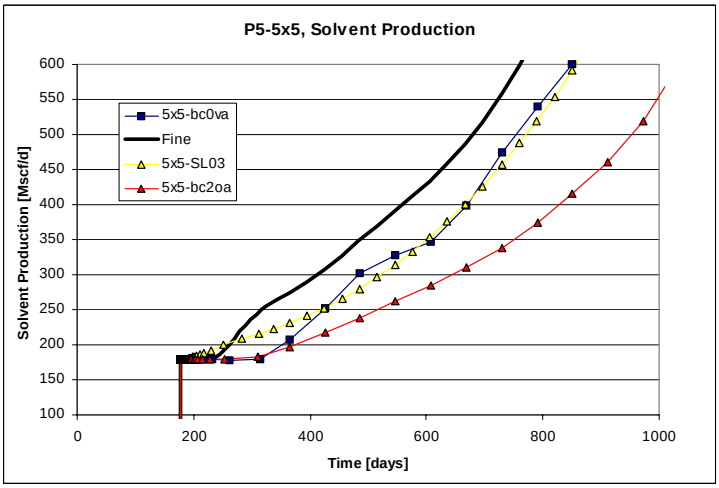

Figure 5.29. The figure compares the solvent production rate at breakthrough time of the P5 fine grid and the upscaled P5-5x5 model using Standard boundary conditions, Effective flux boundary conditions and straight line relative permeability functions with a global mixing factor. The bc0va system predicts slightly late breakthrough with a good production profile. The SL-03 predicts early breakthrough due to the dispersive features of this system.

5.6 S1 permeability distribution.

The S1 permeability distribution, given in figure 5.30, of 100x100 grid blocks is obtained from the **StreamSim** home page. Although there are 100x100 blocks, each 2 subsequent blocks are equal and therefore the permeability distribution is effectively 50x50. The fine grid simulations have been carried out on the 100x100 grid.

It is seen that the bedding is at an angle of some 30 degrees relative to the flow direction and that in the bedding direction the correlation length is about 0.5. For the flow direction we have used a correlation length of 0.3 resulting in a heterogeneity index of 1.30.

The fine grid properties are as follows:

Number of x-direction grid blocks	100
Number of z direction grid blocks	100
x-direction grid block size	3.048 m (10 ft)
y-direction grid block size	6.096 m (20 ft)
z-direction grid block size	1.524 m (5 ft)
kz-multiplier for fine grid simulations	0.1
Porosity	0.2

The grid has been upscaled to 10x10 grid blocks.

S1 fine grid permeability distribution

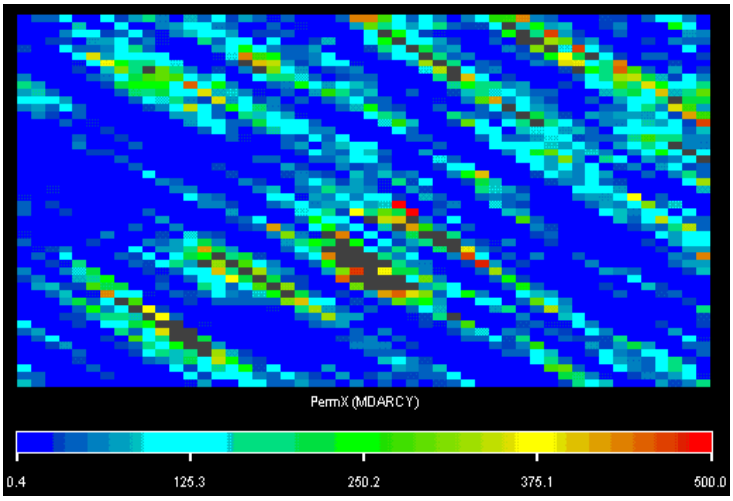

Figure 5.30. S1 100x100 permeability distribution. It is seen in contrast to the previous permeability distributions that the permeability pattern of the S1 distribution is dipping about 30 degrees.

S1 coarse grid permeability distribution

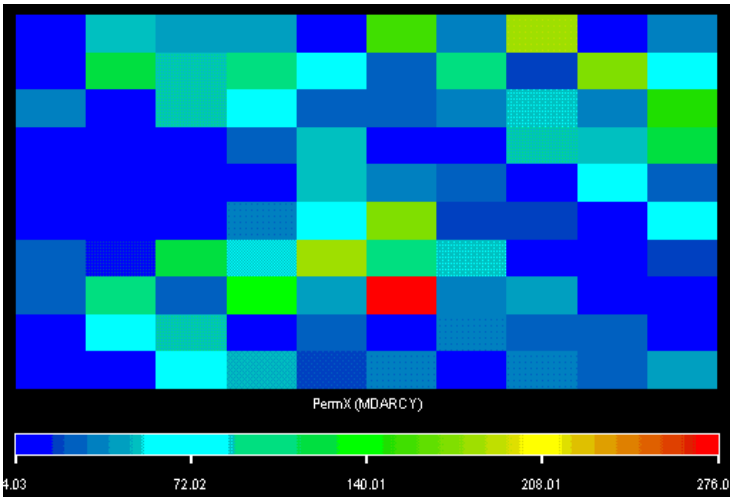

Figure 5.31. S1 10x10 permeability distribution.

S1 fine grid oil saturation

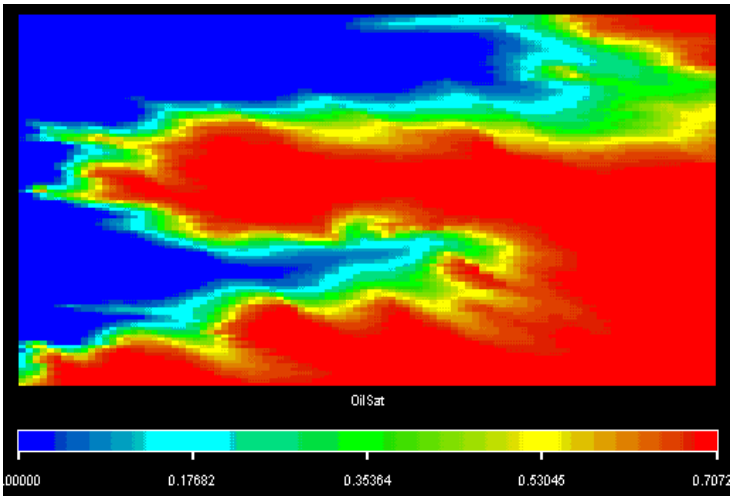

Figure 5.32. S1 Fine grid oil saturation after 1.5 year solvent injection.

S1 coarse grid oil saturation using standard boundary conditions and volume averaging (bc0va)

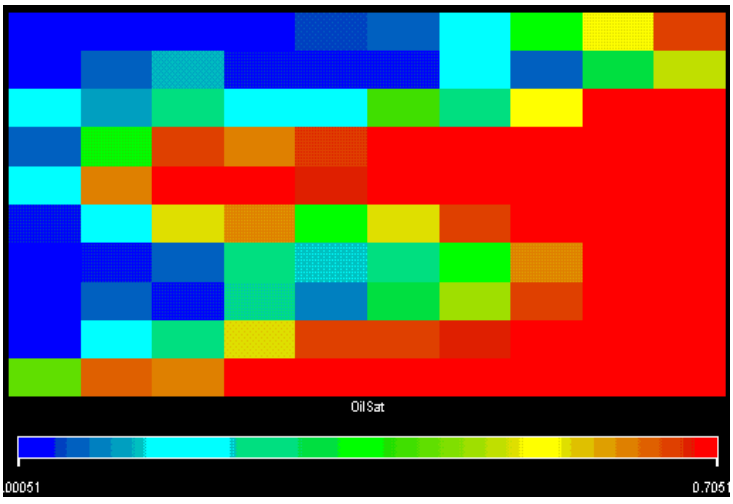

Figure 5.33. S1 bc0va, oil saturation after 1.5 year solvent injection. It is seen that the saturation distribution is very well reproduced on the coarse scale. The bc0va solvent profile is seen to match the fine grid results very well.

S1 coarse grid oil saturation using effective flux boundary conditions and outlet averaging (bc2oa)

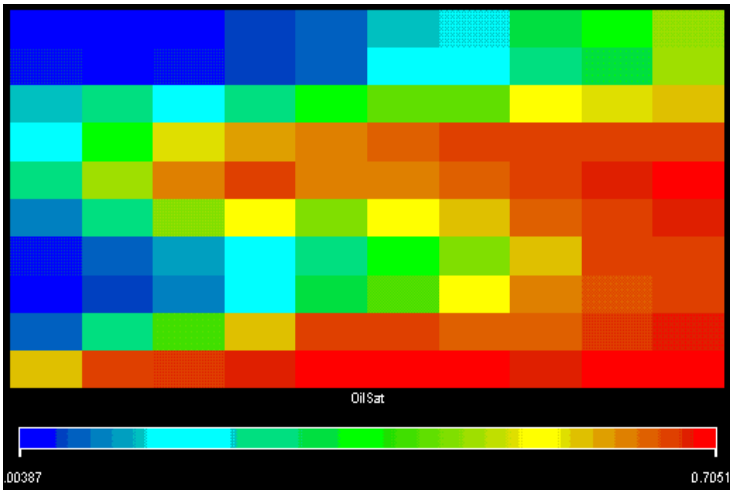

Figure 5.34. S1 bc2oa, oil saturation after 1.5 years of solvent injection. In this case the fronts are more dispersed due to numerical dispersion.

S1 coarse grid oil saturation using straight line functions and constant ω factor (SL-1.0)

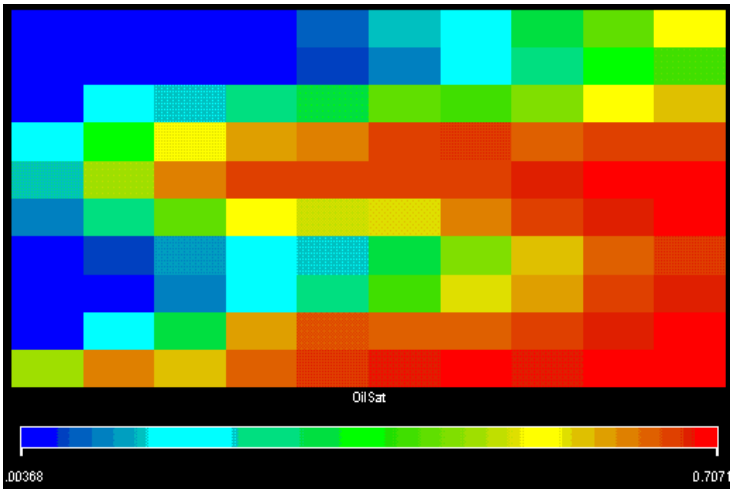

Figure 5.35. S1 SL-1.0, oil saturation after 1.5 years of solvent injection. Also here the fronts are more dispersed due to numerical dispersion and straight line relative permeability functions. An omega factor of 1.0 ensures full mixing within the cells and component viscosities therefore being equal to the quarter power mixture viscosity. This slows down the solvent flow.

S1 coarse grid oil saturation using straight line functions and constant ω factor (SL-03)

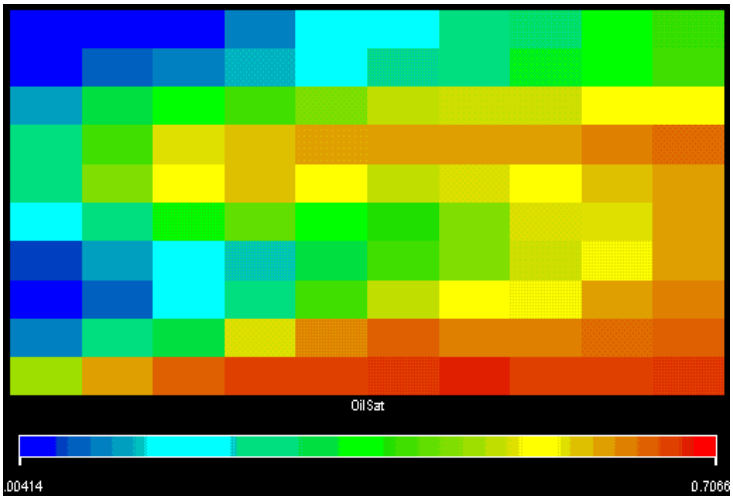

Figure 5.36. S1 SL-0.3, oil saturation after 1.5 years of solvent injection. In this case the fronts dispersion is enhanced due to the combination of straight line functions and an omega factor of 0.3 increasing the solvent flow.

S1 solvent production

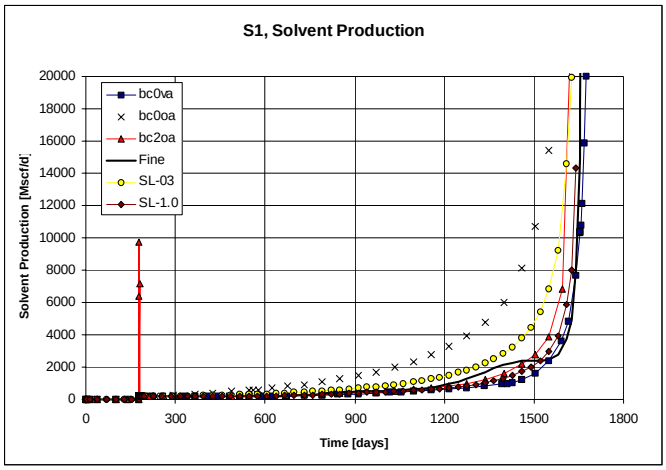

Figure 5.37. The figure compares the solvent production ratio f the S1 fine grid and the upscaled S1 10x10 model using standard boundary conditions, effective flux boundary conditions and straight line relative permeability functions with a global mixing factor respectively. Compared to the previous cases results using standard boundary conditions with outlet averaging (bc0oa) has been included also. Bc0oa and SL-03 predicts much too high solvent production.

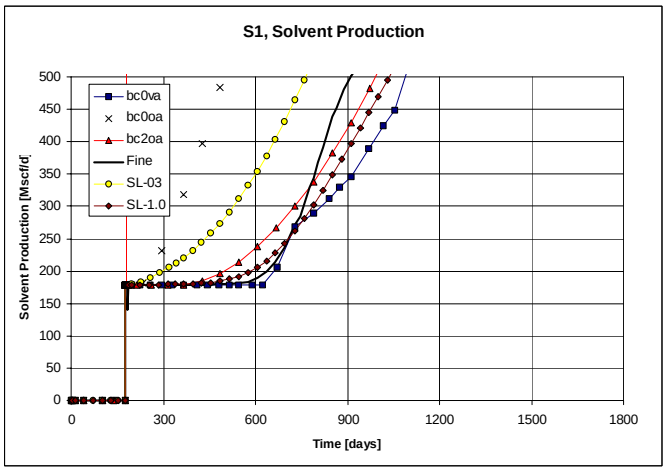

Figure 5.38. The figure compares the solvent production rate of the S1 fine grid and the upscaled S1 10x10 model using standard boundary conditions, effective flux boundary conditions and straight line relative permeability functions with a global mixing factor. It is seen that using straight line functions in combination with complete mixing (ω=1) predicts too early breakthrough. The bc0va model predicts a slightly late breakthrough.

S1 reservoir pressure

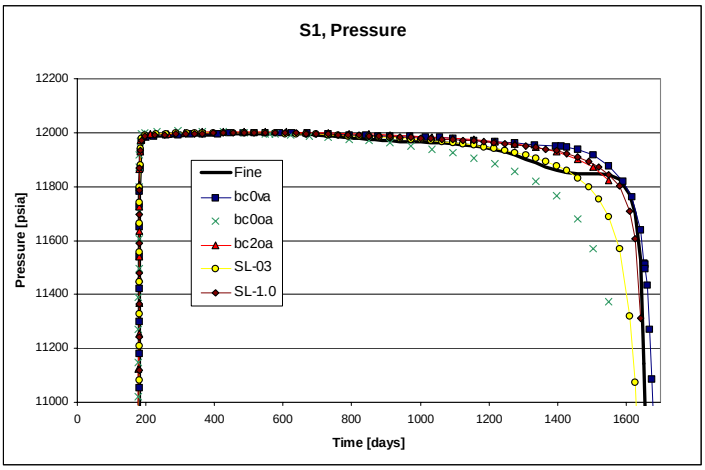

Figure 5.39. The figure compares the average pressure of the SS fine grid and the upscaled S1 10x10 model using standard boundary conditions, Effective flux boundary conditions and straight line relative permeability functions with a global mixing factor.

Real permeability distributions

5.7 T2D

The T2D permeability distributions consists of 243x435 grid block x-section from an existing reservoir.

The fine grid properties are as follows:

X-direction grid block size	8.53 m (28 ft)
Y-direction grid block size	5.18 m (17 ft)
Z-direction grid block size	0.98 m (3.2 ft)
Porosity	0.08

The coarse grid is upscaled to 9x15 grid blocks corresponding to an upscaling factor of 783, a factor of 27 in the x-direction and a factor of 29 in the z-direction.

The heterogeneity index is calculated to be 4810 indicating a very high variation in the permeability distributions.

T2D fine grid permeability distribution

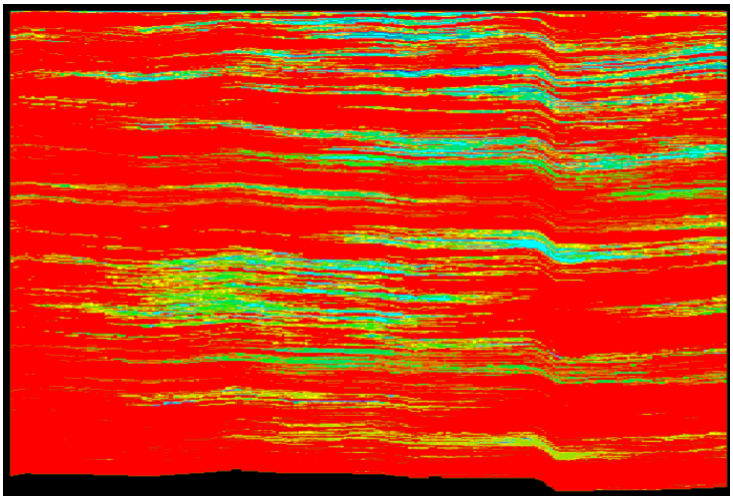

Figure 5.40. T2D fine grid permeability distribution consisting of 243x435 gridblocks, the horizontal permeability correlation length is seen to be in excess of .5. The permeability ranges between 0.001 and 72 mD.

T2D coarse grid permeability distribution

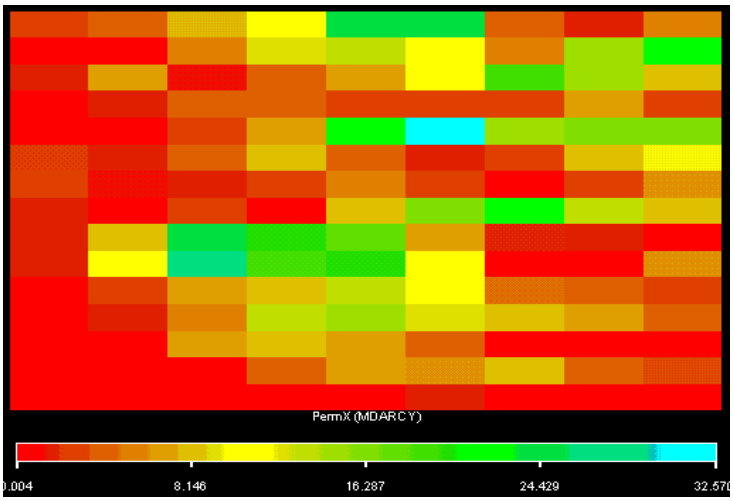

Figure 5.41 T2D 9x15 permeability distribution.

T2D fine grid oil saturation

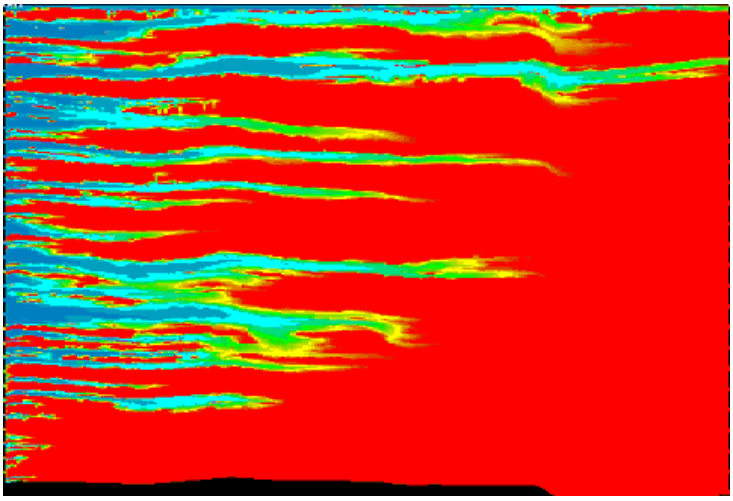

Figure 5.42. T2D fine grid oil-saturation distribution after 5 years of solvent injection. It is seen how the solvent fingers through the high permeability layers.

T2D coarse grid oil saturation using standard boundary conditions and volume averaging (bc0va)

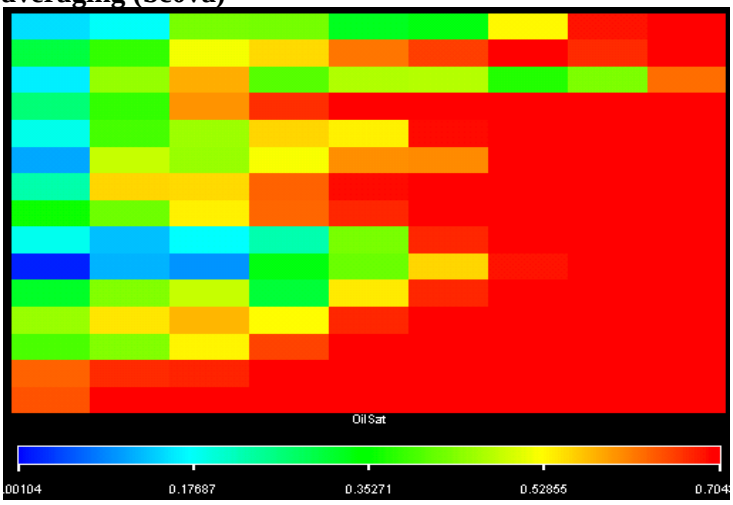

Figure 5.43. T2D-bcova 9x15 coarse grid oil-saturation distribution after 5 years of solvent injection. By comparing to the fine grid distribution in figure 41 it is seen that the channeling features are well represented on the coarse scale. By inspecting the plot it is seen how oil is bypassed within a coarse grid due to the shape of the pseudo relative permeability functions.

T2D coarse grid oil saturation using effective flux boundary conditions and outlet averaging (bc2oa)

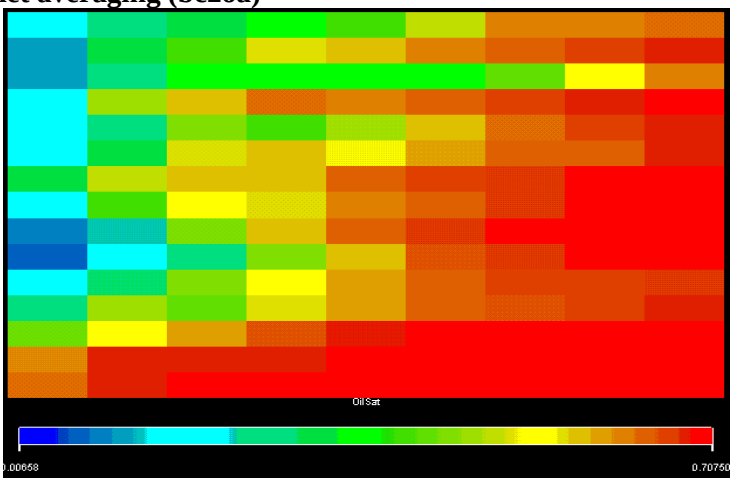

Figure 5.44. T2D-bc2oa , 9x15 coarse grid oil-saturation distribution after 5 years of solvent injection. By inspecting the plot it is seen that the solvent front is more dispersed than what is observed when using the bc0va model. The reason for this is that in this case the effective flux boundary conditions are used with outlet averaging of concentrations which does not correct for numerical dispersion as the volume averaging does.

T2D coarse grid oil saturation using straight line functions and constant ω factor (SL-0.3)

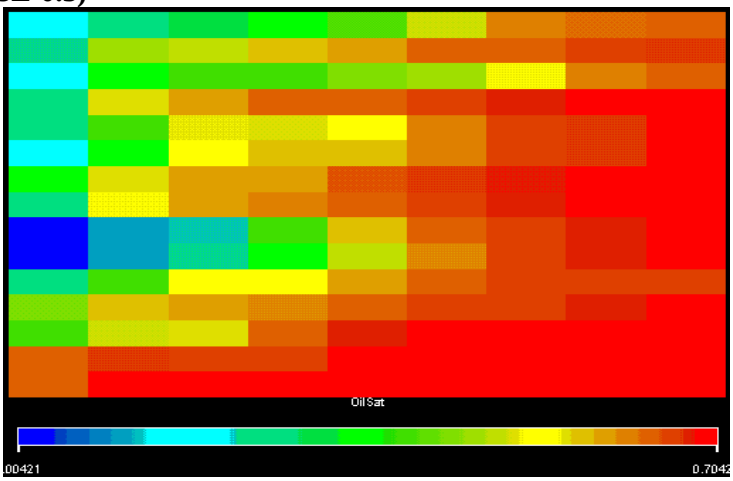

Figure 5.45. T2D-SL03, 9x15 coarse grid oil-saturation distribution after 5 years of solvent injection. It is seen how the ω-factor promotes the solvent flow by reduced mixing and lower effective solvent viscosity than the effective oil viscosity.

T2D coarse grid oil saturation using straight line functions and constant ω factor (SL-1.0)

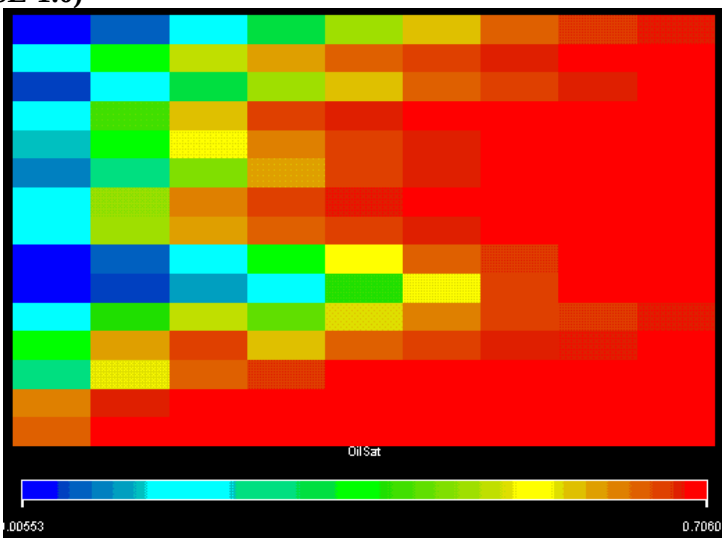

Figure 5.46. T2D-SL1.0, 9x15 coarse grid oil-saturation distribution. In this case the ω factor is equal to 1.0 corresponding to a homogeneous coarse grid blocks and therefore complete mixing between the oil and the solvent. In this case the effective solvent and oil viscosity are equal to the quarter power mixture viscosity.

T2D solvent production

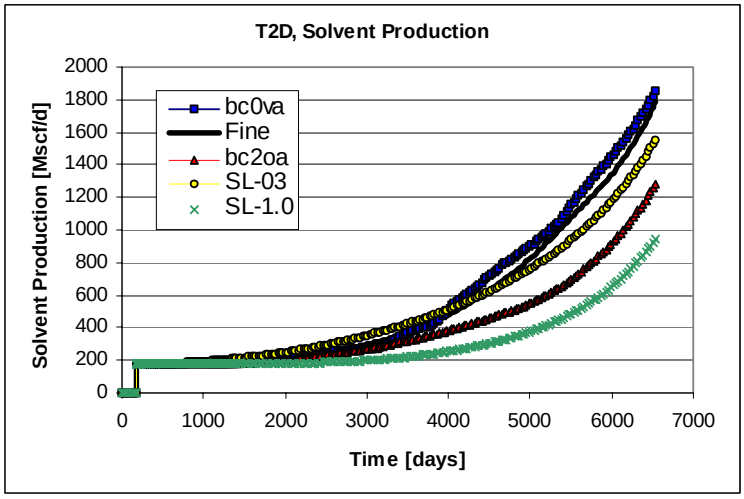

Figure 5.47-a. The figure compares the solvent production rate of the T2D-1 fine grid and the upscaled T2D model using standard boundary conditions, Effective flux boundary conditions and straight line relative permeability functions with a global mixing factor. The bc0va model captures the fine grid profile well.

T2D solvent production

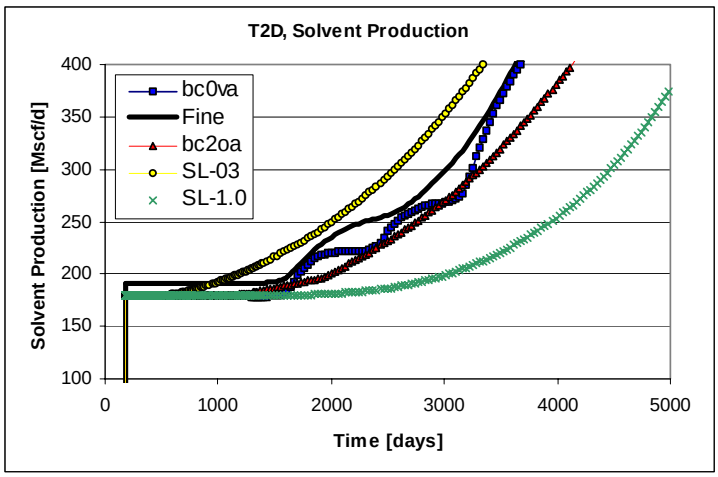

Figure 5.47-b. The figure compares the solvent production rate of the T2D-1 fine grid to the upscaled 9x15 models at the time of solvent break through. It is seen that the bc0va model matches the breakthrough time very well. The shape of the bc0va production profile is due to a combination of the individual fingers breaking through and the volume averaging of concentrations.

T2D reservoir pressure

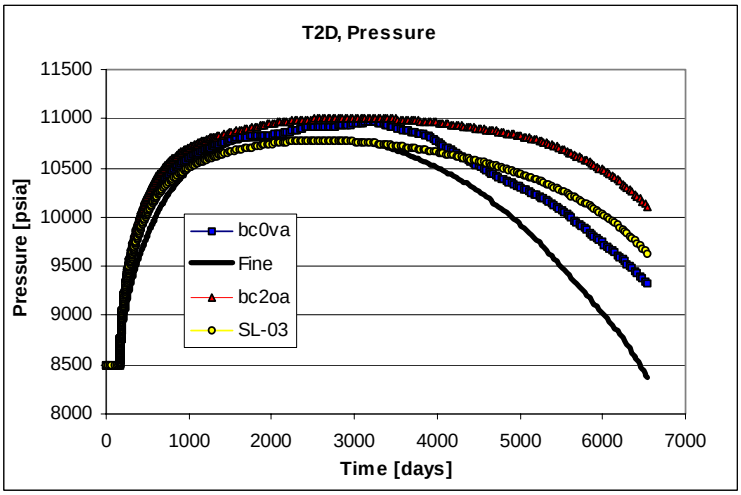

Figure 5.48. The figure compares the average pressure of the T2D fine grid and the upscaled T2D 9x15 model using standard boundary conditions, Effective flux boundary conditions and straight line relative permeability functions with a global mixing factor. None of the coarse grid models are capable of accurately reproducing the fine grid pressure behavior at late times.

5.8 SPE10-1-xz

In this case we have taken the top xy layer of the grid nr. in the SPE-10 comparison case and used this as an xz cross section- layer of 60x220 grid blocks. The grid has then been upscaled to 10x11 grid blocks corresponding to an upscaling factor of 120.

The fine grid dimensions are as follows:

Number of x-direction grid blocks	100
Number of z direction grid blocks	100
x-direction grid block size	3.048 m (10 ft)
y-direction grid block size	6.096 m (20 ft)
z-direction grid block size	1.524 m (5 ft)
kz-multiplier for fine grid simulations	0.1
kz-multiplier	0.1
Porosity	0.2

The heterogeneity index is calculated to be 4.5.

SPE-10-XZ fine and coarse grid permeability distributions

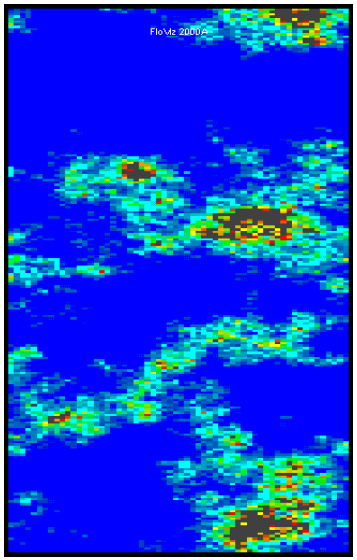

Figure 5.49. SPE10-1-xz Fine grid permeability

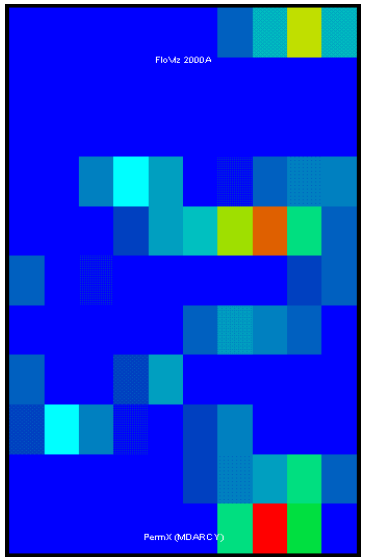

Figure 5.50. SPE10-1-xz Coarse grid permeability

Figure 5.49 and 5.50 illustrate the SPE10-1-xz fine grid and coarse grid permeabilities. The fine grid consists of 60x220 grid blocks and the coarse grid of 10x11 grid blocks, which corresponds to an upscaling ratio of 120, a factor of 6 in the x-direction and a factor of 20 in the z direction. The permeability range from less than 1 mD to 587 mD for the coarse grid and between 0 and 3300 mD for the fine grid.

SPE-10-XZ fine and coarse grid oil saturation

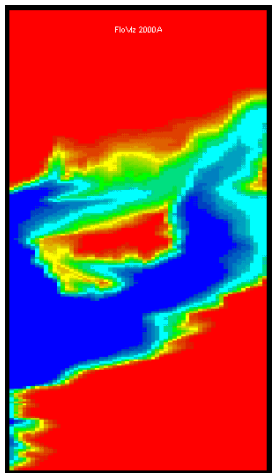

Figure 5.51. fine grid oil saturation

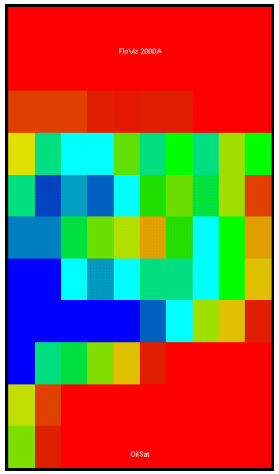

Figure 5.52. bc0va oil saturation

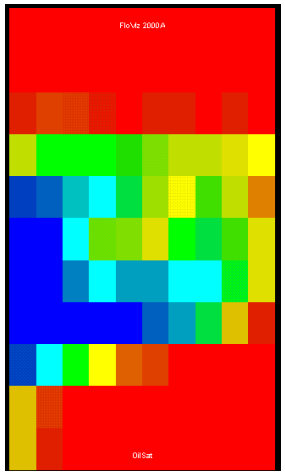

Figure 5.53. SL-03 oil saturation

Figure 5.51 – 5.53. Oil saturation after 1.5 year of solvent injection for the fine grid, standard boundary conditions with a local ω factor and for straight lines and a global ω of 0.3. It is seen that there is not much difference in the saturation plot indicating that using straight lines with a global omega factor is probably sufficient to capture the flow behavior for this system.

SPE-10-XZ solvent production

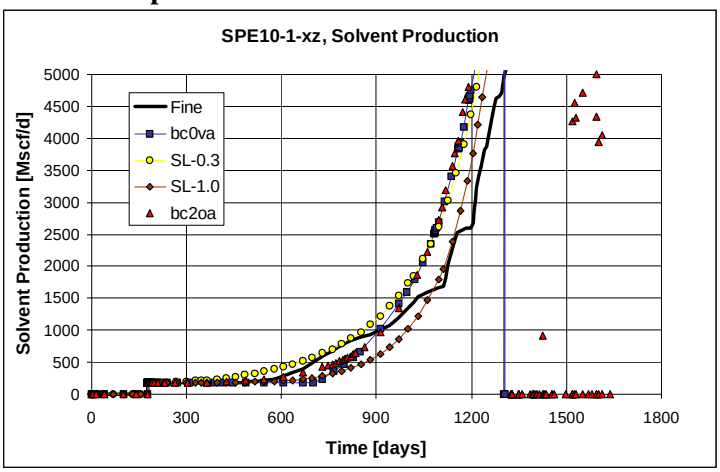

Figure 5.54. The figure compares the solvent production rate obtained from the fine grid to the production profiles obtained using the STBC, EFBC and SL-0.3 and SL-1.0.

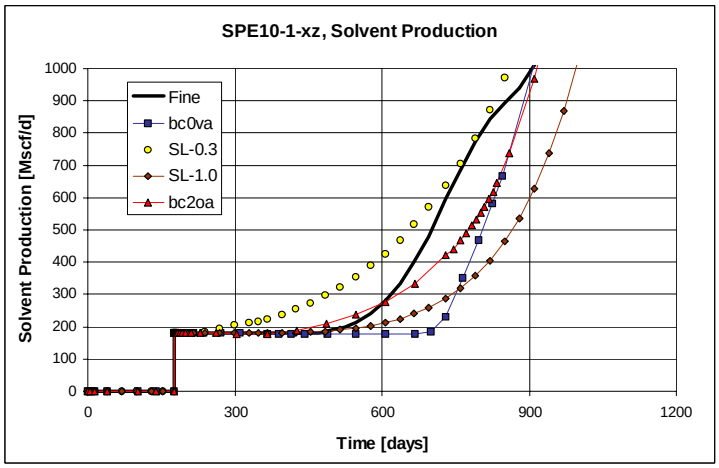

Figure 5.55. Here we compare the solvent production breakthrough times and production profile in the first 1000 days. It is seen that the bc0va model breaks through some 300 days late but is however able to reproduce the profile quite well. The bc2oa breaks through a little early and shows signs of a more dispersed front than the bc0va. The SL-0.3 and SL-1.0 illustrate how the breakthrough time can be matched by adjusting the ω factor.

SPE-10-XZ reservoir pressure

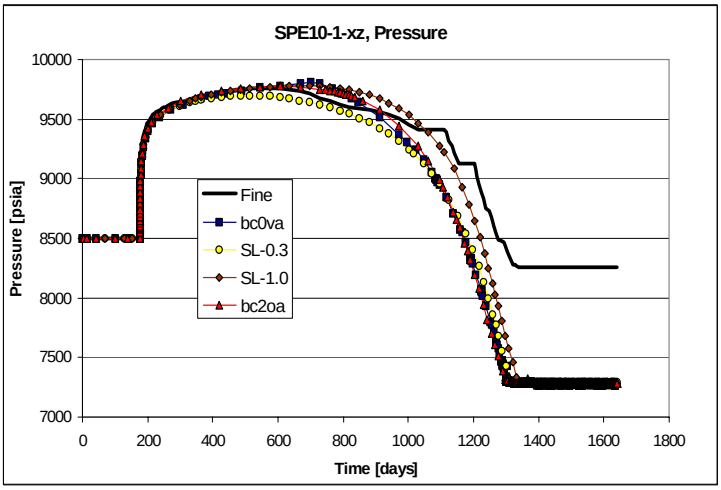

Figure 5.56. The figure compares the average pressure obtained from the fine grid to the production profiles obtained using the STBC, EFBC and SL-0.3 and SL-1.0. It is seen that the first 1000 days the overall pressure profile is captured by all the coarse models, while at late time the coarse grid pressure fall well below the fine grid results.

5.9 Discussion

In the 6 cases presented here we have attempted to test the upscaling methodology with 2 different sets of boundary conditions, the Effective Flux Boundary Conditions with outlet averaged concentrations and the Standard Boundary Conditions with volume averaged concentrations. The upscaled results have been compared to fine grid reference results and to coarse grid results where only the absolute permeability distribution have been upscaled and using straight line relative permeability functions.

The fine grid and coarse grid simulations have been carried out using the Chears simulator. The upscaling simulations have been carried out using our adapted version of the Renorm upscaling software. The renorm simulations are carried out on the fine grid contained in each coarse grid domain.

The fine grid simulations have been carried out with straight line permeability functions and an omega factor equal to one, i.e. allowing complete mixing between solvent and oil in each cell. The coarse grid simulations have been carried out with the pseudo relative permeability functions and the omega

factor that has been calculated from the Renorm calculations. For each coarse grid block a separate pseudo function and omega factor is specified.

The cases presented are 2 dimensional cases where the flow direction is parallel to the gridding, meaning that we have only carried out the upscaling in the main flow direction, i.e. along the positive x-axis.

For a 3 dimensional case, where flow potentially could take place along positive and negative x, y and z-axis directions, a total of 6 flow directions, we would have to consider upscaling for all 6 flow directions. The methodology for doing this would be the same as for the 2 dimensional case presented here, a total of 6 simulations would have to be carried out resulting in 6 pseudo curves and omega factors for each coarse grid block.

The largest grid upscaled in this study is the T2D distribution which consists of 243x435, a total of 105705 grid blocks. The time to carry out the upscaling to 9x15 grid blocks was roughly 2 hours on a Dell Precision 330 workstation running Linux, with a processor of 1.4 GHz and 512 MB of RAM.

Evaluation of the ω-factor

The ω-factor has been included as a local parameter evaluated for each grid block. The evaluation method used to for the cases presented here is somewhat simplistic, as the evaluation has been carried out at specific solvent saturation not taking the actual heterogeneity into account. The consequence of this is probably that the ω-factor has been assigned a too high value for many grid blocks. In order to improve this a proper automatic matching of effective solvent viscosity and effective hydrocarbon viscosity should be implemented in the procedure.

Boundary Conditions

We have compared the use of Standard Boundary conditions with volume averaged concentrations (bc0va) to the Effective Flux Boundary conditions with outlet averaged concentrations (bc2oa). The bc0va pseudo functions are based only on the fine grid simulation of the particular coarse grid sub-domain and includes correction for numerical dispersion because of the volume averaging. The bc2oa conditions take the surrounding permeability field into account which results in an attenuation of the fractional flow. The use of outlet averaging, however, allows for faster breakthrough. When comparing the dynamically upscaled results to results where only the absolute permeability has been upscaled and the solvent flow is controlled by a global ω-factor (e.g. SL-03) it is seen that for some of the cases, that the SL functions produce good results suggesting that a complicated dynamic upscaling may not be required.

For other cases, however, it is seen that the SL cases can not reproduce the correct flow profile. This is particularly evident for the more layered cases, i.e. permeability distributions with long correlation lenghts. If we consider the layered case Layer-1/100 or the T2D case it is seen from these cases that the SL models can not reproduce the fine grid flow behavior. The bc2oa model is also not able to reproduce these cases where extreme channeling takes place, due to the attenuation of the fractional flow imposed by the Effective Flux conditions and the outlet averaging of concentrations.

The bc0va model preserves a sharp solvent front due to the volume averaging and can produce high solvent flow rates due to the more aggressive pseudo functions.

The results from the 6 case studies are summarized below.

1. Layered

In the layered case we upscaled a 100x100 layered grid to a 10x10 homogeneous grid. The bc0va conditions were able to reproduce layered behavior and followed the production profiles of the fine grid behavior with good accuracy. Both the bc2oa and the SL-model were not able to reproduce the features of the layered system

2. P4

The P4 distribution is derived using the GSLIb software and has a correlation length of 0.25 and a heterogeneity index of 2.06. All models in this case reproduce the fine grid behavior quite well. It is seen, however, that the SL-03 model breaks through early and that the bc0va model breaks through late while the bc2oa model matches the break through time reasonably well. The reason for this is probably the different omega values used for the 3 models. The SL-03 model uses an ω of 0.3 for all grid blocks. The bc2oa and bc0va models use local ω-factors for each block, for the bc2oa the ω has been calculated using outlet averaging while the calculation for the bc0va has been carried out using volume averaging, which will result in higher ω values for the bc0va than for the bc2oa. For both pseudo models the ω-factor is higher than 0.3 for the majority of the grid blocks. By increasing the ω-factor for the SL case and reducing it for the bc0va case we could probably obtain a match on break through time for all three models.

3. P5

The P5 system is similar to the P4 case, however, with permeability correlation length of 0.7 and a heterogeneity index of 3.40. As for the P4 case

it is also seen that all three upscaling models recreate the fine grid behavior quite well. The Sl-03 model breaks through first while the bc0va and bc2oa models are seen to break through slightly late. It is also seen that the shape of the bc0va solvent production curve closely resembles the fine grid solvent production profile. Breakthrough times for all models could be improved by adjusting the omega value.

The P5 case has also been upscaled to a 5x5 grid. It is seen that only the bc0va model is able to capture the production profile.

4. S1

In the S1 system the bedding planes are seen to be at an angle of some 30 degrees to the flow direction. The heterogeneity index has been calculated to be 1.30 assuming a correlation length of 0.3. By inspecting the solvent saturation plots it is seen that the bc0va model closely resembles the fine grid model while the bc2oa and SL models are highly dispersed. The production profile comparisons show that the bc0va model matches the breakthrough time and the shape of the production profile well, while the other models do not reproduce the solvent production profile.

5. T2D

The T2D case represents a cross section from a real reservoir and is highly heterogeneous. The system is upscaled from 243x453 grid blocks to 9x15 grid blocks. The horizontal correlation length are about 0.7 with a heterogeneity index of 4810. From the solvent saturation plots it is seen that the SL-03 case is highly dispersed leading to a much premature breakthrough. The other cases predict a reasonable breakthrough time, however, only the bc0va model is capable of reproducing the solvent production profile throughout.

6. SPE-10-XZ

The SPE-10-XZ case is a 60x220 fine grid upscaled to a coarse grid of 10x11 grid blocks. It is seen from the results that none of the models reproduce the fine grid results. The bc0va model predicts a much to late breakthrough, however, as for the other cases the shape of solvent production profile after breakthrough is similar to what is seen from the fine grid result.

5.10 Conclusion

In this project we are focusing on upscaling a continuous miscible gas injection process in which water is immobile. Upscaling methods are generally

considered to be system dependent and therefore it can be difficult to apply a method that works for one system to a system of different character.

The results from the coarse grid simulations have been compared to fine grid reference results and to coarse grid simulations using straight line relative permeability functions, i.e. with no upscaling of relative permeability functions, and a constant mixing parameter, ω. Simulations have been carried out on systems of different heterogeneity correlation lengths.

The results show that in most cases the standard boundary conditions with volume averaged concentrations (bc0va) provide good results. The volume averaging effectively controls numerical dispersion and the pseudo relative permeability functions are able to transfer the flow behavior induced by the fine grid heterogeneity on to the coarse grid. For highly heterogeneous systems with long correlation lengths this becomes especially true.

In cases with short correlation lengths, the breakthrough for the bc0va model takes place to late. It is possible that the volume averaging corrects to much for numerical dispersion for these systems leading to the late breakthrough. It is also possible that the omega factors used are too high slowing down the solvent flow. Other parameters also affect the breakthrough time, for example the absolute permeability and the kv/kh ratio. The important feature of the bc0va model is that it is able to reproduce production profile and saturation distribution more accurately than the other models that suffer from numerical dispersion.

When using the Effective Flux Boundary Conditions in combination with outlet averaging, the displacement front is seen to be more dispersed. For short correlation lengths the breakthrough may take place early due to the outlet averaging, while for systems with long correlation lengths the breakthrough can be delayed due to the nature of the EFBC conditions.

For some systems of short correlation lengths it may not be necessary to use pseudo relative permeability functions as the systems exhibit a rather homogeneous behavior on the simulation scale. For these systems it is sufficient to use straight line permeability functions with a global viscosity mixing parameter, ω, to control the velocity of the injected solvent. It is possible to control the numerical dispersion by introducing a critical solvent saturation.

5.11 Suggestions for future work

The upscaling methodology has up to this stage been tested on 2 dimensional permeability realizations of different size and types of heterogeneity. When upscaling we have used 2 different combinations of boundary conditions and concentration averaging, the Standard Boundary Conditions with Volume Averaging (bc0va) and the Effective Flux Boundary Conditions with Outlet Averaging (bc2oa), to create pseudo functions for the coarse grid simulations. For the cases tested here it has been found that for systems with long correlation lengths, the bc0va, provides the best results on the coarse scale. For systems of shorter correlation lengths the results indicate that the use of pseudo relative permeability functions may not be required and that straight line functions with a global ω-factor is adequate.

In order to improve the methodology the following suggestions may be taken into account.

1. The calculation of the ω-factor needs to be improved. As suggested in chapter 4, by using a matching procedure for comparing the effective hydrocarbon viscosity to the effective solvent viscosity for each coarse grid block, it is possible to obtain local ω-factor that more accurately incorporates the effects of heterogeneity than the simplified procedure used here.

2. Test the upscaling method for 3-dimensional systems. One problem that arises here is the availability of a reservoir simulator which can use directional relative permeability functions.

3. Test the method on more permeability realisations and other fluid systems with different viscosity and density ratios.

4. In order to incorporate the effects of gravity in the upscaling, the evaluation of a separate density ω-factor can be included in the calculations.

5. It is possible to use parallel processing to speed up the upscaling as the sub grid simulations are run independently.

VISCOSITY

6 Modelling of Viscosity

6.1 Introduction

The viscosity of reservoir fluids is an important parameter due to the inverse proportional influence on the fluid flow velocity through Darcy´s law. For modelling purposes we therefore require knowledge of how the viscosity is affected by changes in pressure and fluid composition. For reservoir flow calculations the temperature is normally assumed to be constant. For flow processes in the well and through surface facilities the influence of temperature must be included.

Laboratory tests

The physical properties and behavior of reservoir fluids are determined from a wide range of different laboratory experiments. The viscosity of a reservoir oil is measured at reservoir temperature at a number of pressure points above and below the saturation pressure. One method which is commonly used for viscosity measurements is the rolling ball viscometer method, where the time is measured for a steel ball to roll through the fluid at a specific angle.

For gas injection processes, the knowledge of viscosity is required not only as a function of pressure but also as a function of composition and therefore if gas injection is planned, it is necessary to carry out more experiments in order to determine how the injected gas interacts with the reservoir oil. For example, it is important to know at what pressure does the injected gas dissolve in the oil and how does this affect the properties of the oil. Experimental methods for investigating these effects includes:

- Swelling test where the injection gas is added to a known amount of oil in steps. Between each step mixture properties can be measured.
- Slim tube experiments where oil is displaced by gas at different conditions in order to investigate the relation between miscibility and displacement efficiency.

When injected gas goes into solution with the oil, the viscosity of the resultant fluid may change significantly from the viscosity of the original fluid. As it is very labour-intensive to experimentally determine the effects of fluid

interactions on resultant fluid properties, there is a need for modelling methods that can predict the outcome of an "experiment" with good accuracy.

6.2 Representing Viscosity in Reservoir Simulation

There are in general 3 ways of representing viscosity behavior in a reservoir simulator depending on the type of reservoir fluids and processes that are to be modelled. For so-called black oil simulations, where the injected and in-situ fluids are considered to be immiscible, the viscosity can be included in reservoir models using look up tables that have been derived from laboratory experiments. These tables are functions of pressure and solution gas.

If the injected fluid mixes with the reservoir fluid, the viscosity of the resultant fluid becomes a function of pressure as well as of the compositional changes of the phases in the reservoir. This makes the prediction of viscosity more complicated and therefore not easily handled by look up tables. For miscible processes it is possible to use an extension of the black oil formulation, e.g. the Todd Langstaff miscible formulation, where viscosity and other properties are determined from 2 component mixing rules combining the initial phase properties into resultant phase properties using mixing parameters.

An alternative to the miscible approach is compositional simulation which uses a cubic equation of state to calculate the fluid phase properties. In compositional reservoir simulation, viscosity is normally calculated by the Lohrenz Bray Clark (LBC) [36] method. The LBC method is correlating the fluid viscosity to the reduced fluid density which is obtained from the EOS calculations.

Recently a new method for calculating viscosity, termed the Friction Theory method [35, 54], has been developed at the Technical University of Denmark. This method uses the attractive and repulsive pressure terms in a cubic equation of state, such as the Soave-Redlich-Kwong or the Peng-Robinson, to calculate the viscosity of a characterized oil. The new method for calculating viscosity of hydrocarbon mixtures have been implemented into the CHEARS Reservoir simulator.

An introduction will be given to the Lohrenz Bray Clark method and the Friction theory method and subsequently results are presented where the performance of the two methods have been compared. The comparison have been carried out for pressure depletion as well as for a gas injection case.

6.3 Lohrenz Bray Clark method

In reservoir simulation the Lohrenz-Bray-Clark[36] correlation has been widely used. This correlation is based on a reduced fluid density of the mixture. The Lohrenz Bray Clark viscosity correlation was published in 1964. The method for reservoir liquids is based on the concept of residual viscosities and the principle of corresponding states. The method was evaluated by comparing experimental and calculated results for 260 different reservoir oils ranging from black oils to highly volatile oils. The average absolute deviation was found to be 16 %. The average absolute deviation for gas calculations was found to be 4 %. In reservoir simulation the fluid density is normally calculated by a cubic equation of state such as the Soave-Redlich-Kwong or the Peng-Robinson. The LBC correlation is given by the following equation, correlating the viscosity, μ, to the reduced density, ρ_r, the low pressure viscosity μ^o and the 5 constants a_1 through a_5.

6.1 $$[(\mu-\mu^o)\lambda+10^{-4}]^{\frac{1}{4}} = a_1 + a_2\rho_r + a_3\rho_r^2 + a_4\rho_r^3 + a_5\rho_r^4$$

where the reduced density is given by $\rho_r = \rho/\rho_c$ and μ^o can be determined from equation 6.2

6.2 $$\mu^o = 34\times10^{-5}T_r^{0.94}/\lambda, \qquad \text{for } T_r \le 1.5 \text{ and}$$

$$\mu^o = 17.78\times10^{-5}(4.58T_r - 1.67)^{\frac{5}{8}}/\lambda, \qquad \text{for } T_r > 1.5$$

where the reduced temperature T_r is calculated by $T_r = T/T_c$ and the λ factor is calculated by the following equation

6.3 $$\lambda = T_c^{\frac{1}{6}} M^{-\frac{1}{2}} P_c^{-\frac{2}{3}}$$

6.3.1 Peneloux Volume Shift

The predicted viscosity is obviously very sensitive to the fluid densities that the calculations are based on. In compositional reservoir simulation the density is calculated from the molar volume obtained from the cubic equation of state in use, such as the standard 2-parameter Soave Redlich Kwong and Peng Robinson equations of state. The 2 parameter cubic equations of state, however, are not very well suited for accurate liquid density calculations due to the inaccuracy of the molar volume calculations. Peneloux [43] introduced a method for including a volume correction term in the equations of state in order to improve the molar volume calculation. The volume shift takes the following form:

6.4 $$v^{cor} = v - c$$

The concept of volume shift may improve the Lohrenz Bray Clark viscosity predictions significantly. Jhaveri and Younggren[47] applied the volume shift to the Peng Robinson equation by defining a dimensionless parameter as follows:

6.5 $$S_E = c / b$$

The dimensionless volume shift is calculated by the following correlation

6.6 $$S_E = 1 - \psi / M^{\chi}$$

where M is the molecular weight and χ and Ψ are positive cofficients. For paraffins the value of coefficients are χ = 0.1823 and Ψ = 2.258.

6.3.2 Model Tuning

If experimental data are available it is normal practice to tune the viscosity predictions against the experimental data. The viscosity, calculated by the LBC method, is tuned by adjusting the critical volume of the pseudo components of the fluid characterisation. This procedure only affects the

viscosity calculation as the critical molar volume is not used in other calculations. The maniplation of the critical volume directly affects the reduced density through the following relation

6.7 $$\rho_r = \frac{v_c}{v}$$

The Lohrenz Bray Clark Method is given in more detail in Appendix B.

6.4 Friction Theory

A new methodology for calculating hydrocarbon mixture viscosities has been developed at the IVC-SEP, Technical University of Denmark. The method is termed the Friction Theory. As part of this project, the *Friction Theory* methodology has been implemented in the CHEARS reservoir simulator in order to compare its performance to the standard Lohrenz Bray Clark correlation.

The Friction theory separates the total viscosity, η, into a dilute gas viscosity, $\eta_{0,mx}$, term and a residual friction term, $\eta_{f,mx}$.

6.8 $$\eta = \eta_{0,mx} + \eta_{f,mx}$$

The dilute gas viscosity is defined as the viscosity at the zero density limit, while the residual term is related to friction concepts of classical mechanics. For an n-component mixture the residual friction term is expressed by the following equation:

6.9 $$\eta_{f,mx} = \kappa_{r,mx} p_r + \kappa_{a,mx} p_a + \kappa_{rr,mx} p_r^2$$

where $\kappa_{r,mx}$ is a linear repulsive viscous friction coefficient, the $\kappa_{a,mx}$ is a linear attractive viscous friction coefficient and $\kappa_{rr,mx}$ is a quadratic repulsive friction coefficient. The pressure terms p_a and p_r represent the Van der Waals

attractive and repulsive pressure terms of the mixture. These can be obtained from a cubic equation of state. The friction theory is given in more detail in Appendix C.

6.5 Implementation of the Friction Theory Method.

The CHEARS simulator is Chevron's (Chevron-Texaco) in-house reservoir simulator. We received the source code of the CHEARS 98A simulator version suitable for Pc's via an agreement between Chevron and the Technical university of Denmark. This allowed us to implement and test new calculation methods in the simulator. For this project it was decided to implement the Friction Theory (FT) viscosity calculation method in order to test the method in a reservoir simulation context and to compare the performance to the normally used Lohrenz Bray Clark method. After spending significant time mapping out the Chears simulation code and the data structure we were able to implement the Friction Theory as a separate subroutine in the simulator. When the software starts, the user is prompted to specify which viscosity calculation routine he/she wishes to use. The comparisons are carried out by running a simulation with each viscosity model. The calculated liquid and gas viscosities are printed to an external file as a function of pressure and can after simulation be compared to the experimental values. The first version of the FT method implemented into the simulator could only handle simple hydrocarbon mixtures of pure components, i.e. the method was not extended to pseudo-components at this time. Extensive testing was carried out for both pure components as well as for binary mixtures where experimental data were available. At a later stage when the FT method was generalized for reservoir oil descriptions [35], the simulator version was updated with the extended FT viscosity model.

The procedure for running the simulator with the FT model is as follows. The PVT data that is normally required for carrying out a compositional simulation run is specified via the input deck. The additional data required for the FT model is input via 2 extra include files that must be placed in the directory where the simulations are carried out. An example of an input deck and the include files are given in Appendix E.

6.6 Comparing the Viscosity Modelling Methods

In the following, the Friction Theory calculation method will be compared to the Lohrenz Bray Clark method. The comparison are carried out for several different reservoir oils.

6.6.1 Reservoir Oils

The friction theory has been generalized for reservoir oil so that it can be used with pseudo components and mixing rules[35]. We have compared the performance of the Friction Theory and the Lohrenz Bray Clark method on 12 reservoir oils. The oils range from black oils to volatile oils for which we have experimental viscosity data.

Results are presented where comparisons have been carried out for all the oils in a depletion scenario and for one of the oils in a gas injection scenario.

In the depletion cases the reservoir model is produced from initial pressure to a pressure below the saturation pressure using the Lohrenz Bray Clark and the Friction Theory respectively. The calculated viscosities are subsequently compared to the experimental viscosity data. In all the figures, used for comparison of the viscosity calculation methods, the viscosity is given in CentiPoise and pressure is given in Psia.

The oils that have been used for the comparisons are given in the table below:

	Reservoir Pres.	Reservoir Temp.	Bubble Point	Viscosity at P_{sat}
	Bara / Psia	K / F	Bara / Psia	CentiPoise
AM-1	204 / 2965	330 / 135	174 / 2530	3.1
Chevron-1	804 / 11661	381 / 226	250 / 3623	0.128
Danesh-1	284 / 4114.5	377 / 220	182 / 2634.5	0.373
Danesh-2	395 / 5726.5	363 / 195	316 / 4580.5	0.5
Elf-1	274 / 3984	338 / 148.5	270 / 3922	1.24
Elf-23	211 / 3066	345 / 161.2	199 / 2882	4.62
Elf-24	213 / 3097	346 / 163.2	209 / 3027	5.73
Elf-26		346 / 163.4	134 / 1938	0.81
NSO-1		371 / 208	203 / 2951	0.299
NSO-2		366 / 200	274 / 3981	0.404
NSO-3		344 / 160	159 / 2305	2.1
Chevron-2		346 / 163	109 / 1585	11.89

Table 6.1. The tabulated oils have been characterised and used in the Chears simulator in order to calculate viscosity as a function of pressure using the Lohrenz Bray Clark (LBC) and the Friction theory methods respectively. When testing the LBC method, we have used the 2-parameter Peng Robinson density, both with and without the dimensionless Peneloux volume shift as proposed by Jhaveri and Younggren (eq. 6.6).

6.6.2 Characterization

The oils have been characterised by the following components:

N2, CO2, H2S, C1, C2, C3, iC4, nC4, iC5, nC5, C6, C7+

The C7+ fraction has been characterised by 4 pseudo-components. This means that the oils are characterised by a total of 15 components, if the oil contains H_2S, otherwise by 14 components. The characterisation has been carried out by means of the SPECS PVT software developed at the IVC-SEP at the Technical University of Denmark. The initial characterisation is adjusted until the experimentally determined saturation pressure is matched. This has been carried out by adjusting the specific gravity of the plus fraction until a match has been accomplished.

The compositions of the oils are given in Appendix A. The final characterisations for the oils are also given in Appendix A. The critical parameters for the 11 base components are tabulated values and can be found in several references. We have used the tables given in Ali Danesh's book[47]. The Peng Robinson Equation of state is used in the simulations and therefore the same EOS has been selected to characterize the oils in SPECS.

6.7 Prediction of Viscosity

As the LBC method is dependent on the accuracy of which the liquid density is predicted by the Peng Robinson EOS, the viscosity prediction has been carried out with and without the dimensionless Peneloux shift for the density calculations. The volume shift given by eq. 6.6 has been applied to the pseudocomponents only. The reason for this is that the LBC correlation in general underpredicts the viscosity, i.e. the density is too low. When the volume shift is applied to the pseudocomponents through equation 6.6 this results in a density increase and hence a viscosity increase.

When predicting the viscosity using the Friction theory method the standard 2 parameter Peng Robinson EOS is used. This gives initial viscosity predictions from the 2 methods which can be compared to experimental results.

6.7.1 Tuning

In order to improve the viscosity calculation performance it is possible to tune the models to match experimental viscosity data. The Lohrenz Bray Clark method is tuned by adjusting the critical molar volume of the heaviest pseudo component. As the critical volume is only used for the viscosity calculation this tuning does not affect other properties of the model.

The Friction theory model is tuned by adjusting the critical viscosity of the pseudo components.

6.7.2 Comparisons

The purpose of this study is to compare the two viscosity calculation methods in a reservoir simulation context. In depletion cases we can compare the predictive performance of the methods to the experimental results that we have available. Based on this initial comparison the viscosity models can be tuned to match the experimental data better.

However, after the models have been tuned it is necessary to ask the question whether or not the tuning process may invalidate the predictive capabilities of the model in a gas injection scenario. This is a valid question considering the fact that the potential fraction of injection gas has not been included in the tuning process. In order to validate the models for gas injection, we need experimental data on mixtures of the reservoir oils and the injection gas, e.g. from swelling tests. If we do not have these data it becomes difficult to carry out the performance evaluation. If the two tuned viscosity calculation methods produce inconsistent results, how can this be interpreted and which method delivers the most reliable result ?

We have included one miscible gas injection example where the Chevron-1 oil is displaced by CO_2. The comparison is carried out in the first instance to investigate to which extent the outcome of the simulations differ when using one or the other viscosity calculation method. The results from this comparison show that both models appear to behave consistent and the observed difference in the production performance is related to the initial difference between the tuned models rather than to the gas injection.

6.7.3 Simulation model

The model used for the simulations is a small homogeneous 2 dimensional model which runs through very fast. The model has the following properties:

nx = 50, ny = 1, nz = 5

Grid block size x-direction	61 m (200 ft)
Grid block size y-direction	61 m (200 ft)
Grid block size z-direction	30.5 m (100 ft)
Porosity	0.2
Permeability	50 mD
Relative Permeability	Straight Lines

6.8 Results, *Depletion*

The simulation results for the 12 different oils are shown in the following pages. 2 figures for each oil present the viscosity calculated by the LBC method and the Friction theory method compared to experimental results. The first figure gives the predicted values and the second figure presents the results obtained after tuning.

6.8.1 AM-1

The results for the AM-1 oil is given in the figure below. The composition of the oil is given in table-1 in Appendix-A. The oil has been characterised by the 11 base component and 4 pseudo-components covering the C7+ fraction. The characterisation is given in table 2 in Appendix-A. The viscosity has been calculated by means of the Lohrenz Bray Clark method and the Friction Theory in prediction mode and after tuning methods. The results are compared with experimental data in figure 6.1 and 6.2.

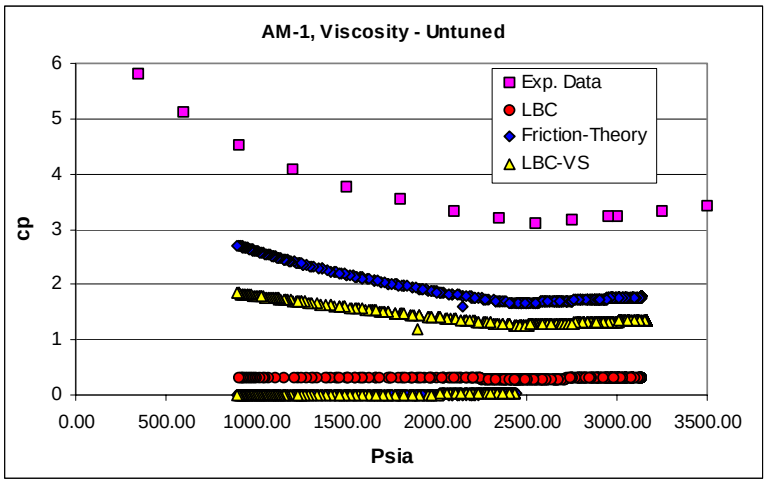

Figure 6.1. Experimental viscosity data for the AM-1 oil is compared to predictions using the Friction theory method and the LBC method respectively. The results from the LBC method are generated first with no Peneloux shift (LBC) and by using volume shift for the pseudo components (LBC-VS). It is seen that for this oil the LBC-VS predicts the viscosity within some 58 % and the Friction theory prediction is within 45%.

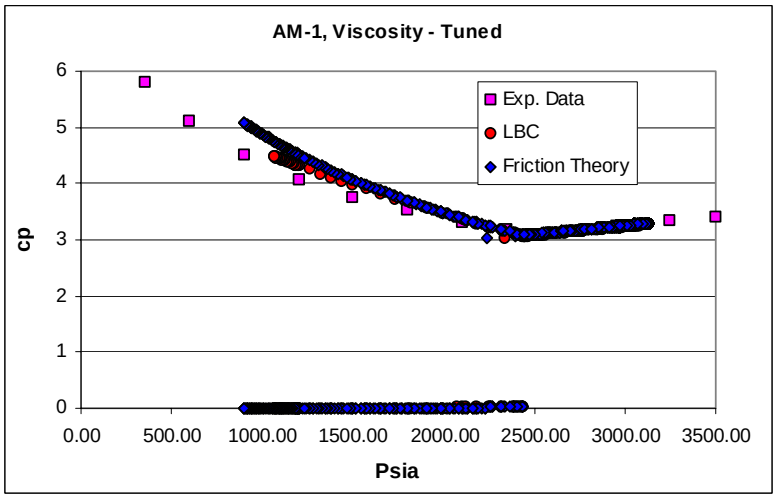

Figure 6.2. Experimental viscosity data compared to calculated values after tuning the LBC and the Friction theory methods. It is seen that the both methods are reproducing the experimental data very well, especially above the saturation point while at lower pressures the methods over predicts slightly.

6.8.2 Chevron-1

The results for the Chevron-1 oil is given in the figures below. The composition of the oil is given in table-2 in Appendix-A. The oil has been characterised by the 11 base component and 4 pseudo-components covering the C7+ fraction. The characterisation is given in table 4 in Appendix-A. The viscosity has then been calculated by means of the LBC and the Friction theory methods. These are compared with experimental data in figure 6.3.

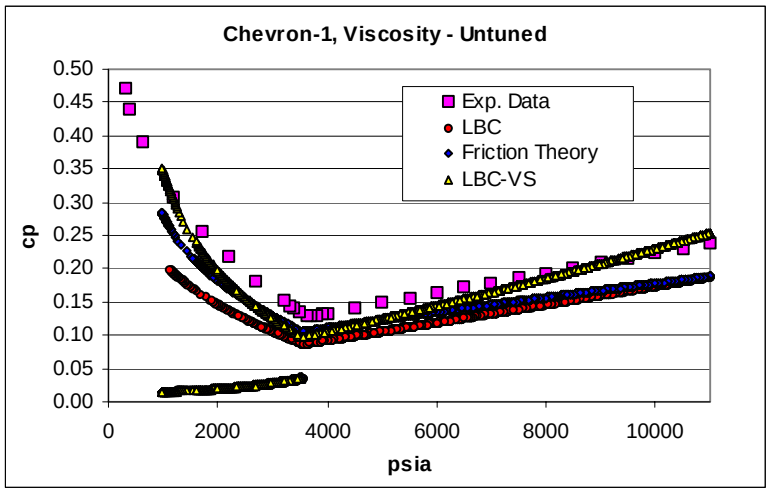

Figure 6.3. Experimental viscosity data for the Chevron-1 oil is compared to predictions using the Friction theory method and the LBC method respectively. The results from the LBC method are generated first with no Peneloux shift (LBC) and by using volume shift for the pseudo components (LBC-VS). It is seen that the LBC-VS predicts the viscosity within some 23 % while the Friction theory prediction is within 15%.

The calculation methods have subsequently been tuned against the experimental data, this is done for the LBC method by tuning the critical volume of the heaviest pseudo component, and for the friction theory method by tuning the critical viscosity of the pseudo components. The results after the tuning process is given in figure 6.4.

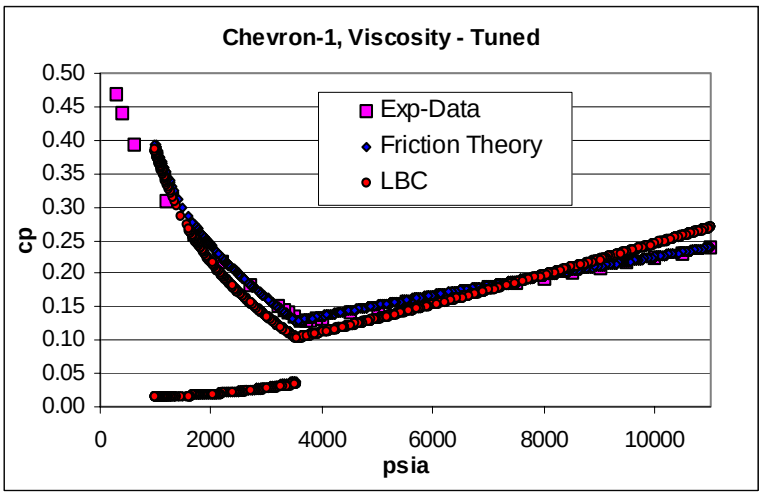

Figure 6.4. Experimental viscosity data compared to calculated values after tuning the LBC and the Friction theory methods. It is seen that the friction theory method is reproducing the experimental data very well, above and below the saturation point, while the tuned LBC method gives reasonable results, however, it is seen that the shape of the curve is wrong, overpredicting at high pressures and underpredicting at lower pressures.

6.8.3 Danesh-1

The results for the Danesh-1 oil is given in the figures below. The composition of the oil is given in table 5 in Appendix-A. The oil has been characterised by the 11 base component and 4 pseudo-components covering the C7+ fraction. The characterisation is given in table 6 in Appendix-A. The viscosity has been calculated by means of the Lohrenz Bray Clark method and the Friction Theory in prediction mode and after tuning methods. The results are compared with experimental data in figure 6.5 and 6.6.

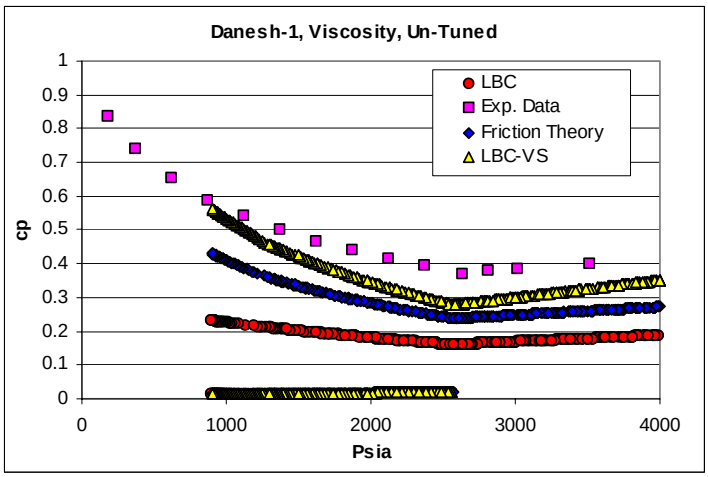

Figure 6.5. Experimental viscosity data for the Danesh-1 oil is compared to predictions using the Friction theory method and the LBC method respectively. The results from the LBC method are generated first with no Peneloux shift (LBC) and by using volume shift for the pseudo components (LBC-VS). It is seen that the LBC-VS predicts the viscosity within about 26 % while the Friction theory prediction is within 38%.

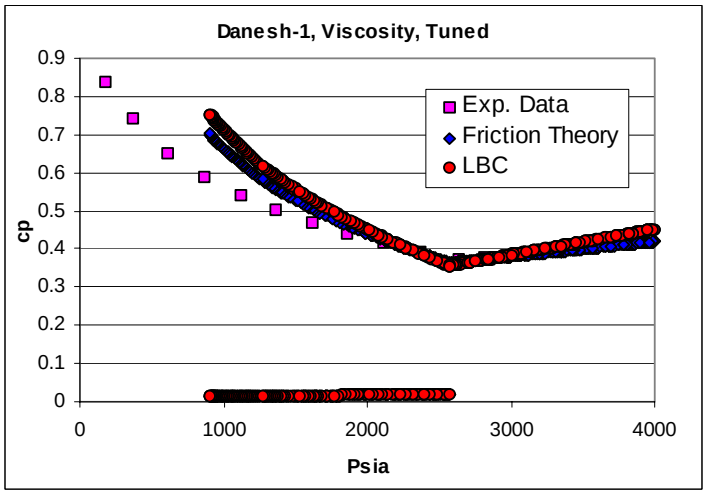

Figure 6.6. Experimental viscosity data compared to calculated values after tuning the LBC and the Friction theory methods. It is seen that the friction theory method is reproducing the experimental data very well, especially above the saturation point while at lower pressures the method overpredicts slightly. The tuned LBC method gives reasonable results, however, it is seen that the shape of the curve is wrong with a max deviaton of some 16% above the saturation pressure and about 25% below.

6.8.4 Danesh-2

The results for the Danesh-2 oil is given in the figures below. The composition of the oil is given in table 7 in Appendix-A. The oil has been characterised by the 11 base component and 4 pseudo-components covering the C7+ fraction. The characterisation is given in table 8 in Appendix-A. The viscosity has been calculated by means of the Lohrenz Bray Clark method and the Friction Theory in prediction mode and after tuning methods. The results are compared with experimental data in figure 6.7 and 6.8.

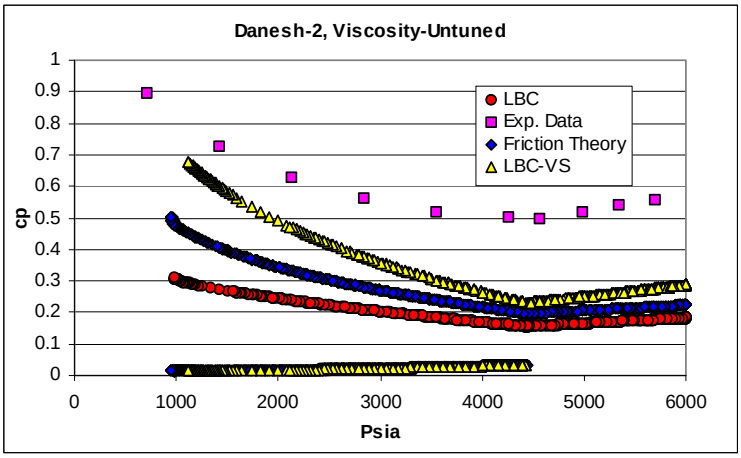

Figure 6.7. Experimental viscosity data for the Danesh-2 oil is compared to predictions using the Friction theory method and the LBC method respectively. The results from the LBC method are generated first with no Peneloux shift (LBC) and by using volume shift for the pseudo components (LBC-VS). It is seen that both the LBC-VS and the FT predictions are in excess of 50%.

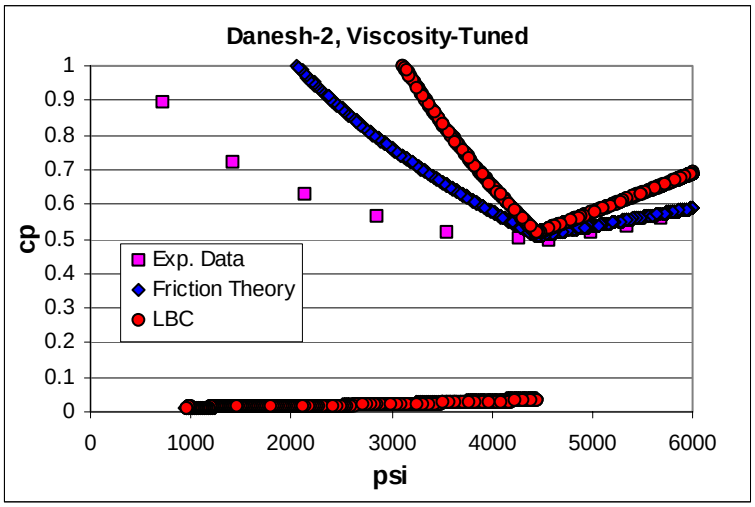

Figure 6.8. Experimental viscosity data compared to calculated values after tuning the LBC and the Friction theory methods. It is seen that for this oil the LBC model fails to reproduce the viscosity above and below the saturation point while the the Friction Theory method is reproducing the experimental data very well above the saturation pressures but fails below.

6.8.5 NSO-1

The results for the NSO-1 oil is given in the figures below. The composition of the oil is given in table 9 in Appendix-A. The oil has been characterised by the 11 base component and 4 pseudo-components covering the C7+ fraction. The characterisation is given in table 10 in Appendix-A. The viscosity has been calculated by means of the Lohrenz Bray Clark method and the Friction Theory in prediction mode and after tuning methods. The results are compared with experimental data in figure 6.9 and 6.10.

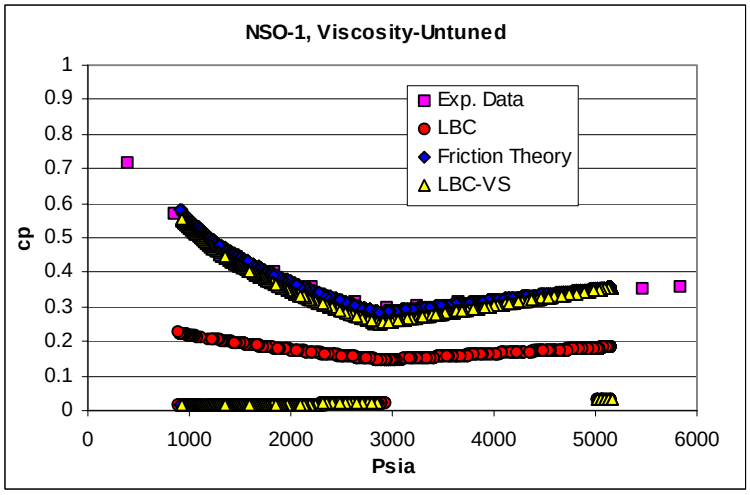

Figure 6.9. Experimental viscosity data for the NSO-1 oil is compared to predictions using the Friction theory method and the LBC method respectively. The results from the LBC method are generated first with no Peneloux shift (LBC) and by using volume shift for the pseudo components (LBC-VS). The FT predicts the viscosity within 3% while the LBC-VS is within 17 %.

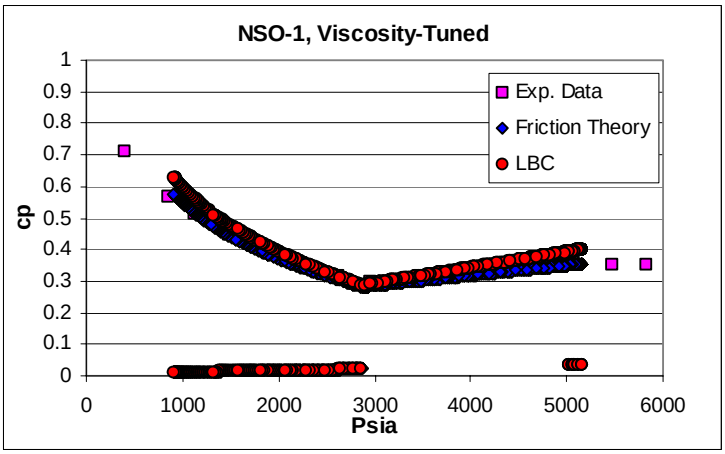

Figure 6.10. Experimental viscosity data compared to calculated values after tuning the LBC and the Friction theory methods. It is seen that for this oil the LBC model reproduces the viscosity with reasonable accuracy with deviations of some 12 % at high and low pressures. The Friction Theory method is reproducing the experimental data very well throughout.

6.8.6 NSO-2

The results for the NSO-2 oil is given in the figures below. The composition of the oil is given in table 11 in Appendix-A. The oil has been characterised by the 11 base component and 4 pseudo-components covering the C7+ fraction. The characterisation is given in table 12 in Appendix-A. The viscosity has been calculated by means of the Lohrenz Bray Clark method and the Friction Theory in prediction mode and after tuning methods. The results are compared with experimental data in figure 6.11 and 6.12.

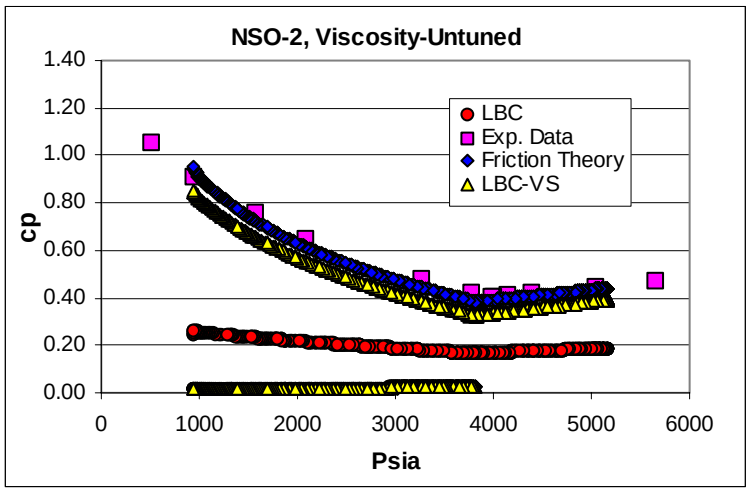

Figure 6.11. Experimental viscosity data for the NSO-2 oil is compared to predictions using the Friction theory method and the LBC method respectively. The results from the LBC method are generated first with no Peneloux shift (LBC) and by using volume shift for the pseudo components (LBC-VS). The FT predicts the viscosity within 5% while the LBC-VS exhibits a deviation of some 20 %.

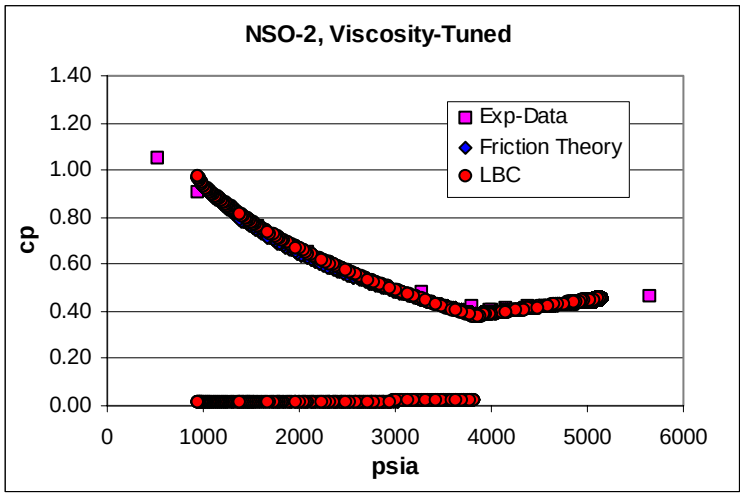

Figure 6.12. Experimental viscosity data compared to calculated values after tuning the LBC and the Friction theory methods. It is seen that for this oil, both models reproduce the viscosity with good accuracy (less than 5%).

6.8.7 NSO-3

The results for the NSO-3 oil is given in the figures below. The composition of the oil is given in table 13 in Appendix-A. The oil has been characterised by the 11 base component and 4 pseudo-components covering the C7+ fraction. The characterisation is given in table 14 in Appendix-A. The viscosity has been calculated by means of the Lohrenz Bray Clark method and the Friction Theory in prediction mode and after tuning methods. The results are compared with experimental data in figure 6.13 and 6.14.

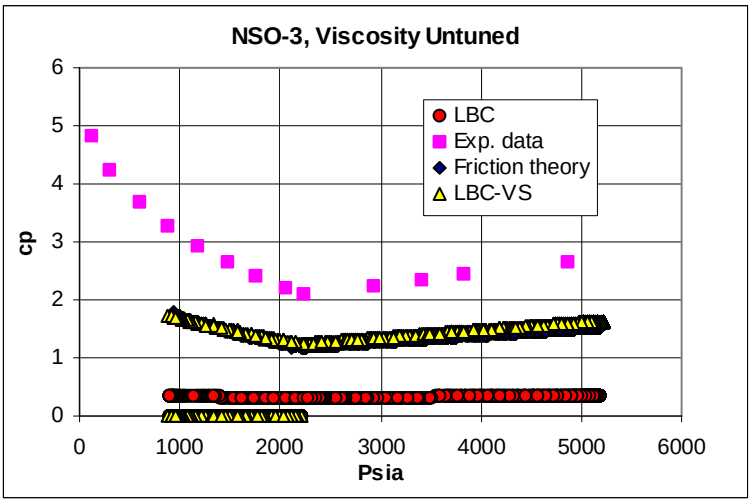

Figure 6.13. Experimental viscosity data for the NSO-3 oil is compared to predictions using the Friction theory method and the LBC method respectively. The results from the LBC method are generated first with no Peneloux shift (LBC) and then by using volume shift for the pseudo components (LBC-VS). For this oil the LBC-VS predicts the viscosity within some 40% and the Friction theory prediction is within 43%.

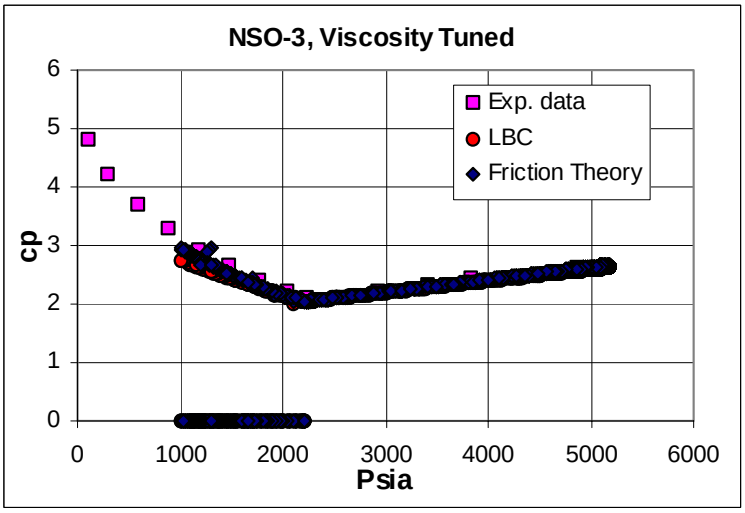

Figure 6.14: Experimental viscosity data compared to calculated values after tuning the LBC and the Friction theory methods. It is seen that for this oil both models reproduce the viscosity with good accuracy (less than 5%).

6.8.8 Elf-1

The results for the ELF-1 oil is given in the figures below. The composition of the oil is given in table 15 in Appendix-A. The oil has been characterised by the 11 base component and 4 pseudo-components covering the C7+ fraction. The characterisation is given in table 16 in Appendix-A. The viscosity has been calculated by means of the Lohrenz Bray Clark method and the Friction Theory in prediction mode and after tuning methods. The results are compared with experimental data in figure 6.15 and 6.16.

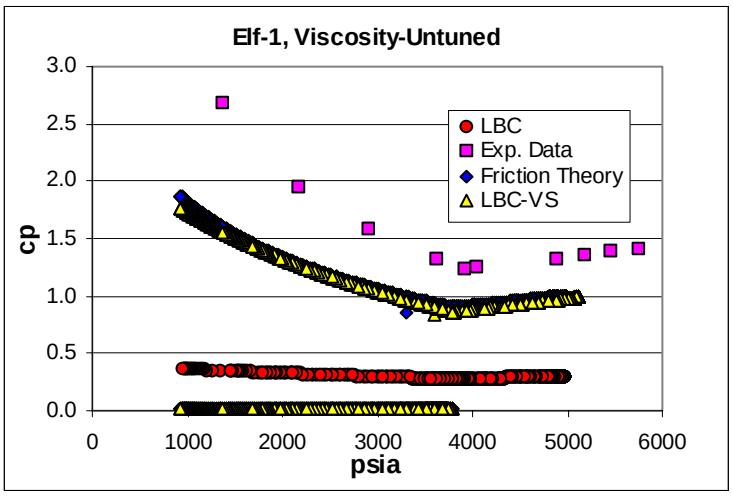

Figure 6.15. Experimental viscosity data for the Elf-1 oil is compared to predictions using the Friction theory method and the LBC method respectively. The results from the LBC method are generated first with no Peneloux shift (LBC) and then by using volume shift for the pseudo components (LBC-VS). It is seen that the LBC-VS predicts the viscosity within some 34% and the Friction theory prediction is within 30%.

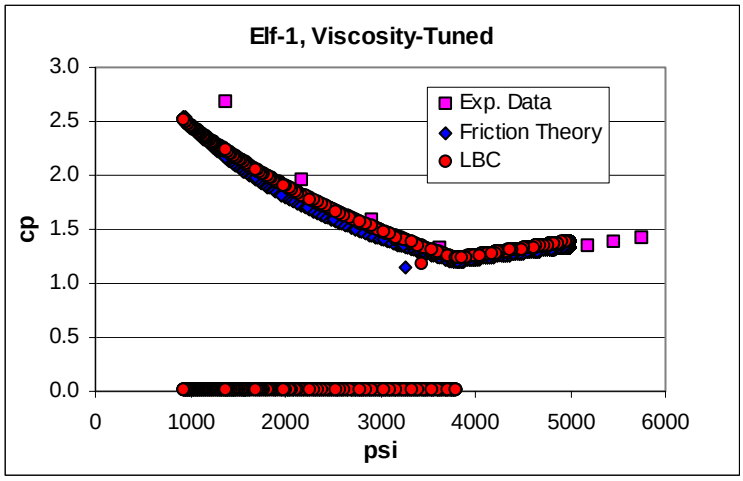

Figure 6.16. Experimental viscosity data compared to calculated values after tuning the LBC and the Friction theory methods. It is seen that for this oil both models reproduce the viscosity with good accuracy at high pressure. Below 2000 psia the deviation increases above 10 %.

6.8.9 Elf-23

The results for the ELF-23 oil is given in the figures below. The composition of the oil is given in table 17 in Appendix-A. The oil has been characterised by the 11 base component and 4 pseudo-components covering the C7+ fraction. The characterisation is given in table 18 in Appendix-A. The viscosity has been calculated by means of the Lohrenz Bray Clark method and the Friction Theory in prediction mode and after tuning methods. The results are compared with experimental data in figure 6.17 and 6.18.

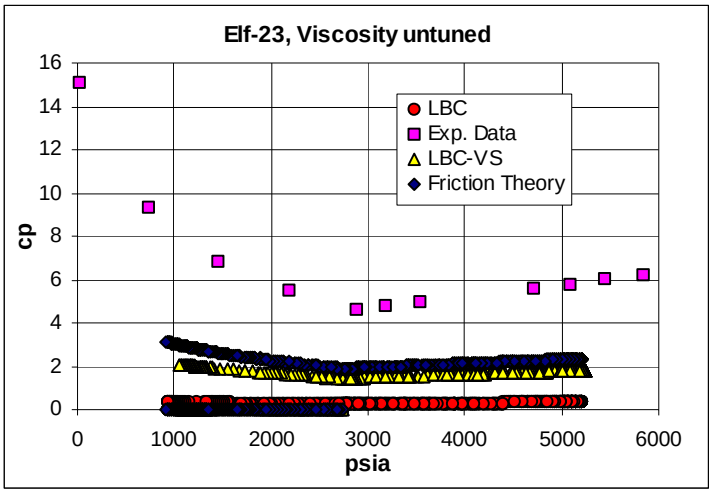

Figure 6.17. Experimental viscosity data for the Elf-23 oil is compared to predictions using the Friction theory method and the LBC method respectively. The results from the LBC method are shown first with no Peneloux shift (LBC) and then by using volume shift for the pseudo components (LBC-VS). For this oils both the FT method and the LBC predictions are more than 50 % lower than the experimental measurements.

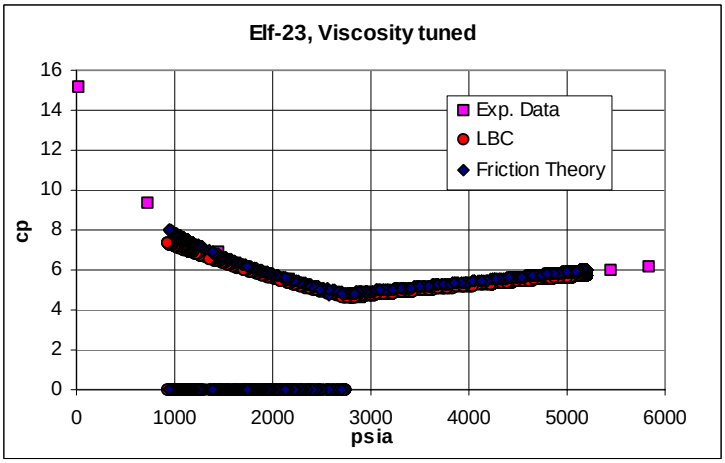

Figure 6.18. Experimental viscosity data compared to calculated values after tuning the LBC and the Friction theory methods. Both models reproduce the viscosity with good accuracy after tuning.

6.8.10 Elf-24

The results for the ELF-24 oil is given in the figures below. The composition of the oil is given in table 19 in Appendix-A. The oil has been characterised by the 11 base component and 4 pseudo-components covering the C7+ fraction. The characterisation is given in table 20 in Appendix-A. The viscosity has been calculated by means of the Lohrenz Bray Clark method and the Friction Theory in prediction mode and after tuning methods. The results are compared with experimental data in figure 6.19 and 6.20.

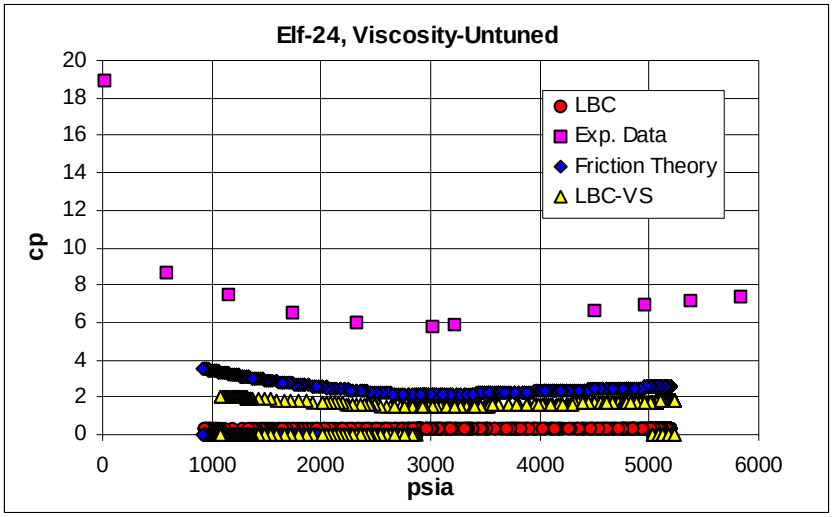

Figure 6.19. Experimental viscosity data for the Elf-24 oil is compared to predictions using the Friction theory method and the LBC method respectively. The results from the LBC method are generated first with no Peneloux shift (LBC) and then by using volume shift for the pseudo components (LBC-VS).

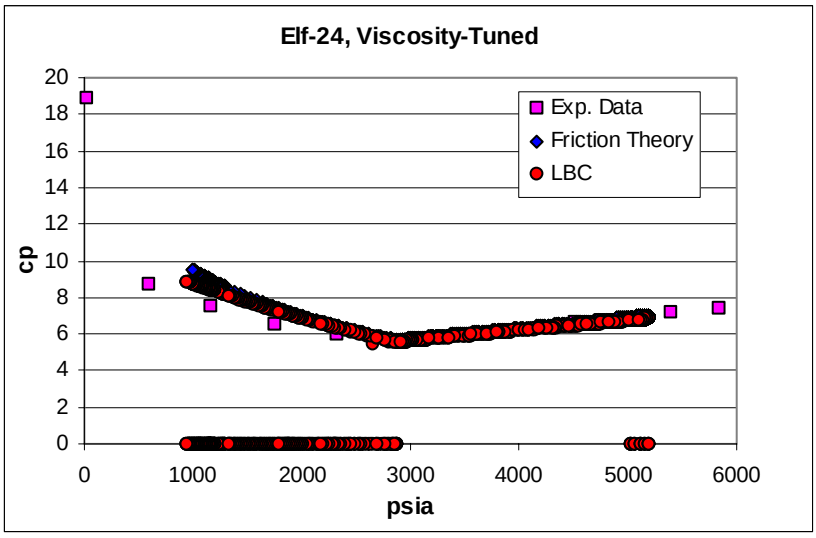

Figure 6.20. Experimental viscosity data compared to calculated values after tuning the LBC and the Friction theory methods. It is seen that for this oil both models reproduce the viscosity with good accuracy.

6.8.11 Elf-26

The results for the ELF-26 oil is given in the figures below. The composition of the oil is given in table 21 in Appendix-A. The oil has been characterised by the 11 base component and 4 pseudo-components covering the C7+ fraction. The characterisation is given in table 22 in Appendix-A. The viscosity has been calculated by means of the Lohrenz Bray Clark method and the Friction Theory in prediction mode and after tuning methods. The results are compared with experimental data in figure 6.21 and 6.22.

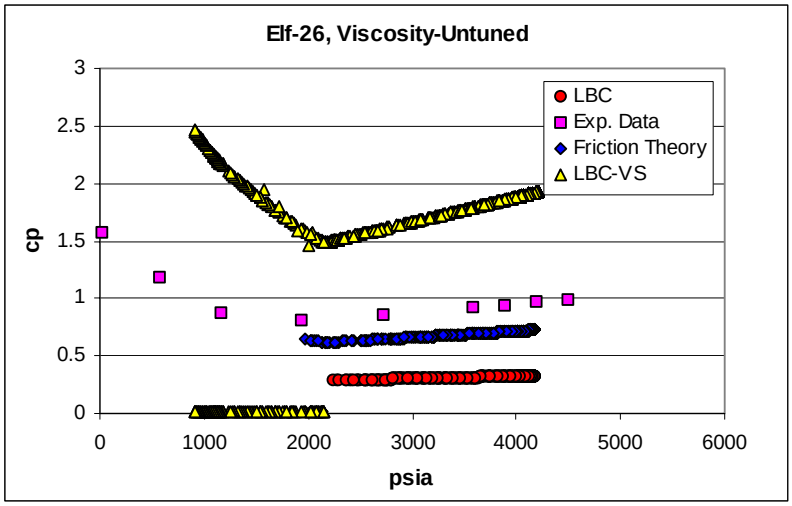

Figure 6.21. Experimental viscosity data for the Elf-26 oil is compared to predictions using the Friction theory method and the LBC method respectively. The results from the LBC method are generated first with no Peneloux shift (LBC) and then by using volume shift for the pseudo components (LBC-VS). It is seen that for this oil the LBC-VS predicts the viscosity to be close to 100% higher than the experimental values. The Friction Theory prediction is within 25%.

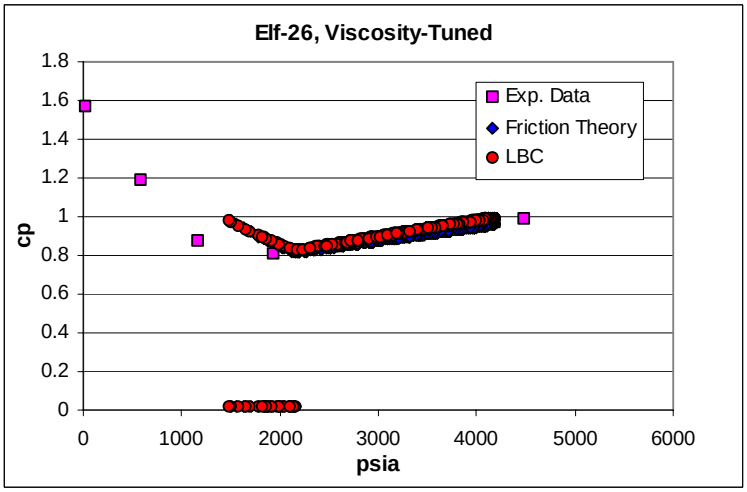

Figure 6.22. Experimental viscosity data compared to calculated values after tuning the LBC and the Friction theory methods. It is seen that for this oil both models reproduce the viscosity with good accuracy above saturation pressure while below saturation pressure both models tend to over predict the viscosity.

6.8.12 Chevron-2

The results for the Chevron-2 oil is given in the figures below. The composition of the oil is given in table 23 in Appendix-A. The oil has been characterised by the 11 base component and 4 pseudo-components covering the C7+ fraction. The characterisation is given in table 24 in Appendix-A. The viscosity has been calculated by means of the Lohrenz Bray Clark method and the Friction Theory in prediction mode and after tuning methods. The results are compared with experimental data in figure 6.23 and 6.24.

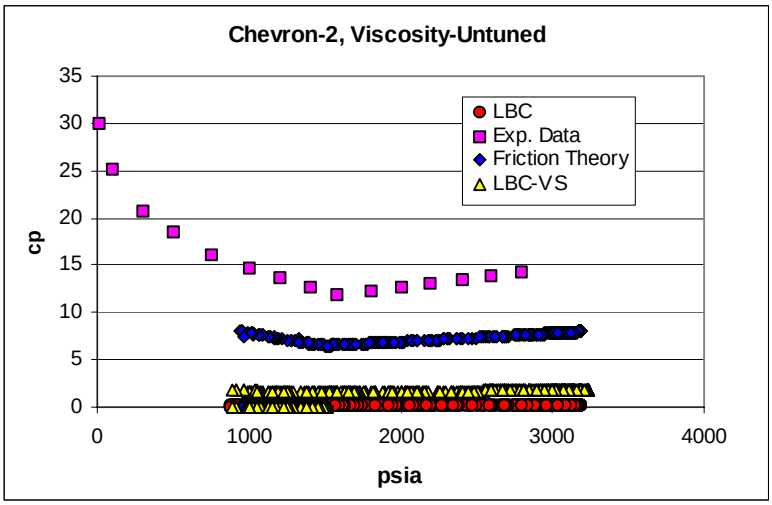

Figure 6.23. Experimental viscosity data for the Chevron-2 oil is compared to predictions using the Friction theory method and the LBC method respectively. The results from the LBC method are generated first with no Peneloux shift (LBC) and then by using volume shift for the pseudo components (LBC-VS). It is seen that the LBC-VS prediction is in excess of 80% lower than experimental data while the Friction theory prediction is between 40 and 50% lower.

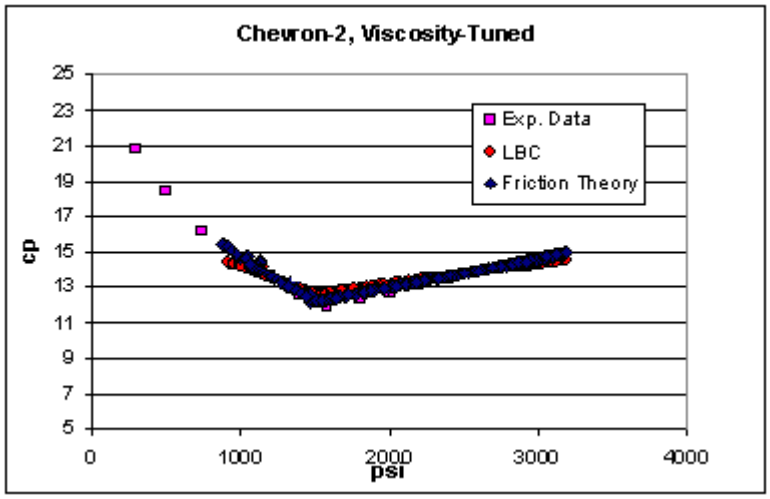

Figure 6.24. Experimental viscosity data compared to calculated values after tuning the LBC and the Friction theory methods. It is seen that for this oil the tuned Friction Theory method accurately reproduces the experimental data. The tuned LBC model reproduces the experimental data within 5%, due to an incorrect slope of the data curve.

6.9 Chevron-1, Gas Injection

A miscible gas injection example where the Chevron-1 oil is displaced by CO_2 is presented here. The following figure shows the viscosity of the resultant mixture calculated by the tuned LBC and the FT methods. We do not attempt to analyze or evaluate the viscosity calculation in a quantitative sense, as we do not have experimental data to support this. We can however use the figure to compare the performance of viscosity calculation models to identify deviations between the models that are not consistent with the initial tuning.

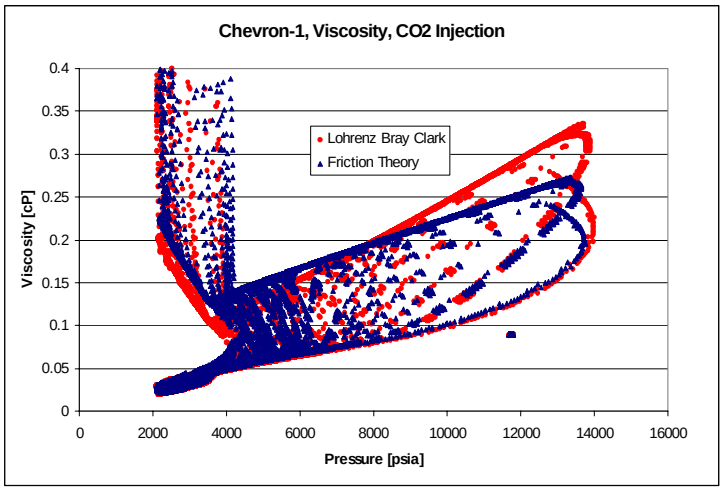

Figure 6.25: The Chevron-1 system has been run with CO_2 injection using both the Friction Theory and the LBC methods. It is seen that the depletion lines from figure 6.4 are unchanged. Further more is is seen that the models qualitatively behave in the same manner when introducing a higher fraction of CO_2 into the system.

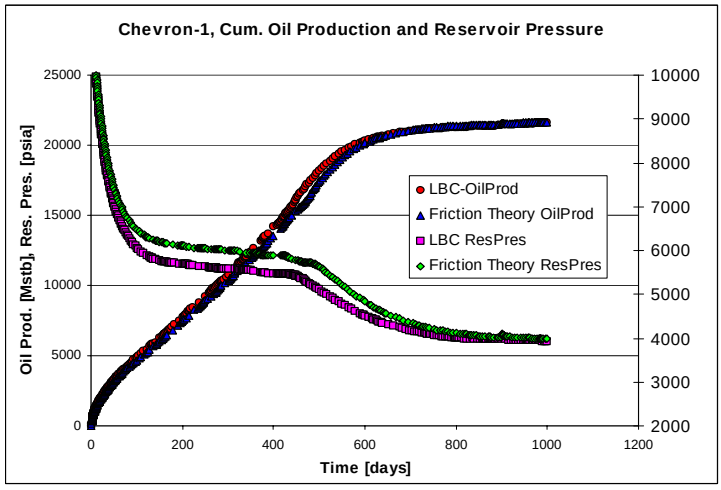

Figure 6.26: The figure shows cumulative oil production and average reservoir pressure when using the 2 viscosity models respectively for the Chevron-1 oil in a CO_2 gas injection. Both models seem to give consistent results for this system. The difference in average reservoir pressure between the models is explained by the initial viscosity difference between the two tuned models.

The comparison is carried out to investigate to which extent the outcome of the simulations differ when using one or the other viscosity calculation

method. The results from this comparison show that the both models appear to behave consistent and the observed difference in the production performance is related to the initial difference between the tuned models rather than to the gas injection.

6.10 Conclusion

Table 6.2 shows the deviation of the viscosity models relative to the experimental data in prediction mode and after tuning. The deviation is evaluated at pressures above the saturation pressures. At lower pressures below the saturation pressure the deviations in some cases are higher than tabulated here. It is seen that the LBC model in all the cases significantly under-predicts the viscosity and that the predictions deteriorate for the heavier oils. For the heaviest oil, the Chevron-2 oil, the LBC prediction is more than 20 times lower than the experimental data.

The deviations from experimental values are plotted in figure 6.27. It is seen that the FT method is the most accurate model and that for 2 of the oils the predicted values are within 5%. After tuning the FT model is capable of reproducing the viscosity above saturation pressure for all the oils with a deviation of less than 3%. The tuned LBC model reproduces 6 of the oils within 3% deviation while for the remaining 6 oils, the deviation ranges from 4 to 16 %.

	Exp. Data [cP]	FT %	LBC %	LBC-VS %	FT-tuned %	LBC-tuned %
AM-1	3	40	90	58	< 1	< 1
Chevron-1	0.13	15	38	23	< 1	15
Danesh-1	0.39	38	56	26	< 1	7
Danesh-2	0.5	60	70	54	< 2	16
NSO-1	0.3	3	50	17	< 1	14
NSO-2	0.41	5	59	20	3	4
NSO-3	2.1	43	81	40	3	< 1
Elf-1	1.28	30	77	34	< 1	< 2
Elf-23	4.4	50	93	64	< 2	< 2
Elf-24	5.9	66	94	75	< 2	< 2
Elf-26	0.85	25	65	*~100*	< 2	< 2
Chevron-2	12	42	95	83	3	5

Table 6.2: The table gives the deviations in % from experimental viscosity data above saturation pressure before and after tuning. It is seen that the tuned FT model consistently reproduces the viscosity with a very good accuracy of 3% deviation or less. All predicted values are lower than the experimental data except the LBC-VS prediction of the Elf-26 oil.

From the results presented here it is clear that the Friction Theory method is superior to the Lohrenz Bray Clark method. The simple tuning provided results with a deviation of less than 3% for all 12 oils tested here. The FT method does not increase computing time compared to the LBC method.

The method is presently being improved further for a wider range of oils.

A single gas injection case was presented where we compared the production performance of the tuned LBC model to the tuned FT model, in order to investigate if the models exhibited a different behavior when subjected to gas injection rather than depletion. From the production and pressure curves in figure 6.26 it is seen that the models behave consistent. In order to evaluate if the actual viscosity values are accurate it is necessary to compare to experimental data of oil-CO_2 mixtures, e.g. obtained from swelling tests.

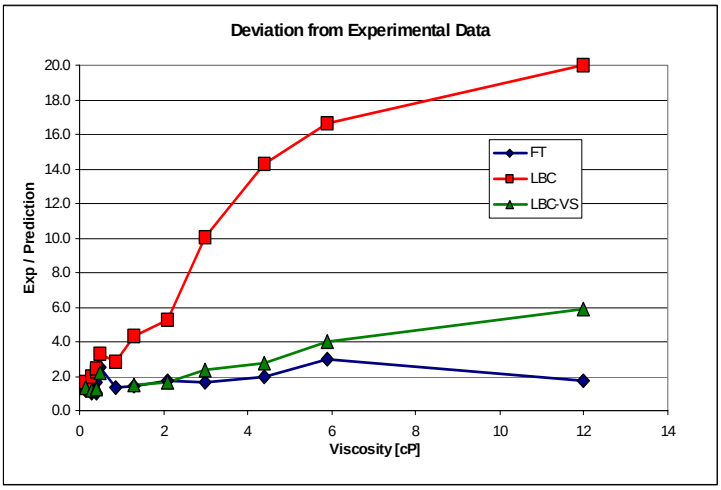

Figure 6.27: The figure illustrates the ratio between experimental data and model results when using the LBC, the LBC-VS and the FT methods respectively for the 12 oils ranging from 0.13 cP to the heaviest oil of 12 cP.

6.11 Suggestions for future work

The Friction Theory model provides for much improved viscosity calculations compared to the normally used Lohrenz Bray Clark model. In order to build further confidence in the Friction Theory model for gas injections studies it is suggested that the model is tested against experimental data on mixtures of oils and injection gases at realistic reservoir conditions.

7 References:

1. Stone H.L., *Rigorous Black Oil Pseudo Functions*, SPE 21207, 1991
2. Zhang H.R, Sorbie K.S., *The Upscaling of Miscible and Immiscible Displacement Processes in Porous Media*, SPE 29931, 1995
3. Darman N.H., Sorbie K.S., Pickup G.E.,*The Development of Pseudo Functions for Gravity Dominated Immiscible Gas Displacements*, SPE-51941, 1999
4. Chase C.A., Todd M.R., *Numerical Simulation of CO2 Flood Performance*, SPE-10514, 1984
5. Darman N.H., Sorbie K.S., Pickup G.E., *Upscaling Immiscible Gas Displacements: Quantitative Use of Fine Grid Flow Data in Grid Coarsening Schemes*, SPE59452, 2000
6. Kyte J.R., Berry D.W., *New Pseudo Functions to Control Numerical Dispersion*, SPE-5105, 1975
7. Fayers F.J., Haajizadeh M., Lin C.Y., Taggart J., *Use of the 4-Component Todd and Langstaff Method as an Upscaling Technique in Simulating Gas Injection Projects*, SPE-59340, 2000
8. Zhou D., Jensen C., Tang R., Arif H., *A New Formulation for Simulating Near Miscible Displacement Processes*, SPE-56623, 1999
9. Peters B.M., Zhou D., Blunt M.J., *Experimental Investigation of Scaling Factors that Describe Miscible Floods in Layered Systems*, SPE-39624, 1999
10. Christie M.A., King P.R., Barker J.W., Culverville I.D., *A Renormalisation Based Upscaling Technique for WAG Floods in Heterogeneous Reservoirs*, SPE-29127, 1995
11. King M.J., Blunt M.J., Mansfield M., Christie M.A., *Rapid Evaluation of the Impact of Heterogeneity on Miscible Gas Injection*, SPE-26079, 1993
12. Wallstrom T.C., Hou S., Christie M.A., Durlofsky L.J., Sharp D.H., *Application of a new Two Phase Upscaling Technique to Realistic Reservoir Cross Sections*, SPE-51939, 1999
13. Christie M.A., Clifford P.J., *Fast Procedure for Upscaling Compositional Simulation*, SPE-50992, 1998
14. Christie M.A., Blunt M.J., Tenth SPE Comparative Solution Project: *A Comparison of Upscaling Techniques*, SPE-66599, 2001

15. Fayers F.J., Foakes A.P., Lin C.Y., Pucket D.A., *An Improved Three Phase Flow Model Incorporating Compositional Variance,* SPE-59313, 2000

16. Wallstrom T.C., Hou S., Christie M.A., Durlofsky L.J., Sharp D.H., Zou Q., *Effective Medium Boundary Conditions for Upscaling Relative Permeabilities*, Transport in Porous Media, 1999

17. Wallstrom T.C., Hou S., Christie M.A., Durlofsky L.J.,Sharp D.H., Zou Q., *Application of Effective Flux Boundary Conditions to two phase upscaling in Porous Media.*, Submitted to Transport in Porous media, 2001

18. Wallstrom T.C., Hou S., Christie M.A., Durlofsky L.J., Sharp D.H., Zou Q., *Effective Flux Boundary Conditions for Upscaling Porous Media Equations*, Submitted to Transport in Porous media, 2001

19. Hearn C.L., *Simulation of Stratified Waterflooding by Pseudo relative Permeability Curves,* SPE-2929, 1971

20. Barker J.W., Fayers F.J., *Transport Coefficients for Compositional Simulation with Coarse Grids in Heterogeneous Media,* SPE-22591, 1991

21. Todd M.R., Longstaff W.J., *The Development, Testing and Application of a Numerical Simulator for Predicting Miscible Flood Performance.*, SPE-3483, 1972

22. Barker J.W., Thibeau S., *A Critical Review of the Use of Pseudo Relative Permeabilities for Upscaling*, SPE-35491, 1996

23. Blackwell R.J., Rayne J.R., Terry W.M., *Factors Influencing the Efficiency of Miscible Displacement,* AIME, 1959

24. Thiele M.R., Batycky R.P., Blunt M.J., Orr F.M., *Simulating Flow in Heterogeneous Systems Using Streamtubes and Streamlines,* SPE-27834, 1996

25. Johns R.T., Fayers F.J., Orr F.M., *Effect of Gas Enrichment and Dispersion on nearly Miscible Displacements in Condensing/Vaporizing Drives,* SPE-24938, 1992

26. Kossack C.A., *The Multiple Step Scale-Up Process Using Pseudo Functions in Heterogeneous reservoirs: A Numerical Validation of the Process.*, SPE-21623, 1990

27. Fanchi J.R., *Integrated Flow of Modelling of Miscible Gas Injection Processes,* SPE-59342, 2000

28. Arbogast T., Bryant S.L., *Numerical Subgrid Upscaling for Waterflood Simulations,* SPE-66375, 2001.

29. Lenormand R., *Calculation of Fractional Flow for Dynamic Upscaling,* IEA Proc 1999

30. Nekrassov A., Behr A., Brusilovsky A., Hafner F., Polonsky D., *Approximation of the Mass Exchange, Convection and Dispersion Fluxes in the Compositional Reservoir Simulation,* SPE-66387, 2001.

31. Thiele M.R., Batycky R.P., Blunt M.J., *A Streamline Based 3D Field Scale Compositional Reservoir Simulator*, SPE-38889, 1997.

32. Zhou D., Fayers F.J., Orr F.M., *Scaling of Multiphase Flow in Simple Heterogeneous Porous Media,*SPE-27833, 1994

33. Jessen K., Stenby E.H., Orr F.M., *Interplay of Phase Behavior and Numerical Dispersion in Finite Difference Compositional Simulation,* SPE-75134, 2002

34. Al-Syabi Z., Danesh A., Tohidi B., Todd A.C., Tehrani D.H., *A Residual Correction for Predicting the Viscosity of Petroleum Reservoir Fluids over Wide Ranges of Pressure and Temperature.Chemical Engineering Science*, SPE-2001.

35. Quinones-Cisneros S.E., Zéberg-Mikkelsen C.K., Stenby E.H., *The Friction Theory for Viscosity Modeling: extension to crude oil systems*, Chemical Engineering Science, 2001.

36. Lohrenz J., Bray B.G., Clark C.R., *Calculating Viscosities of Reservoir Fluids from their Compositions*, JPT, 1964.

37. Thiele M.R., Blunt M.J., Orr F.M., *Modelling Flow in Heterogeneous Media using Streamtubes I, Miscible and Immiscible Displacements,* In Situ, 1995.

38. Thiele M.R., Blunt M.J., Orr F.M., *Modelling Flow in Heterogeneous Media using Streamtubes II, Compositional Displacements,* In Situ, 1995.

39. Jacks H.H., Smith O.J.E., Mattax C.C., *The Modelling of a Three Dimensional Reservoir with a Two Dimensional Reservoir Simulator - The Use of Dynamic Pseudo Functions,* SPE 4071, 1973

40. Coats K.H., Dempsey J.R., Henderson J.H., *The Use of Vertical Equilibrium in Two-Dimensional Simulation of Three-Dimensional Reservoir Performance,* SPE-2797, 1972

41. Soave G., *Equilibrium Constants from a Modified Redlich Kwong Equation of State,* Chem. Eng. Sci.,27, 1197-1203, 1972

42. Peng D.Y., Robinson D.B., *A new Two-Constant Equation of State,* Ind. Eng. Chem. Process Des. Dev., 15(1), 59-64, 1976

43. Peneloux A., Rauzy E., Freze R., *A Consistent Correction for Redlich-Kwong-Soave Volumes,* J. Fluid Phase Equilibria, 8, 7-23, 1982

44. Macleod D.B., *On a Relation Between Surface Tension, Density,* Trans. Faraday Soc., 19, 38-43, 1923

45. Sugden S., *The Parachors and Valency (Routledge 1930); A List of Parachors,* Brit. Assoc. Report. 1932

46. Durlofsky L.J., Jones R.C., Milliken W.J., *A nonuninform coarsening approach for the scale up of displacement processes in heterogeneous porous media,* Advances in water resources 20, 335-347, 1997

47. Danesh A., *PVT and Phase Behavior of Petroleum Reservoir Fluids*

48. Whitson C. H., Brulé M. R., *Phase Behavior,* SPE Monograph Volume 20

49. Pedersen K. S., Fredenslund Aa., Thomassen P., *Properties of Oils and Natural Gases*

50. Gelhar L.W., Axnes C.L., *Three Dimensional Stochastic Analysis of Macrodispersion in Aquifers,* Water Resources Research 19, no 1, 161-180, 1983

51. Christie M.A., Bond D.J., *Detailed Simulation of Unstable Processes in Miscible Flooding,* SPE-14896, 1987

52. Christie M.A., *Numerical Techniques for High Resolution Simulation of Instabilities,* SPE-16005, 1987

53. Jákupsstovu S., Zhou D., Kamath J. Durlofsky L., Stenby E.H., *Upscaling of Miscible Displacement Processes,* Nordic symposium on Petrophysics no. 6, Trondhjem 2001

54. Quinones-Cisneros S.E., Zéberg-Mikkelsen C.K., Stenby E.H., *One Parameter Friction Theory Model for Viscosity,* Fluid Phase equilibria 178 (2001) 1-16, 2001

55. Zhang D., Soll W.E., *Uncertainty and Upscaling in Porous Media Flow,* Earth and Environmental sciences, Prog. Rep. 1998-2000

56. Stryjek R., Vera J.H., *An improved Peng Robinson Equation of State for Pure Compounds and Mixtures,* Canadian jouirnal of Chemical Engineering Vol 64, April 1986

57. Blunt M., Christie M., *Theory of Viscous Fingering in Two Phase, Three Component Flow,* SPE Advanced Technology Series, April 1994

58. Christie M.A., Bond D.J., *Multidimensional Flux-Corrected Transport for Reservoir Simulation* 13505, 1985

59. Lenormand R., Thierry A., Wang B., *Transport Equations for Miscible Displacement in Heterogeneous Porous Media: A Streamtube Approach,* ECMOR 4, Røros, Norway 1994

60. Stoneley R., *An Introduction to Petroleum Exploration for Non Geologists,* Oxford, JAPEC

61. Dake L.P., *Fundamentals of Reservoir Engineering,* Elsevier

8 Appendix A: Reservoir Fluids

All the oils have been characterised by the following components:

N2, CO2, H2S, C1, C2, C3, iC4, nC4, iC5, nC5, C6, C7+

The C7+ fraction has been characterised by 4 pseudo-components. This means that the oils are characterised by a total of 15 components if the oil contains H_2S, otherwise by 14 components. The characterisation has been carried out by means of the SPECS PVT software developed at the IVC-SEP at the Technical University of Denmark. The initial characterisation is adjusted until the experimentally determined saturation pressure is matched. This has been carried out by adjusting the specific gravity of the plus fraction until a match has been accomplished.

The critical parameters for the 11 base components are tabulated values and can be found in several references. We have used the tables given in Ali Danesh's book [47]. The Peng Robinson Equation of state is used in the simulations and therefore the same EOS has been selected to characterize the oils in SPECS.

The critical parameters for the 11 base components common to all the oils are given in the following table.

Component	**T_c**	**P_c**	**V_c**	**ω**	**MW**	**η_c**
Name	**[K]**	**Bar**	**Cc/mole**		**g/mole**	**micropoise**
N2	126.2000	34.0000	89.2000	0.0380	28.0140	174.1790
CO2	304.2000	73.8300	94.0000	0.2240	44.0100	376.8720
H2S	373.5000	89.6300	98.5000	0.0940	34.0820	600.0000
Methane	190.6000	45.9900	98.6000	0.0120	16.0430	152.9300
Ethane	305.4000	48.7200	145.5000	0.1000	30.0700	217.5620
Propane	369.8000	42.4800	200.0000	0.1520	44.0970	249.7340
i-Butane	408.1000	36.4800	262.7000	0.1770	58.1230	271.1550
n-Butane	425.2000	37.9600	255.0000	0.2000	58.1230	257.6820
i-Pentane	460.4000	33.8100	305.8000	0.2275	72.1500	275.0730
n-Pentane	469.6000	33.7000	313.0000	0.2520	72.1500	258.6510
Hexane	507.4000	30.2500	371.0000	0.3013	86.1770	257.8410

Table A1, Base Component Properties

Oil #1 AM-1

		Oil #1			
		mole %			mole %
1	Nitrogen	0.07	26	Hexadecanes	2.82
2	Carbon Dioxide	0.06	27	Heptadecanes	3.06
3	Hydrogen Sulfide	0	28	Octadecanes	2.57
4	Methane	42.06	29	Nonadecanes	1.97
5	Ethane	1.56	30	Eicosanes	1.99
6	Propane	0.2	31	Uncosanes	1.79
7	i-Butane	0.15	32	Docosanes	1.62
8	n-Butane	0.17	33	Tricosanes	1.43
9	i-Pentane	0.22	34	Tetracosanes	1.27
10	n-Pentane	0.21	35	Pentacosanes	1.16
11	Hexane	0.56	36	Hexacosanes	1.08
12	Benzene	0.04	37	Heptacosanes	1.03
13	Heptanes	1.67	38	Octacosanes	0.98
14	Tolouene	0.19	39	Nonacosanes	0.95
15	Octanes	2.07	40	Triacontanes	0.88
16	Ethylbenzene	0.08	41	Uncontanes	0.78
17	Xylenes	0.23	42	Docontanes	0.67
18	Nonanes	1.52	43	Tricontanes	0.6
19	Decanes	2.09	44	Tetracontanes	0.51
20	Undecanes	2.1	45	Pentacontanes	0.49
21	Dodecanes	2.28			
22	Tridecanes	2.81	46	Tetracontanes	0.51
23	Tridecanes	2.81	47	Pentacontanes	0.49
24	Tetradecanes	3.12			
25	Pentadecanes	3.16	48	Hexacontanes plus	5.73

Table A2. Oil #1

Component	Z	TC	Pc	Vc	OM	MW	nc	
Name		[K]	Bar	cc/mole			Micropoise	
C7	0.278	619.588	26.990	492.206	0.477	142.732	292.628	552.21
C16	0.126	708.932	17.558	795.632	0.842	263.266	291.761	550.57
C24	0.088	796.553	14.738	1001.466	1.145	396.090	312.309	589.35
C36	0.055	952.401	13.291	1232.908	1.314	652.425	363.165	685.31

Table A3. Oil #1 - Characterisations of Pseudocomponents

Oil #2 Chevron-1

	Oil #2			
	mole %	weight %		
Hydrogen Sulfide	12.39	7.8		
Carbon Dioxide	3.01	2.45		
Nitrogen	0.82	0.43		
Methane	44.13	13.08		
Ethane	8.78	4.88		
Propane	4.58	3.73		
i-Butane	1.05	1.13		
n-Butane	2.67	2.87		
i-Pentane	1.36	1.82		
n-Pentane	1.41	1.88		
Hexane	2.27	3.52		
Heptanes	2.51	4.44		
Octanes	2.69	5.32		
Nonanes	2.12	4.74		
Decanes	1.75	4.33		
Undecanes	1.32	3.59		
Dodecanes	1.04	3.1		
Tridecanes	0.96	3.12		
Tetradecanes	0.75	2.64		
Pentadecanes	0.66	2.52		
Hexadecanes	0.52	2.13		
Heptadecanes	0.43	1.87		
Octadecanes	0.38	1.78		
Nonadecanes	0.36	1.76		
Heptanes plus	17.53	56.41		
Undecanes plus	8.46	37.58		
Eicosanes plus	2.04	15.07		

Table A4. Oil #2

Component	Z	TC	Pc	Vc	OM	MW	nc	
Name		[K]	Bar	cc/mole			micropoise	
C7	0.073	627.550	30.610	445.090	0.181	107.283	275.322	489.78
C10	0.055	651.647	25.296	544.619	0.400	157.441	291.874	477.33
C15	0.028	697.771	20.840	681.618	0.714	235.173	309.944	469.86
C21	0.020	795.973	17.847	861.954	1.169	379.896	347.537	454.12

Table A5. Oil #2 Characterisation of Pseudo components

Oil #3 Danesh-1 (Good Oil)

	Oil #3			
	mole %	weight %	MW	Density
Nitrogen	0.16	0.05		
Carbon Dioxide	0.91	0.43		
Hydrogen Sulfide	0	0		
Methane	36.47	6.24		
Ethane	9.67	3.1		
Propane	6.95	3.27		
i-Butane	1.44	0.89		
n-Butane	3.93	2.44		
i-Pentane	1.44	1.11		
n-Pentane	1.41	1.09		
Hexane	4.33	3.97		
Heptanes +	33.29	77.41		

Table A6. Oil #3

Component	Z	TC	Pc	Vc	OM	MW	nc	
Name		[K]	Bar	cc/mole			micropoise	
C7	0.1574	601.289	30.437	430.534	0.397	124.675	297.796	518.099
C10	0.083	669.778	20.605	664.854	0.679	208.675	291.745	507.572
C15	0.0571	741.824	16.698	859.287	0.958	308.197	302.977	527.114
C21	0.0353	877.735	14.401	1096.274	1.270	509.775	343.293	597.255

Table A7. Oil #3 Characterisation of Pseudo components

Oil #4 Danesh-2 (Ex. 2.1)

	Oil #4			
	mole %	weight %	MW	Density
Nitrogen	0.9			
Carbon Dioxide	1.49			
Hydrogen Sulfide	0			
Methane	51.54			
Ethane	6.57			
Propane	4.83			
i-Butane	0.68			
n-Butane	2.39			
i-Pentane	0.91			
n-Pentane	1.47			
Hexane	2.17			
Heptanes	4.3			
Octanes	3.96			
Nonanes	1.93			
Decanes	1.66			
Undecanes	1.38			
Dodecanes +	13.82			

Table A8. Oil #4

Component	Z	TC	Pc	Vc	OM	MW	nc	
Name		[K]	Bar	cc/mole			micropoise	
C7	0.1185	591.057	37.114	354.041	0.330	109.071	318.820	1116.244
C11	0.0797	655.420	24.970	553.571	0.593	181.232	310.160	1086.596
C17	0.0431	722.593	19.971	727.157	0.857	268.839	320.238	1123.372
C24	0.0291	841.644	17.226	926.305	1.194	432.633	358.865	1260.952

Table A9. Oil #4 Characterisation of Pseudo components

Oil #5 North Sea Oil -1

	Oil #5			
	mole %	weight %		
Nitrogen	0.41			
Carbon Dioxide	0.44			
Hydrogen Sulfide	0			
Methane	40.48			
Ethane	7.74			
Propane	8.2			
i-Butane	1.23			
n-Butane	4.22			
i-Pentane	1.43			
n-Pentane	2.21			
Hexane	2.83			
Heptanes	4.13			
Octanes	4.31			
Nonanes	3.13			
Decanes	2.439			
Undecanes	1.88			
Dodecanes	1.674			
Tridecanes	1.573			
Tetradecanes	1.207			
Pentadecanes	1.232			
Hexadecanes	0.985			
Heptadecanes	0.977			
Octadecanes	0.911			
Nonadecanes	0.585			
Eicosanes +	6.382			

Table A10. Oil #5

Component	Z	TC	Pc	Vc	OM	MW	nc	
Name		[K]	Bar	cc/mole			micropoise	
C7	0.1579	598.138	35.365	374.063	0.359	115.776	317.442	315.192
C16	0.076	664.129	23.517	589.736	0.633	193.270	307.073	304.897
C24	0.052	750.781	16.653	869.395	0.986	316.714	305.973	303.805
C36	0.0263	923.370	11.656	1322.408	1.294	610.916	323.649	321.356

Table A11. Oil #5 Characterisation of Pseudo components

Oil #6 North Sea Oil -2

	Oil #6			
	mole %	weight %		
Nitrogen	0.34			
Carbon Dioxide	0.84			
Hydrogen Sulfide	0			
Methane	49.23			
Ethane	6.32			
Propane	4.46			
i-Butane	0.86			
n-Butane	2.18			
i-Pentane	0.93			
n-Pentane	1.33			
Hexane	2.06			
Heptanes	3.33			
Octanes	4.06			
Nonanes	2.76			
Decanes	1.33			
Undecanes	1.79			
Dodecanes	1.7			
Tridecanes	1.81			
Tetradecanes	1.46			
Pentadecanes	1.49			
Hexadecanes	1.08			
Heptadecanes	1.13			
Octadecanes	0.99			
Nonadecanes	0.88			
Eicosanes +	7.64			

Table A12. Oil #6

Component	Z	TC	Pc	Vc	OM	MW	nc	
Name		[K]	Bar	cc/mole			micropoise	
C7	0.168	610.011	32.874	406.908	0.408	126.333	314.806	322.840
C14	0.070	686.522	21.219	662.233	0.726	223.590	306.699	314.526
C20	0.049	774.682	15.424	946.412	1.073	356.953	307.041	316.052
C35	0.027	946.334	11.411	1364.472	1.297	658.211	329.862	342.157

Table A13. Oil #6 Characterisation of Pseudo components

Oil #7, NSO #3

	Oil #7			
	mole %	weight %		
N2	0.33			
CO2	0.19			
H2S				
Methane	35.42			
Ethane	3.36			
Propane	0.9			
i-Butane	0.69			
n-Butane	0.26			
i-Pentane	0.26			
n-Pentane	0.14			
Hexane	0.72			
Heptane+	57.73			

Table A14. Oil #7

Component	Z	TC	Pc	Vc	OM	MW	nc	
Name		[K]	Bar	cc/mole			micropoise	
C7	0.2789	615.338	28.539	465.581	0.452	137.000	297.901	1553.717
C15	0.1445	702.625	19.040	739.106	0.803	249.000	299.942	1557.724
C23	0.0974	792.764	15.991	936.864	1.119	381.502	323.909	1677.098
C35	0.0566	949.758	14.632	1148.22	1.316	634.359	381.982	1970.377

Table A15. Oil #7 Characterisation of Pseudo components

Oil #8, Elf –1

	Oil #8			
	Mole %	Weight %	MW	Density
Nitrogen	0.08			
Carbon Dioxide	0.27			
Hydrogen Sulfide				
Methane	49.71			
Ethane	3			
Propane	1.38			
i-Butane	0.52			
n-Butane	1			
i-Pentane	0.8			
n-Pentane	0.73			
Hexane	2.29			
Heptanes	2.76			
Octanes	3.11			
Nonanes	2.72			
Decanes	3.02			
Undecanes +	28.62			

Table A16. Oil #8

Component	Z	TC	Pc	Vc	OM	MW	nc	
Name		[K]	Bar	cc/mole			micropoise	
C7	0.1989	620.738	30.640	440.373	0.453	137.507	312.474	443.482
C15	0.1008	705.441	19.845	716.572	0.803	248.795	307.998	426.99
C23	0.0628	790.154	16.306	920.327	1.109	376.260	326.065	444.177
C34	0.0398	939.625	14.443	1150.15	1.315	617.355	374.238	498.869

Table A17. Oil #8 Characterisation of Pseudo components

Oil #9, Elf –23

	Elf-23			
	mole %	weight %	MW	Density
Nitrogen	0.13			
Carbon Dioxide	0.09			
Hydrogen Sulfide				
Methane	41.32			
Ethane	0.78			
Propane	0.84			
i-Butane	0.21			
n-Butane	0.69			
i-Pentane	0.44			
n-Pentane	0.38			
Hexane	1.32			
Heptanes	2.17			
Octanes	2.99			
Nonanes	3.25			
Decanes	3.87			
Undecanes +	41.53		343.3	0.9433

Table A18. Oil #9

Component	Z	TC	Pc	Vc	OM	MW	nc	nc
Name		[K]	Bar	cc/mole			micropoise	
C7	0.261	638.563	29.302	470.006	0.515	153.605	319.065	909.537
C17	0.137	732.671	17.895	804.683	0.914	289.336	308.069	897.404
C27	0.087	829.856	14.290	1057.417	1.233	450.010	323.899	944.524
C41	0.053	986.971	12.355	1330.074	1.293	731.015	363.979	1055.09

Table A19. Oil #9 Characterisation of Pseudo components

Oil #10, Elf –24

	elf-24			
	mole %	weight %	MW	Density
Nitrogen	0.81			
Carbon Dioxide	0.08			
Hydrogen Sulfide				
Methane	42.14			
Ethane	0.46			
Propane	0.27			
i-Butane	0.12			
n-Butane	0.23			
i-Pentane	0.22			
n-Pentane	0.15			
Hexane	0.88			
Heptanes	1.75			
Octanes	2.63			
Nonanes	3.12			
Decanes	4			
Undecanes +	43.14		347.8	0.9457

Table A20. Oil #10

Component	Z	TC	Pc	Vc	ω	MW	nc	nc
Name		[K]	Bar	cc/mole		g/mol	μP	μP
C7	0.2745	644.588	28.0512	470.006	0.543	160.789	316.584	880.149
C18	0.1322	739.943	16.9852	804.683	0.949	303.536	304.248	845.851
C28	0.0862	835.364	13.6434	1057.417	1.252	464.396	318.680	885.975
C42	0.0534	990.248	11.7439	1330.074	1.285	745.353	355.118	987.277

Table A21. Oil #10 Characterisation of Pseudo components

Oil #11, Elf –26

	elf-26			
	mole %	weight %	MW	Density
Nitrogen	0.013			
Carbon Dioxide	1.375			
Hydrogen Sulfide				
Methane	32.095			
Ethane	3.361			
Propane	4.618			
i-Butane	1.463			
n-Butane	3.429			
i-Pentane	2.469			
n-Pentane	0.508			
Hexane	2.459			
Heptanes	3.233			
Octanes	5.711			
Nonanes	4.81			
Decanes	3.963			
Undecanes +	30.495			

Table A22. Oil #11

Component	Z	TC	Pc	Vc	OM	MW	nc	nc
Name		[K]	Bar	cc/mole			micropoise	
C7	0.21	610.241	35.322	381.370	0.392	124.619	327.980	433.308
C12	0.135	664.358	23.371	593.100	0.635	194.391	306.660	381.891
C18	0.088	731.862	17.052	835.881	0.922	293.565	300.542	399.04
C27	0.049	857.323	13.127	1153.354	1.252	488.564	317.197	453.696

Table A23. Oil #11 Characterisation of Pseudo components

Oil #12, Kuito (Chevron – 2)

	mole %	MW	Density
Nitrogen	0.0003	Undecanes	0.0254
Carbon Dioxide	0.0113	Dodecanes	0.0299
Hydrogen Sulfide		Tridecanes	0.0349
Methane	0.2786	Tetradecanes	0.0358
Ethane	0.0101	Pentadecanes	0.0351
Propane	0.0031	Hexadecanes	0.0313
i-Butane	0.0018	Heptadecanes	0.0326
n-Butane	0.0032	Octadecanes	0.0282
i-Pentane	0.0022	Nonadecanes	0.0221
n-Pentane	0.0025		
Hexane	0.0054		
Heptanes	0.0137		
Octanes	0.0194		
Nonanes	0.0266		
Eicosanes +	0.3227	520	

Table A24. Oil #12

Component	Z	TC	Pc	Vc	OM	MW	nc	nc
Name		[K]	Bar	cc/mole			micropoise	
C7	0.337	658.390	24.989	555.394	0.609	178.912	308.088	726.587
C19	0.176	762.214	15.430	934.244	1.037	340.052	300.576	708.871
C33	0.103	875.122	11.128	1315.747	1.339	554.864	301.749	711.637
C50	0.066	1023.96	9.032	1668.353	1.192	856.659	317.791	749.470

Table A25. Oil #12 Characterisation of Pseudo components

9 Appendix B: Lohrenz Bray Clark method

In reservoir simulation the Lohrenz Bray Clark [1] correlation has been widely used. This correlation is based on a reduced fluid density of the mixture. The fluid density is normally calculated by an equation of state. The correlation does not always match the viscosity very well and therefore it is normal practice to tune the calculated viscosity against laboratory experiments. The normal way to tune the viscosity is by adjusting the critical volume of the heaviest component of the fluid characterisation. This only affects the viscosity calculation.

The Lohrenz Bray Clark viscosity correlation was published in 1964. The method for reservoir liquids is based on the concept of residual viscosities and the **principle of corresponding states**. The method was evaluated by comparing experimental and calculated results for 260 different reservoir oils ranging from black oils to highly volatile oils. The average absolute deviation was found to be 16 %. **[x]**. For reservoir gases a series of previously published correlations were used. The average absolute deviation for gas calculations was found to be 4 %.

9.1.1 Lohrenz Bray Clark Methodology

The LBC method is based on the Jossi [xx] method for calculating pure component viscosity. Jossi et al correlated the residual viscosity to the reduced density for pure compounds as follows:

B.1 $$[(\mu - \mu^o)\lambda + 10^{-4}]^{\frac{1}{4}} = a_1 + a_2\rho_r + a_3\rho_r^2 + a_4\rho_r^3 + a_5\rho_r^4$$

Where

a_1 = 0.102300

a_2 = 0.023364

a_3 = 0.058533

a_4 = -0.040758

a_5 = 0.0093324

and the reduced viscosity ρ_r is given by $\rho_r = \rho / \rho_c$

and μ^o is the low pressure viscosity which can be determined as

B.2 $\mu^o = 34\times10^{-5} T_r^{0.94} / \lambda$, for $T_r \le 1.5$, and

$\mu^o = 17.78\times10^{-5} (4.58T_r - 1.67)^{\frac{5}{8}} / \lambda$, for $T_r > 1.5$

where the reduced temperature T_r is calculated by $T_r = T / T_c$

The λ factor is calculated by the following equation

B.3 $$\lambda = T_c^{\frac{1}{6}} M^{-\frac{1}{2}} P_c^{-\frac{2}{3}}$$

Lohrenz Bray Clark extended the above equations for pure components to mixtures by using the following mixing rules:

B.4 $$\mu^0 = \left(\sum_{i=1}^{N} x_i \mu_i^0 M_i^{1/2} \right) \Big/ \left(\sum_{i=1}^{N} x_i M_i^{1/2} \right)$$

B.5 $$\lambda = \left(\sum_{i=1}^{N} x_i T_{ci} \right)^{1/6} \left(\sum_{i=1}^{N} x_i M_i \right)^{-1/2} \left(\sum_{i=1}^{N} x_i P_{ci} \right)^{2/3}$$

B.6 $$\rho_{Mc} = (v_c)^{-1} = \left(\sum_{i=1}^{N} x_i v_{ci} \right)^{-1}$$

and

B.7 $$\rho_r = v_c / v$$

The critical molar volume for the C7+ fraction was correlated to viscosity data of several reservoir fluids through the following equation.

B.7 $$(v_c)_{C7+} = 1.3468 + 9.4404\times10^{-4} M_{C7+} - 1.72651 S_{C7+} + 4.4083\times10^{-3} M_{C7+} S_{C7+}$$

where M and S are the molecular weight and specific gravity respectively.

10 Appendix C: Friction Theory

A new methodology for calculating hydrocarbon mixture viscosities has been developed at the IVC-SEP, Technical University of Denmark. The method is termed the *Friction Theory*. As part of this project, the *Friction Theory* methodology has been implemented in the CHEARS reservoir simulator in order to compare its performance to the standard *Lohrenz Bray Clark* correlation.

The Friction theory separates the total viscosity into a dilute gas viscosity, η_0, term and a residual friction term, η_f.

C.1 $$\eta = \eta_{0,mx} + \eta_{f,mx}$$

The dilute gas viscosity is defined as the viscosity at the zero density limit, while the residual term is related to friction concepts of classical mechanics. For an n-component mixture the residual friction term is expressed by the following equation:

C.2 $$\eta_{f,mx} = \kappa_{r,mx} p_r + \kappa_{a,mx} p_a + \kappa_{r,mx} p_r^2$$

p_a and p_r are the Van der Waals attractive and repulsive pressure terms of the mixture. These can be optained from a cubic equation state. The mixture friction coefficients κ_r, κ_r and κ_{rr} are obtained from the following mixing rules:

C.3 $$\kappa_{r,mx} = \sum_{i=1}^{n} \frac{z_i \eta_{c,i} \kappa_{r,i}}{P_{ci}}$$

C.4 $$\kappa_{a,mx} = \sum_{i=1}^{n} \frac{z_i \eta_{c,i} \kappa_{a,i}}{P_{ci}}$$

C.5 $$\kappa_{rr,mx} = \sum_{i=1}^{n} \frac{z_i \eta_{c,i} \hat{\kappa}_{rr,i}}{p_{ci}^2}$$

with

C.6 $$z_i = \frac{x_i}{MW_i^{\varepsilon} MM}$$

where

C.7 $$MM = \sum_{i=1}^{n} \frac{x_i}{MW_i^{\varepsilon}}$$

where ε is a mixing exponent used to improve the results. A value of .30 is used for ε.

And η_c is the component critical viscosity.

The critical viscosity for pure components are given in Table 2, For pseudo components the following equation is used .

C.8 $$\eta_c = K_c \frac{\sqrt{MW}\, P_c^{2/3}}{T_c^{1/6}}$$

Where the value of the proportionality constant, K_c, is set to 7.9483 as default. K_c can be used to tune the Friction Theory viscosity predictions to experimental viscosity data.

C.9 $$\hat{\kappa}_{r,i} = \hat{\kappa}_{r,i}^{c} + \Delta\hat{\kappa}_{r,i}$$

C.10 $$\hat{\kappa}_{a,i} = \hat{\kappa}^{c}_{a,i} + \Delta\hat{\kappa}_{a,i}$$

C.11 $$\hat{\kappa}_{rr,i} = \hat{\kappa}^{c}_{rr,i} + \Delta\hat{\kappa}_{rr,i}$$

with the following empirical expressions for the residual terms:

C.12 $$\Delta\hat{\kappa}_{r,i} = \kappa_{r,0,0}(\Gamma - 1) + (\kappa_{r,1,0} + \kappa_{r,1,1}\psi)(\exp(\Gamma - 1) - 1) + (\kappa_{r,2,0} + \kappa_{r,2,1}\psi + \kappa_{r,2,2}\psi^2)(\exp(2\Gamma - 2) - 1)$$

and

C.13 $$\Delta\hat{\kappa}_{a,i} = \kappa_{a,0,0}(\Gamma - 1) + (\kappa_{a,1,0} + \kappa_{a,1,1}\psi)(\exp(\Gamma - 1) - 1) + (\kappa_{a,2,0} + \kappa_{a,2,1}\psi + \kappa_{a,2,2}\psi^2)(\exp(2\Gamma - 2) - 1)$$

and

C.14 $$\Delta\hat{\kappa}_{rr,i} = \kappa_{r,2,1}\psi)(\exp(2\Gamma) - 1)(\Gamma - 1)^2$$

where

C.15 $$\psi = \frac{RTc_i}{Pc_i}$$

and

C.16 $$\Gamma = \frac{Tc_i}{T}$$

The Dilute Gas Viscosity is calculated as follows:

C.17 $$\eta_0 = 40.785 \frac{\sqrt{MWT}}{\upsilon^{2/3}\Omega^*} F_c$$

where

C.18 $$\Omega^* = \frac{1.16145}{T^{*0.14874}} + \frac{0.52487}{\exp(o.77320T^*)} + \frac{2.16178}{\exp(2.43787T^*)} - 0.0006435T^{*0.14874} \sin(18.02323T^* - 7.27371)$$

and

C.19 $$T^* = \frac{1.2593T}{T_c}$$

and

C.20 $$F_c = 1 - 0.2756\omega$$

where ω is the accentric factor

The friction theory parameters for the Peng Robinson Equation of State are given in the following table,

ka00	-0.0489197
ka10	0.270572
ka11	-1.10473e-4
ka20	-0.0448111
ka21	4.08972e-5
ka22	-5.79765e-9
kr00	-0.357875
kr10	0.637572
kr11	-6.02128e-5
kr20	-0.079024
kr21	3.72408e-5
kr22	-5.65610e-9
krr21	1.37290e-8
kac	-0.140464
krc	0.0119902
krrc	0.000855115

Table C.1. Friction theory parameters for the Peng Robinson Equation of State

Critical Viscosities

N_2	174.179
CO_2	376.872
H_2S	600.0
Methane	152.930
Ethane	217.562
Propane	249.734
i-Butane	271.155
n-Butane	257.682
i-Pentane	257.073
n-Pentane	258.651
Hexane	257.841

Table C.2. Critical Viscosity values for the pure components

10.1.1 Tuning of The Friction Theory Method

The tuning of the Friction Theory Method is carried out by adjusting the proportionality constant, K_c, in equation C.8, and thereby tuning the critical viscosities of the pseudo components.

11 Appendix D: Fluid Data

```
* FLUID PROPERTIES
*-------------------------------------------------------
RESTEMP   231
*              DENSITY
WATERPROP      1.034
*              PRESS    FVF        VISCOSITY
               14.700   1.0240     0.4500
               1000.0   1.0220     0.4500
               2000.0   1.0190     0.4500
               3000.0   1.0180     0.4500
               4000.0   1.0160     0.4500
               5000.0   1.0140     0.4500
*
*
*
*
*              DENSITY
OILPROP         0.8722
*
* PRESSURE  FVF      VISC     RS      COMPR     DVIS      a
   14.50     1.06630  0.49466       0.0000   1.35E-05   1.24E-04
0.00659
  541.00   1.21976 0.37213  233.7831  2.26E-05  1.78E-04 0.02645
 1067.50   1.35918 0.28588  479.1242  2.69E-05  1.87E-04 0.04196
 1594.00   1.50074 0.22690  734.8677  3.07E-05  1.89E-04 0.05908
 2120.50   1.65955 0.18351 1025.1934  3.43E-05  1.87E-04 0.07909
 2647.00   1.84822 0.15044 1371.6625  3.80E-05  1.81E-04 0.10315
 3173.50   2.08505 0.12449 1805.9986  4.19E-05  1.73E-04 0.13290
 3800.00   2.40506 0.09693 2389.2906  4.62E-05  1.25E-04 0.13290
 4700.00   2.51000 0.09000 5841.0     4.73E-05  1.16E-04 0.13290
 5700.00   2.52000 0.09000 6500.0     4.73E-05  1.16E-04 0.13290
 6700.00   2.53000 0.09000 6650.0     4.73E-05  1.16E-04 0.13290
 7700.00   2.54000 0.09000 7750.0     4.73E-05  1.16E-04 0.13290
 9700.00   2.55000 0.09000 7850.0     4.73E-05  1.16E-04 0.13290
12700.00   2.56000 0.09000 8850.0     4.73E-05  1.16E-04 0.13290
*
*
*
```

```
*
*

*               SP Grav
GASPROP          0.9178
*           PRESSURE       FVF       VISC
               14.50   4.76259   0.01062
              541.00   3.77932   0.01405
             1067.50   2.79606   0.01527
             1594.00   1.81279   0.01704
             2120.50   1.33955   0.01967
             2647.00   1.07204   0.02338
             3173.50   0.90923   0.02839
             3800.00   0.81008   0.03231
             4700.00   0.6903    0.03427
             5700.00   0.61822   0.03659
             6700.00   0.57039   0.04417
             7700.00   0.53039   0.04417
             9700.00   0.47125   0.04870
             12700.00  0.42125   0.04970
*
*
* *               DENSITY
SOLVENTPROP     0.8592
*           PRESSURE       FVF       VISC
               14.50   239.074     0.01303
              541.00   5.97436   0.01363
             1067.50   2.85166   0.01474
             1594.00   1.83162   0.01650
             2120.50   1.35196   0.01889
             2647.00   1.08794   0.02168
             3173.50   0.92748   0.02459
             3800.00   0.82216   0.02742
             4700.00   0.6903    0.03227
             5700.00   0.61822   0.03659
             6700.00   0.57039   0.04417
             7700.00   0.53039   0.04717
             9700.00   0.47125   0.05638
             12700.00  0.42125   0.06680
*
```

12 Appendix E: Input Deck

The following tables illustrate the necessary PVT input data that the simulator needs for equation of state calculations and for the viscosity calculations.

```
*-------------------------------------------------------
---
*     FLUID PROPERTIES
*-------------------------------------------------------
---
*
*
COMPONENTS
*
N2                      28.014
CO2                     44.01
H2S                     34.082
C1                      16.043
C2                      30.07
C3                      44.097
iC4                     58.123
nC4                     58.123
iC5                     72.15
nC5                     72.15
C6                      86.177


ORIGINALPREOS
*
EOSPARMS
*     Pc          Tc        Vc       w           sc
*     psi         F
*
*N2    493.126   -232.510    1.429   0.038
*CO2  1070.808     87.890    1.506   0.224

*H2S  1299.967    212.630    1.578   0.094
*C1    667.025   -116.590    1.579   0.012
*C2    706.620     90.050    2.331   0.100
*C3    616.117    205.970    3.204   0.152
*iC4   529.095    274.910    4.208   0.177
*nC4   550.560    305.690    4.085   0.200
*iC5   490.370    369.050    4.898   0.228
```

Molecular weigth

Critical pressure, temperature and volume. Accentric factor and the dimensionless volume shift

```
*nC5   488.775   385.610   5.014  0.252
*C6    438.737   453.650   5.943  0.301
*

N2    493.126  -232.510   1.429  0.038   0
CO2  1070.808    87.890   1.506  0.224   0
H2S  1299.967   212.630   1.578  0.094   0
C1    667.025  -116.590   1.579  0.012   -0.1540
C2    706.620    90.050   2.331  0.100   -0.1002
C3    616.117   205.970   3.204  0.152   -0.08501
iC4   529.095   274.910   4.208  0.177   -0.07935
nC4   550.560   305.690   4.085  0.200   -0.06413
iC5   490.370   369.050   4.898  0.228   -0.04350
nC5   488.775   385.610   5.014  0.252   -0.04183
C6    438.737   453.650   5.943  0.301   -0.01478


BINTINTCOEF
*
0.000
0.000 0.120
0.020 0.120 0.0
0.060 0.150 0.0 0.0
0.080 0.150 0.0 0.0 0.0
0.080 0.150 0.0 0.0 0.0 0.0
0.080 0.150 0.0 0.0 0.0 0.0 0.0
0.080 0.150 0.0 0.0 0.0 0.0 0.0 0.0
0.080 0.150 0.0 0.0 0.0 0.0 0.0 0.0 0.0
0.080 0.150 0.0 0.0 0.0 0.0 0.0 0.0 0.0 0.0
0.080 0.150 0.0 0.0 0.0 0.0 0.0 0.0 0.0 0.0 0.0
0.080 0.150 0.0 0.0 0.0 0.0 0.0 0.0 0.0 0.0 0.0 0.0
0.080 0.150 0.0 0.0 0.0 0.0 0.0 0.0 0.0 0.0 0.0 0.0 0.0
0.0
*
KVALUES  PREOS  500  15000   500
*
```

Binary Interaction coefficients.

Input for the Friction Theory Subroutine

T_c	P_c	V_c	MW	w	μ_c
126.20	34.00	89.20	28.014	0.0380	174.179
304.20	73.83	94.00	44.010	0.2240	376.872
373.50	89.63	98.50	34.082	0.0940	600.000
190.60	45.99	98.60	16.043	0.0120	152.930
305.40	48.72	145.50	30.070	0.1000	217.562
369.80	42.48	200.00	44.097	0.1520	249.734
408.10	36.48	262.70	58.123	0.1770	271.155
425.20	37.96	255.00	58.123	0.2000	257.682
460.40	33.81	305.80	72.150	0.2275	275.073
469.60	33.70	313.00	72.150	0.2520	258.651
507.40	30.25	371.00	86.177	0.3013	257.841
588.842	37.66	348.10	107.283	0.3207	319.509
628.383	28.55	474.25	150.686	0.4836	311.384
687.542	21.13	665.35	224.649	0.7309	306.513
815.257	13.25	1103.93	413.875	1.1558	296.247

Friction Theory parameters

```
-0.0489197
0.270572
-1.10473e-4
-0.0448111
4.08972e-5
-5.79765e-9
-0.357875
0.637572
-6.02128e-5
-0.079024
3.72408e-5
-5.65610e-9
1.37290e-8
-0.140464
0.0119902
0.000855115
```